

INFORMATION TO USERS

This manuscript has been reproduced from the microfilm master. UMI films the text directly from the original or copy submitted. Thus, some thesis and dissertation copies are in typewriter face, while others may be from any type of computer printer.

The quality of this reproduction is dependent upon the quality of the copy submitted. Broken or indistinct print, colored or poor quality illustrations and photographs, print bleedthrough, substandard margins, and improper alignment can adversely affect reproduction.

In the unlikely event that the author did not send UMI a complete manuscript and there are missing pages, these will be noted. Also, if unauthorized copyright material had to be removed, a note will indicate the deletion.

Oversize materials (e.g., maps, drawings, charts) are reproduced by sectioning the original, beginning at the upper left-hand corner and continuing from left to right in equal sections with small overlaps. Each original is also photographed in one exposure and is included in reduced form at the back of the book.

Photographs included in the original manuscript have been reproduced xerographically in this copy. Higher quality 6" x 9" black and white photographic prints are available for any photographs or illustrations appearing in this copy for an additional charge. Contact UMI directly to order.

U·M·I

University Microfilms International
A Bell & Howell Information Company
300 North Zeeb Road, Ann Arbor, MI 48106-1346 USA
313/761-4700 800/521-0600

Order Number 9213746

**A coupled atmosphere-ocean model in the tropics with various
climatological backgrounds**

Yang, Jiayan, Ph.D.

The Florida State University, 1991

U·M·I
300 N. Zeeb Rd.
Ann Arbor, MI 48106

THE FLORIDA STATE UNIVERSITY
COLLEGE OF ARTS AND SCIENCES

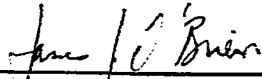
A COUPLED ATMOSPHERE-OCEAN MODEL
IN THE TROPICS WITH
VARIOUS CLIMATOLOGICAL BACKGROUNDS

By
Jiayan Yang

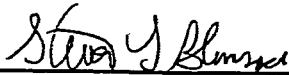
A Dissertation submitted to the
Department of Oceanography
in partial fulfillment of the
requirements for the degree of
Doctor of Philosophy

Degree Awarded:
Fall Semester, 1991

The members of the Committee approve the dissertation of Jiayan Yang defended on September 27, 1991.



James J. O'Brien
Professor Directing Dissertation



Steven L. Blumsack
Outside Committee Member



Allan J. Clarke
Committee Member




William K. Dewar
Committee Member



Richard L. Iverson
Committee Member

Approved:



William C. Burnett, Chair, Department of Oceanography

Acknowledgements

This work was supported by the Office of Naval Research, the National Science Foundation, NOAA and by the Florida State University through time granted on its Cray-YMP Supercomputer.

I would like to express my deepest gratitude and appreciation to my major professor Dr. James J. O'Brien for his support, encouragement and motivation. I wish to thank Drs. Allan Clarke and William Dewar for many invaluable discussions. I would also like to thank Drs. Richard Iverson, Steven Blumsack, Allan Clarke, William Dewar and Christopher Hunter for serving on my advisory committee. Thanks are extended to Dr. Richard Seager who provided the formula of the relationship between the depth of 20°C isotherm and the subsurface temperature.

I thank my colleagues in the Mesoscale Air-Sea Interaction Group for making such an enjoyable place to stay. Special thanks go to Brian Kelly for many discussions.

Finally, I wish to express my deepest appreciation to my wife Lisan Yu for her support, understanding, encouragement, patience, and, especially, for sharing her own scientific expertise which most husbands would envy.

Table of Contents

1. Introduction	1
1.1 Review of coupled atmosphere-ocean models in the tropics	2
1.1.1 <i>Conceptual model and simple model</i>	3
1.1.2 <i>Intermediate models</i>	5
1.1.3 <i>Coupled GCMs and hybrid coupled GCMs</i>	7
1.2 Motivation and objectives	8
2. The physics of coupled instabilities and the ENSO observation	12
2.1 Coupled instabilities	12
2.2 ENSO: the observation	19
3. A simple coupled model with two equilibrium states	27
3.1 The oceanic responses	31
3.2 A simple couples mode	37
4. An intermediate coupled model with a sloping thermocline	52
4.1 The model formulation	52
4.2 The model results and discussion	63
5. Summary	113
Appendix A: Derivation of linearized equations	115
Appendix B: The mean flow effects	118
Appendix C: Derivation of Gill's steady state atmosphere model	121
Appendix D: Derivation of pressure gradients	123
Appendix E: Effects of the mean flow on the SST equation	126
Reference	130

List Of Figures

- Fig.1: The schematic illustration of amplified modes and damped modes when (a) the SST is dominated by upwelling/downwelling; (b) the SST is Fig.1: The schematic illustration of amplified modes and damped modes when (a) the SST is dominated by upwelling/downwelling; (b) the SST is dominated by horizontal advectons (from Hirst, 1986). 15
- Fig.2: The schematic illustration of the delayed action oscillator (from Suarez and Schopf, 1988). 18
- Fig.3: (a) the solution of (2.9) for several parameter choices; (b) the range of parameters of oscillatory solution (from Suarez and Schopf, 1988). 20
- Fig.4: Observed SST anomalies in the eastern Pacific (solid line) and the central Pacific (dashed line) from 1921 to 1978 (from Rasmusson and Carpenter, 1982). 21
- Fig.5: The difference of atmospheric pressure between Easter Island and Darwin, Australia from 1949 to 1978 relative to a mean of 10.3 millibars. The thin line gives monthly means, the heavy line gives the 12-month running mean (from Wyrski, 1982). 23
- Fig.6: SST departures from the seasonal cycle, along the track 100 km off the coast of South America, during the El Nino in 1951, 1953, 1957,1963, 1965, 1969 and 1972 (from Rasmusson and Carpenter, 1982). 24
- Fig.7: The evolution of the composite El Nino (from Rasmusson and Carpenter, 1982). 25
- Fig.8(a): The fates of the coupled oscillations with weak coupling (from Neelin, 1989). 28
- Fig.8(b): The fates of the coupled oscillations with moderate strong coupling (from Neelin, 1989). 29
- Fig.8(c): The fates of the coupled oscillations with strong coupling (from Neelin, 1989). 30

Fig.9: The mean thermocline depth along the equator of the Pacific Ocean as measured by Colin et al. (1971).	33
Fig.10: A schematic picture of wave reflection from a thermocline front.	38
Fig.11: (a) The initial anomalous SST and its induced winds of the first run; (b) the anomalous SST and winds at 1450th day; (c) the anomalous SST and winds at 1950th day.	45
Fig.12: The longitude-time plot of the SST anomalies along the equator for the first run.	46
Fig.13: The initial SST and its induced winds of the second run.	48
Fig.14: The longitude-time plot of the SST anomalies along the equator for the second run.	49
Fig.15: The schematic model formulation.	56
Fig.16: The relation between the depth of the 20°C isotherm and the temperature at 50 meters (from Seager et al., 1988).	62
Fig.17: (a) the thermocline depth; (b) the SST, produced by the model when it was forced by a steady wind.	66
Fig.18: The model thermocline profiles.	69
Fig.19: The initial conditions of the m71odel, (a) the thermocline depth anomalies; (b) the SST anomalies.	71
Fig.20: The evolution of the model variables in the eastern boundary at the equator. (a) SST anomalies; (b) the thermocline depth anomalies; (c) the second layer thickness anomalies (run 1).	72
Fig.21(a): The longitude-time plot of the SST anomalies (run 1).	74
Fig.21(b): The longitude-time plot of the anomalous thermocline depth (run 1).	76
Fig.21(c): The longitude-time plot of the second layer thickness anomalies (run 1).	77
Fig.21(d): The anomalous heat content in the mixed layer.	79
Fig.22: The evolution of the model variables in the eastern boundary at the equator. (a) SST anomalies; (b) the thermocline depth anomalies; (c) the second layer thickness anomalies (run 2).	81

Fig.23(a): The longitude-time plot of the SST anomalies (run 2).	83
Fig.23(b): The longitude-time plot of the anomalous thermocline depth (run 2).	84
Fig.23(c): The longitude-time plot of the second layer thickness anomalies (run 2).	85
Fig.24: The evolution of the model variables in the eastern boundary at the equator. (a) SST anomalies; (b) the thermocline depth anomalies; (c) the second layer thickness anomalies (run 3).	87
Fig.25(a): The longitude-time plot of the SST anomalies (run 3).	88
Fig.25(b): The longitude-time plot of the anomalous thermocline depth (run 3).	89
Fig.25(c): The longitude-time plot of the second layer thickness anomalies (run 3).	90
Fig.26: The evolution of the model variables in the eastern boundary at the equator. (a) SST anomalies; (b) the thermocline depth anomalies; (c) the second layer thickness anomalies (run 4).	93
Fig.27(a): The longitude-time plot of the SST anomalies (run 4).	95
Fig.27(b): The longitude-time plot of the anomalous thermocline depth (run 4).	96
Fig.27(c): The longitude-time plot of the second layer thickness anomalies (run 4).	97
Fig.28: The entrainment coefficient σ as function of mean thermocline depth (the dashed line is from Zebiak and Cane's formula; the solid line is from Seager et al.'s formula which is used in this work).	99
Fig.29: (a) Anomalous SST and wind fields at the 1090th day in experiment#4; (b) anomalous depth of thermocline.	102
Fig.30: (a) Anomalous SST and wind fields at 1250th day in experiment#4; (b) anomalous depth of thermocline.	103
Fig.31: (a) Anomalous SST and wind fields at 90th day in experiment#2; (b) anomalous depth of thermocline.	106
Fig.32: The model conditions of experiment#1 at the 670th day, (a) the anomalous SST and winds; (b) the anomalous thermocline depth.	108

- Fig33: The model conditions of experiment#2 at the 760th day, (a) the anomalous SST and winds; (b) the anomalous thermocline depth. 109
- Fig.34: Low pass (31 day running mean) filtered isotherm fluctuations at (a) 109°30'W and (b) 95° W from 1981 to 1983 (from Halpern, 1984). 111
- Fig. 35: The model configuration in the vertical direction. 124

Abstract

An atmosphere-ocean coupled model is used to study the effects of a zonally sloping thermocline on the coupled oscillatory modes in the tropics. A two and one half layer oceanic model is coupled with the steady state Gill's atmospheric model. A constant depth mixed layer is included in the upper layer. The SST variation is calculated in the mixed layer. The interface of the two active layers is sloping and prescribed as the observed 20°C isotherm in the Pacific Ocean. The formula of Seager et al. (1988) is used to compute the entrained water temperature anomaly.

The unstable waves behave like the propagating modes with greater SST anomalies observed in the eastern Pacific Ocean. It is found that the coupled instabilities are very sensitive to the steepness of the tilted thermocline in the central Pacific Ocean. A series of numerical experiments have been performed, with different thermocline profiles. An interannual oscillation is self-sustained when a realistic thermocline profile is specified. The initial disturbance slowly decays and comes back to the equilibrium state of rest when the thermocline slope becomes steeper. The oscillation amplitude increases significantly when a flatter thermocline is used. An additional numerical experiment is conducted to investigate the role of the western boundary reflection. It is found that the reflection does not change the oscillatory period though it affects the amplitude. A simpler conceptual model is also used to explain the physics.

1. Introduction

Oceanic variability in the tropical ocean, especially interannual fluctuations, has been studied extensively over the past two and a half decades. The great efforts to explore the dynamics of the equatorial oceans have been motivated by the interannual occurrences of global climate fluctuations associated with unstable air-sea interactions in the tropics. The most prominent interannual climate variability in the tropics is the El Niño/Southern Oscillation (ENSO) phenomenon. The ENSO is defined as massive intrusions of warm tropical waters into the eastern equatorial Pacific Ocean and the shifts of the atmospheric pressure between the center in the western Pacific Ocean/eastern Indian Ocean and the center in the eastern Pacific Ocean. The globally catastrophic consequences associated with this climate fluctuation, such as the severe damages to the fishing industry of the southern American countries, disastrous flooding in the eastern coast of America or persistent droughts in Australia have attracted unprecedented joint efforts from both the oceanography and the meteorology communities to tackle the ENSO problems.

The ENSO modelling started with the study of either the ocean or the atmosphere. Wyrтки (1975) suggested that the interannual occurrences of warming SST in the eastern Pacific Ocean are due to the remote forcing in the central and western Pacific Ocean caused by a relaxation of the trade wind. Wyrтки's hypothesis has been supported by many numerical models (e.g., Hurlburt et al., 1976; McCreary, 1976; Inoue and O'Brien,

1984). The atmospheric responses to the anomalous SST fields have also been studied extensively (e.g., Shukla and Wallace, 1983; Keshavamurty, 1982).

The anomalous SST associated with El Niño is usually accompanied by unusual atmospheric conditions. For example, remarkable anomalous conditions of both the atmosphere and the ocean were observed in the tropical Pacific during the International Geophysical Year in 1957 and 1958. Bjerknes (1969) proposed that such unusual atmospheric and oceanographic conditions were not just a unique coincidence but were two aspects of the same phenomenon. There have been more complete measurements taken which support Bjerknes's theory. For example, in May 1982, modest westerly wind anomalies were observed in the western equatorial Pacific Ocean and subsequently extended eastward. This meteorological condition coincided with an eastward expansion of warm SST waters. From the meteorologist's point of view, the westerly wind anomalies were caused by the warm SST. However the SST anomaly itself was amplified by the westerly winds. Such a circular argument indicates that the interaction between the atmosphere and the ocean is the heart of ENSO (Philander, 1990). The full understanding of this phenomenon requires the studies of the interactions between the atmosphere and the ocean.

1.1 Review of coupled atmosphere-ocean models in the tropics

The intriguing hypothesis that ENSO is the result of a strong coupling between the ocean and the atmosphere in the tropics has stimulated the increasing number of studies in the area of tropical air-sea

interactions. To date there have been many coupled atmosphere-ocean models developed to understand the ENSO phenomena. All the models attempt to address the same question: how can the ocean and the atmosphere interact to produce an interannual oscillation? As many models have shown, if a SST anomaly alters the atmosphere in such a way that the induced surface winds further intensify the anomalous SST, then the interactive system of the ocean and the atmosphere becomes unstable. Since the early 1980's, studies of the coupled ocean-atmosphere interactions have developed very rapidly from some highly idealized simple models to the coupled general circulation models of full complexity. All the coupled models can be arranged in a hierarchy of increasing dynamical complexity (McCreary and Anderson, 1991) as: (a) conceptual and simple coupled models, (b) intermediate coupled models, (c) coupled general circulation models (CGCM), and hybrid coupled general circulation models (HCGCM) (HCGCM are those coupled models in which one component is a GCM and the other component is a simple model).

1.1.1 Conceptual model and simple models

As categorized by a recent review paper by McCreary and Anderson (1991), conceptual models are those which drastically reduce the spatial structure of the atmosphere and the ocean to a coupled system which, consisting of a few variables, depends on time only. They represent the ocean and the atmosphere with simplified, but familiar, sets of partial differential equations. Conceptual and simple models usually depend on a number of assumptions in order to reduce the model complexity. Not all of

these simplifications can be rigorously justified in a real coupled system. However, they are very useful to provide a conceptual framework in which essential mechanisms can be identified. Conceptual and simple models are often used to diagnose the more complicated models. There are two primary hypotheses regarding the nature of ENSO in the conceptual and simple models (Hirst, 1990). The first hypothesis is that ENSO may be a self-sustained low-frequency regular oscillation built into the coupled system. The second one is that the coupled system is unstable, and a suitable initial disturbance might "trigger" an ENSO episode.

Several instability analyses have also been conducted on highly idealized models (e.g., Philander et al. 1984; Hirst, 1986; Gill, 1985; Yamagata, 1985; Neelin, 1991). Both the atmospheric and the oceanic models were represented by the linear shallow water equations in the one-layer reduced-gravity model and the equatorial β -plane was used. Gill's atmosphere model was used in these models. Those conceptual and simple models analytically proved that very low frequency instabilities are possible when the linear ocean and atmosphere models, neither of them having instabilities, are coupled together. The essence of developing the linear coupled instabilities is the positive feedbacks between the atmosphere and the ocean.

Although the unstable air-sea interaction is the essential mechanism for the instabilities in all the linear simple models, the evolution and behaviors of different models could be very different. For example, when Philander et al. (1984) assumed that the SST anomaly was proportional to the deviation of the main thermocline depth, i.e., the thermodynamics were completely dominated by the upwelling/

downwelling processes, their model displayed an eastward propagating mode. In contrast, Gill (1985) used an ocean model in which the anomalous SST was solely determined by the anomalous advection of the mean background SST, and his model was dominated by westward propagating disturbances. The different behaviors of these two models will be discussed in Section 2.

1.1.2 Intermediate models

The term intermediate model is used to describe a particular class of coupled ENSO models which are distinguished by being intermediate in complexity between the highly idealized conceptual models and the coupled general circulation models (CGCM). Most of the intermediate models use Gill's steady state atmosphere model or similar models with some modifications to include the moisture processes. The ocean models in this class are basically the shallow water equations with explicit treatments of the thermodynamics. As pointed out by Zebiak (1990), the great utility of this class of models lies in a level of complexity which allows direct comparisons with the observations and easy interpretations of model physics. Intermediate models have played one of the most important roles in the understanding of the physical mechanisms of ENSO.

Anderson and McCreary (1985) (hereafter AM85) used a nonlinear one layer reduced-gravity oceanic model and the original version of Gill's atmospheric model to describe the evolution of SST and wind anomalies associated with ENSO. When both the atmosphere and the ocean were assumed to be cyclic with a wavelength of 15,000 km, AM85 generated an

eastward propagating mode with a period of 2000 days. The physical mechanism for generating the eastward mode in their model is basically the same as that captured in the conceptual model of Yamagata (1985) and Hirst (1986). Zebiak and Cane (1987) (hereafter ZC87) coupled a reduced-gravity oceanic model, topped with a fixed depth mixed layer, to a modified version of Gill's atmosphere model. Some effects of climatological background variations and seasonal variations were included in ZC87. Their model showed the seasonal phase locks of SST anomaly and aperiodicity of ENSO evolution. Schopf and Suarez (1988) (hereafter SS88) developed a coupled model consisting of a two-layer ocean model and a two-layer global atmosphere. The model produced an irregular oscillation. The mechanism of this oscillation is mainly determined by the oceanic long Rossby waves generated in the central Pacific Ocean and the reflected Kelvin waves from the western boundary. By using a nearly identical model to ZC87, Battisti (1988) (hereafter B88) simulated the interannual variabilities but was unable to reproduce the aperiodicity of the model oscillation. B88 did a series of sensitivity tests and convincingly demonstrated that the reflection of long Rossby waves from the western boundary is critical to terminate the SST anomalies in the eastern Pacific Ocean. The physical mechanisms discussed in SS88 and B88 are basically the same, i.e., the delayed negative feedbacks from the reflected Kelvin waves set the oscillation. Battisti and Hirst (1989) argued that this oscillator does not exist in a smaller basin, like the Atlantic and Indian Oceans, because the time lags are too short to allow the anomalous conditions to fully develop in the eastern oceans. The discovery of this delayed action mode is very encouraging because it, for the first time,

dynamically explains why ENSO only occurs in the Pacific Ocean. However, as pointed out by Battisti, Hirst and Sarachik (1989) (hereafter BHS89) and Philander (1990) (hereafter P90), a real ENSO event sometimes behaves like a propagating mode and sometimes behaves like a nonpropagating mode. Hence, both propagating mode and nonpropagating mode likely exist, and some new modes remain to be uncovered.

1.1.3 Coupled GCMs and hybrid coupled GCMs

There has been increasing interest in using the more realistic, three dimensional coupled GCMs. Although simple and intermediate models have been essential to understand the mechanisms of ENSO, they usually depend on a large number of assumptions which are not necessarily rigorously justified. The final understanding and the accurate prediction of ENSO require the coupled GCMs of full complexity. There are various versions of coupled GCMs and hybrid coupled GCMs. Although many CGCMs develop climate drift, in which solutions gradually move away from a realistic climatology, most of them have been able to produce ENSO-like oscillations with interannual time scales. An excellent review and intercomparison of various CGCMs and HCGCMs is given by Neelin et al. (1991). The major disadvantages of using a CGCM are that it usually requires enormous computational resources and the results are sometimes difficult to interpret.

By using an oceanic general circulation model (GCM) coupled with a two-level steady state atmospheric model, Neelin (1989) showed that the model sustained three to four year oscillations. For stronger coupling, a

secondary bifurcation yielded six month coupled oscillations during the warm phase of the ENSO. For weaker coupling, the initial disturbance was gradually damped. Philander et al. (1989) used a coupled general circulation model of the atmosphere and the ocean to study the irregular interannual fluctuations. They compared the results of two different simulations, one with a high model resolution and the other with a coarse resolution. They attributed the significant differences of the two simulations to the absence of the Kelvin waves in the coarse model. Although CGCMs contain more complete physics, simpler layer models remain very useful to isolate and identify certain ENSO mechanisms.

1.2 Motivation and objectives

Although our knowledge of ENSO has increased tremendously over the past decade, there are still some key features that we don't fully understand. For example, one open question in ENSO studies is what is the essential mechanism which deters ENSO from taking a regular cycle, or, what causes the aperiodicity of ENSO? There have been many speculations ranging from nonlinearity to some unknown noises. The real mechanisms are not yet clear. Another problem is the relation between the seasonal and the interannual variabilities, i.e., why ENSO is locked with a particular season. The sensitivity of the ENSO evolution to the initialization and the climatological backgrounds is also poorly known. In fact Neelin (1989) demonstrated that the evolution of ENSO critically depends on the intensity of the atmosphere-ocean coupling. He showed that a reduction of the coupling coefficient by 30% leads to the decaying of

the initial condition in his model. The intensity of air-sea coupling usually strongly depends on the local mean background condition.

In this work, we attempt to study the effects of a pre-existing climatological condition on ENSO evolution. The pre-existing condition in this paper is defined as the persistent climatological background which is not created by ENSO processes. For example, the zonal slope of the main thermocline in the tropics is maintained by the easterly trade wind. Our purpose is to examine the effect of the climatological slope of the thermocline on the development of unstable coupled modes.

Although ZC87 and B88 have considered the thermodynamic effects of the sloping thermocline, the dynamical consequences have never been studied in the existing coupled models. A striking feature of the equatorial oceans is that the SST increases westward, and thus the main thermocline is shoaling eastward. If the thermocline depth varies slowly over one wavelength, the WKBJ method is often useful in estimating the variations of wave amplitudes (e.g., Hughes, 1981; Yang and Yu, 1991). This condition is not valid in the central equatorial Pacific Ocean where the thermocline depth changes rapidly. Gill and King (1985) (hereafter GK85) used a two-layer reduced-gravity model to study such modal energy exchanges. For a very low frequency Kelvin wave, the shoaling thermocline behaves like a step (GK85). Therefore the matching conditions at the step require up to 25% of the incident Kelvin wave's energy be reflected westward as long Rossby waves. Another study conducted by Bussalachi and Cane (1988) (hereafter BC88) found similar results. One of the main results of GK85 is that the eastern Pacific Ocean is not necessarily dominated by the variabilities associated with the first

baroclinic mode even if the remote signals in the western Pacific Ocean are completely dominated by the first vertical mode. The vertical modal energy exchanges can be very efficient for low-frequency Kelvin waves.

If the ocean were free from interacting with the atmosphere, the results of GK85 and BC88 might suggest that a thermocline front is not an effective barrier for zonal energy propagation. However, the subsequent air-sea interaction processes resulting from thermocline reflection and modal decomposition (the term modal decomposition, which was used by Gill and King (1985), is defined as the energy transfers among different vertical modes) could be vitally important in determining the evolution of an unstable coupled mode. As we will discuss in the following sections, the thermocline front can reduce the intensity of tropical air-sea interactions by several processes. First, the westward reflected Rossby waves tend to weaken the opposite SST anomaly in the western Pacific Ocean. The weakened west-east SST difference then further weakens the atmospheric convections. Second, the wind fields induced by the different baroclinic mode Kelvin waves and reflected Rossby waves damp each other. A detailed physical formulation will be given in Section II.

Clearly, one single baroclinic mode is not enough to describe the coupled dynamics in such an inhomogeneous background. We would like to investigate the effect of modal decomposition in the central equatorial Pacific Ocean on the coupled dynamics. Therefore, we use the simplest possible ocean model. This consists of two active upper layers with the thermodynamics included in a constant depth surface mixed layer. The atmosphere model is the original version of the steady state Gill's model. The interface between the two upper layers is prescribed as the observed

20°C isotherm, and the interface between the second layer and the deep ocean is prescribed as a 10°C isotherm. The SST is calculated in a constant depth mixed layer above the upper layer. The mixed layer is treated as in ZC87 except a different formula is used to calculate the entrained water temperature. The temperature of the entrained water is calculated as in Seager et al. (1988) who used the observed data to derive a relation between the depth of the 20°C isotherm and the water temperature at the base of the mixed layer (at 50 meters).

In the next section, we discuss the physics of coupled oscillatory modes and review some ENSO observations. In Section 3, we present a dynamical framework of our research. The effects of an inhomogeneous background on oceanic free waves and coupled air-sea interaction modes will be discussed. We will also use a very simple model, similar to Hirst's (1986) Model III, to explain our physical hypothesis. A multiple layer coupled model of intermediate complexity is introduced in Section 4. In Section 5, we will summarize and conclude the work.

2. The Physics of coupled instabilities and the ENSO observation

2.1 Coupled instabilities

The most important question that all the ENSO relevant coupled models aim to answer is, "how do the atmosphere and the ocean interact to generate such a low-frequency oscillation?". To answer this question, we consider the equation that governs the thermodynamic processes in an ocean mixed-layer:

$$\frac{\partial T}{\partial t} + u \frac{\partial T}{\partial x} + v \frac{\partial T}{\partial y} = \frac{Q - w\Delta T}{H_m}$$

where ΔT is the temperature difference across the base of the mixed layer, H_m is the depth of the mixed layer, w is the entrainment rate at the mixed layer base, Q represents the heat fluxes (radiation, evaporation, etc.) across the ocean surface. If w is estimated by the Kraus-Turner formula, the SST equation can be linearized about a mean state of nonuniform SST $T_0(x,y)$ and an uniform mixed layer depth H_0 . If there is no mean flow (which is unrealistic because the mean current is very important to the total heat balance), the resulting linearized equation (see Appendix A) obtained by Hirst (1986) or Xie et al. (1989) has the form:

$$\frac{\partial T'}{\partial t} + u \frac{\partial T_0}{\partial x} + v \frac{\partial T_0}{\partial y} = \sigma h - \alpha T' \quad (2.1)$$

where T' is the anomalous temperature, and h is the mixed layer depth anomaly. The term $-\alpha T'$ represents Newtonian cooling which tends to

bring the SST back to the equilibrium state. The term σh connects the vertical thermocline displacement to the SST variations.

What is the necessary condition for the coupled instability to develop? Yamagata (1985) considered an ocean mixed-layer governed by the following equations:

$$\frac{\partial u}{\partial t} - \beta y v + g' \frac{\partial h}{\partial x} = -au + \tau^x / (\rho_0 H_0) \quad (2.2a)$$

$$\frac{\partial v}{\partial t} + \beta y u + g' \frac{\partial h}{\partial y} = -av + \tau^y / (\rho_0 H_0) \quad (2.2b)$$

$$\frac{\partial h}{\partial t} + H_0 \left(\frac{\partial u}{\partial x} + \frac{\partial v}{\partial y} \right) = -bh \quad (2.2c)$$

where $-a(u,v)$, $-bh$ are the Rayleigh friction and the Newtonian cooling terms respectively, H_0 is the mean layer thickness, and h is the deviation of the thermocline depth. The wind stress (τ^x, τ^y) is simply related to the low level wind speeds by $(\tau^x, \tau^y) = \gamma (U, V)$. Equation (2.2) can be derived from an ocean mixed-layer with the entrainment rate calculated from the Kraus-Turner formula (Appendix A). Some assumptions (i.e., no mean flow, the pressure gradients induced by anomalous SST are small, etc.) are made in order to simplify the equations. Some of these assumptions can not be rigorously justified when a real coupled system is considered. However, such a simplified system contains some of the essential mechanisms that sustain the ENSO oscillation. Therefore they are useful for the diagnostic studies. An energy integral of the equations (2.2a-c) leads to:

$$\frac{1}{2} \{ H_0 (u^2 + v^2) + g' h^2 \}_t = -a \{ H_0 (u^2 + v^2) \} - b \{ g' h^2 \} + \gamma \{ uU + vV \} / \rho_0 \quad (2.3)$$

where $\{ \}$ denotes the integration over one wavelength in x and from $-\infty$ to $+\infty$ in y . Because the first two terms on right hand side are negative definite, the necessary condition for instability is

$$uU+vV > 0 \quad (2.4)$$

i.e., the ocean current and the wind stress must be positively correlated.

There are two types of unstable modes in such a simple coupled system. If the thermodynamics are dominated by entrainments, equation (2.1) can be replaced by a much simpler equation (after dropping the prime for convenience):

$$T_t = \sigma h - \alpha T \quad (2.5)$$

Philander et al. (1984) coupled an ocean model governed by (2.2) and a SST equation similar to (2.5) to Gill's atmosphere model and found an eastward propagating unstable mode with a speed of about 43 cm/s and a structure similar to a free oceanic Kelvin wave. Gill (1985) and Rennick and Haney (1986) used a different formulation of thermodynamics by assuming that the SST was solely determined by the anomalous zonal advection of the mean SST, i.e.,

$$T_t = -uT_{0x} \quad (2.6)$$

The coupled system which consisted of (2.2), (2.6) and Gill's atmosphere model produced a westward propagating mode. The structure of this coupled mode was similar to long Rossby waves. The different behaviors of these two type modes were physically explained by Hirst (1986). The physics of their different behaviors is schematically shown in Fig.1. In equation (2.5) the SST anomaly is mainly determined by the thermocline depth deviation so that atmospheric heating occurs over the depressed

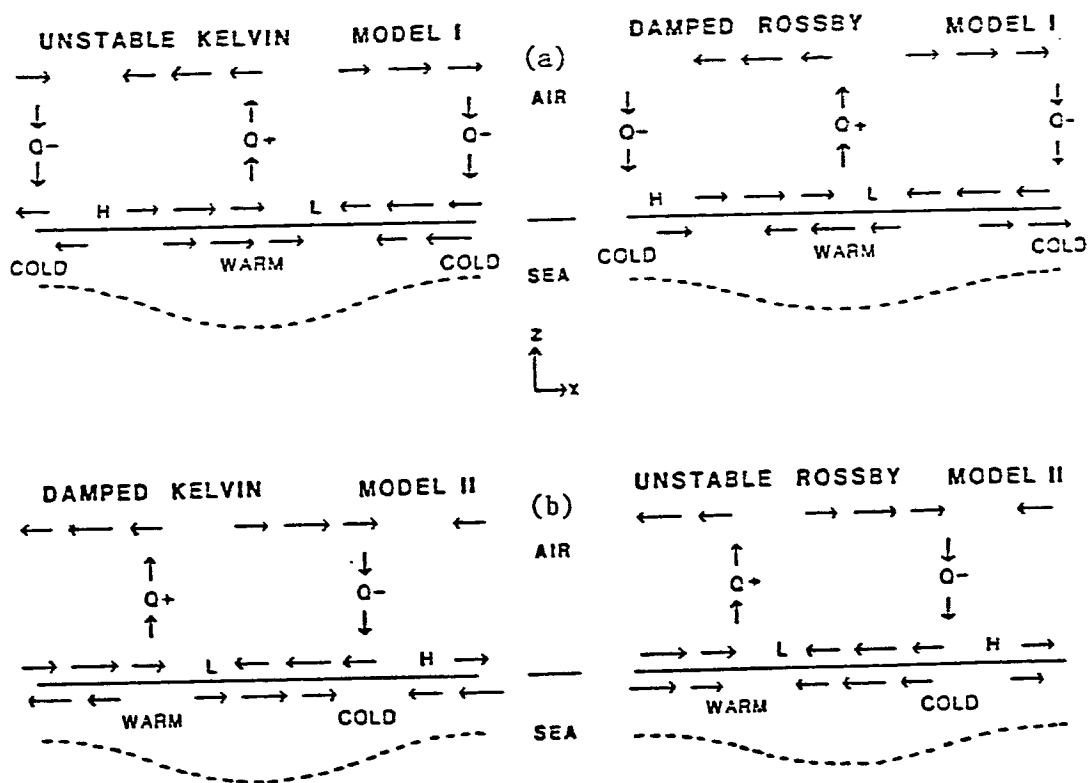


Fig.1: The schematic illustration of amplified modes and damped modes when (a): the SST is dominated by upwelling/downwelling; (b): the SST is dominated by horizontal advectons (from Hirst, 1986).

area of the thermocline (Fig.1(a)). Kelvin waves are amplified because the anomalous currents are in the same direction as the winds, while Rossby waves are damped because the currents are decelerated by the winds. If the SST is governed by (2.6), the currents of long Rossby waves and winds coincide (Fig.1(b)). Hence long Rossby waves are amplified while Kelvin waves are damped. Hirst (1986) further performed a stability analysis to the equation which included both the anomalous advection of mean SST in the zonal direction and the effect of thermocline variation, i.e.,

$$T_t + uT_{0x} = \sigma h - \alpha T \quad (2.7)$$

The meridional advection term vT_{0y} in (2.1) is small (Appendix A) and is neglected in Hirst's analysis. Hirst's results showed that the direction of instability propagation critically depends on the value of σ . It is also possible, within a certain range of parameters, for unstable modes to propagate extremely slowly and even to be stationary.

More complicated models, like Anderson and McCreary (1985), also generated eastward propagating unstable modes. The model selection of unstable modes crucially depends on the competition between the mean zonal SST gradient T_{0x} and the term σh in (2.7). In the real ocean both T_{0x} and σ vary spatially, and the real dominant mode could be either eastward or westward. If the mean background, i.e., the mean SST, the mean current, and the mean upwelling, varies realistically, an eastern ocean localized nonpropagating mode can be dominant (Battisti and Hirst, 1989). This new mode, called the delayed action oscillator, was discussed extensively by Battisti (1988) and Schopf and Suarez (1988). To explain the theory of the delayed action oscillator, we consider the following equation:

$$\frac{\partial T}{\partial t} = -u \frac{\partial}{\partial x} T_0(x,y) + \sigma(H_0(x,y)) h - \alpha T \quad (2.8)$$

where $H_0(x,y)$ is the mean depth of the mixed layer. In the warm pool of the western tropical Pacific Ocean, the horizontal mean SST gradients are small and the effect of vertical entrainment is also very small due to the deep mixed layer. Hence little SST anomaly can be induced by oceanic currents because the first two terms on the right hand side of (2.8) are small. In other word, dynamics are decoupled from thermodynamics in this area. In the eastern Pacific, both horizontal advection of the mean SST and the vertical entrainment become effective. However, the mean SST is low in the eastern tropical Pacific Ocean, hence the atmosphere is less influenced by oceanic perturbations in this area. The strong air-sea coupling occurs in the central Pacific. Fig.2, from Suarez and Schopf (1988), schematically displays how this delayed mode functions. During a warm event, westerly wind anomalies occur in the central and eastern Pacific Ocean. The westerly winds not only intensify the anomalous conditions in the eastern ocean but also generate upwelling long Rossby waves in the western part of the ocean. Since the thermodynamics are decoupled from the dynamics in the western Pacific Ocean, those long Rossby waves propagate freely westward. Upwelling Kelvin waves, resulting from long Rossby wave reflections move back to the eastern Pacific Ocean and terminate the previously existing warm event. This delayed negative feedback is essential for the oscillation to be sustained.

Suarez and Schopf (1988) argued that the essential physics of this complicated mode could be captured in a very simple conceptual model governed by the nonlinear delayed oscillatory equation:

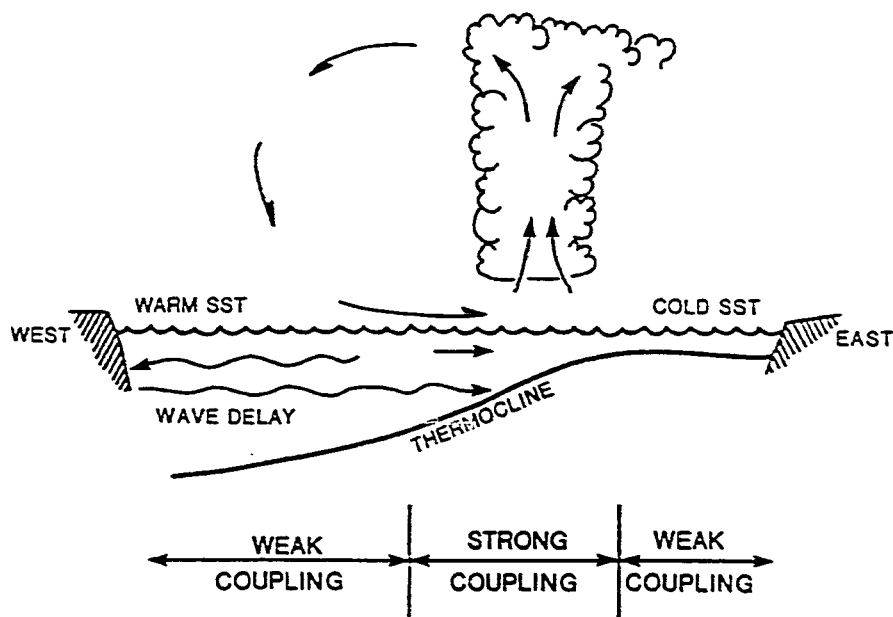


Fig.2: The schematic illustration of the delayed action oscillator (from Suarez and Schopf, 1988).

$$\frac{dT}{dt} = T - T^3 - \alpha T(t-\delta) \quad (2.9)$$

where the first two terms on the right hand side represent the positive feedbacks from the atmosphere and the nonlinear damping respectively, δ is the nondimensional delay time (wave transit time), and α measures the influence of the delayed negative feedbacks associated with reflected Kelvin waves. The model solutions of (2.9) for the different parameters are plotted in Fig.3(a). Fig.3(b) shows the parameter ranges where an oscillatory solution is possible. This model depends on (i) a long delay period and (ii) large delay effects ($\alpha > 1/2$ as suggested by Suarez and Schopf). The first restriction can be satisfied in a large basin like the Pacific Ocean. The second is related to the reflection of the western boundary. The western boundary of the Pacific Ocean is not meridionally straight and not even a wall, but consists of a chains of islands. There had been some suspicions about the reflectibility of long Rossby waves from the western boundary. However, Clarke (1991) argued analytically that the western boundary of the Pacific Ocean is highly reflective. Clarke's results convincingly demonstrate that the model results of Battisti (1988) and Schopf and Suarez (1988), which used the idealized western boundary, can be applied to the real ocean.

2.2 ENSO: the observations

The interannual variations of the oceanic conditions in the tropical Pacific Ocean are clearly shown in Fig.4 where the SST observations, in the period between 1921 and 1978 in the eastern and central Pacific, are plotted. The oscillations are irregular but have a preference for a 3-4 year

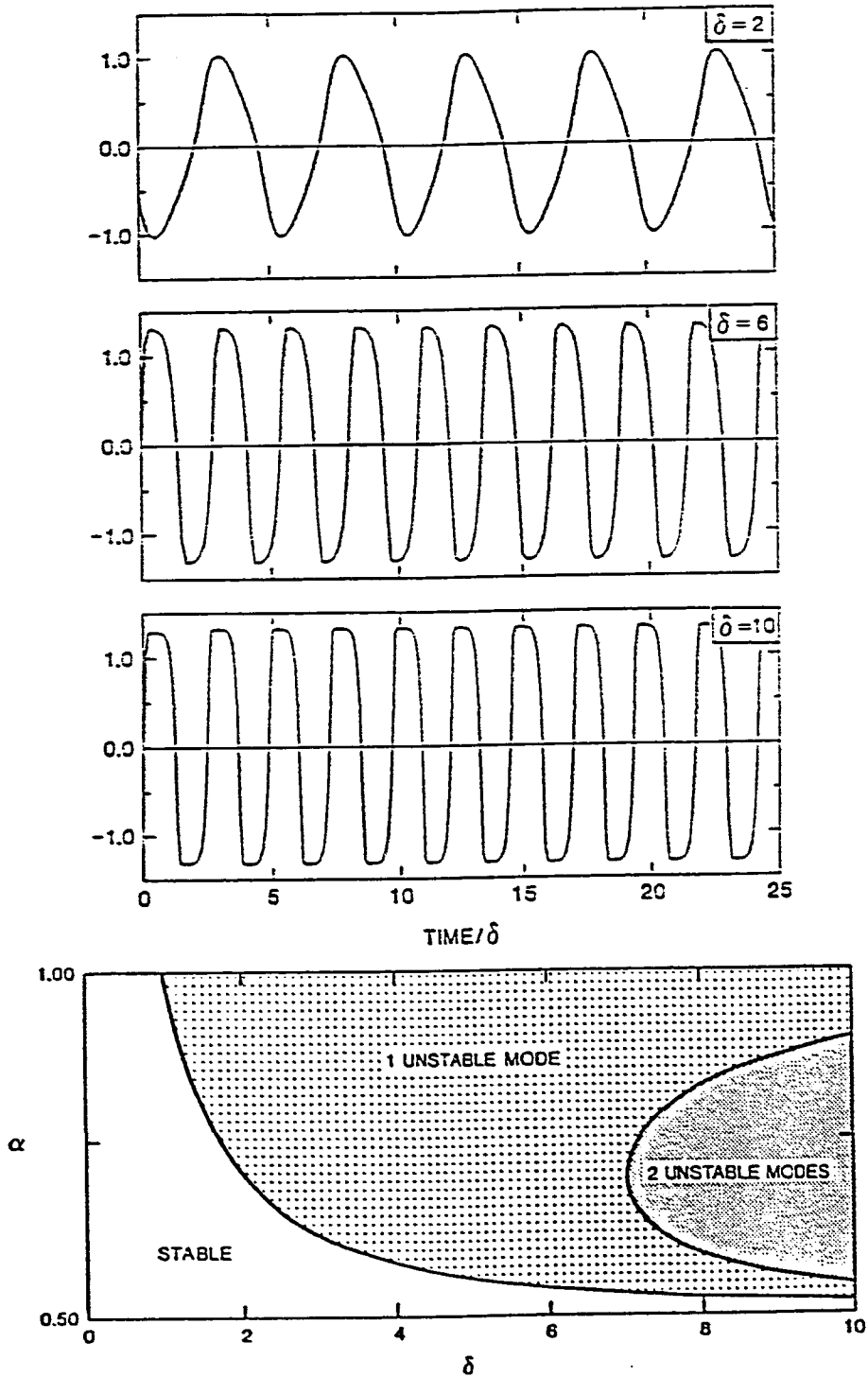


Fig.3: (a) the solution of (2.9) for several parameter choices; (b) the range of parameters of oscillatory solution. (from Suarez and Schopf, 1988).

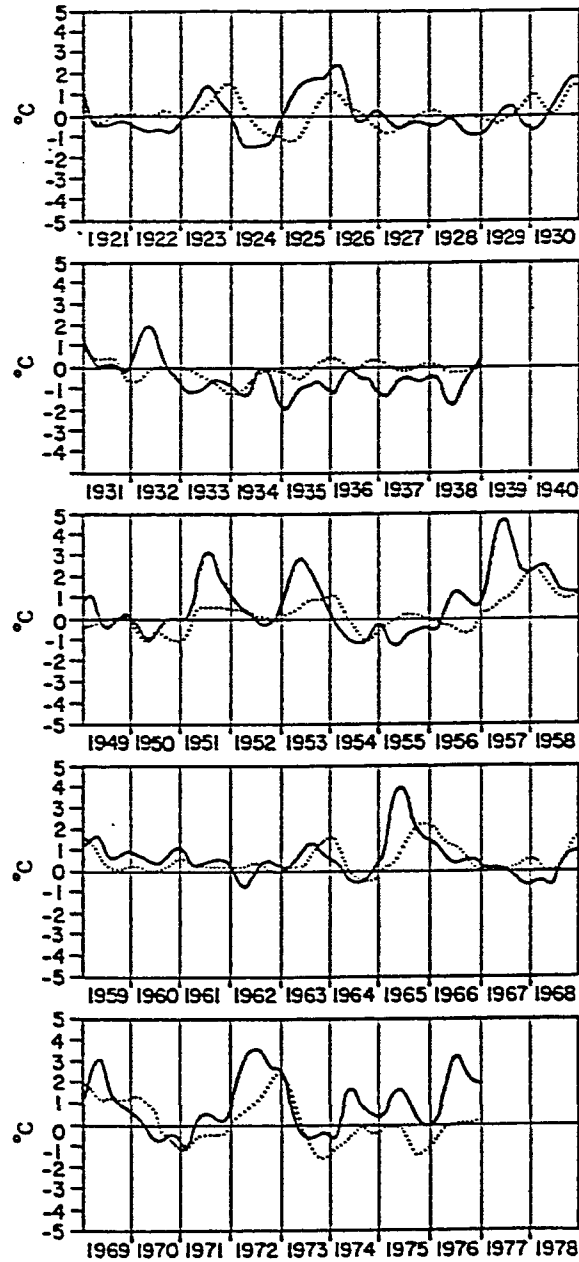


Fig.4: Observed SST anomalies in the eastern Pacific (solid line) and the central Pacific (dashed line) from 1921 to 1978 (from Rasmusson and Carpenter, 1982).

period. The amplitudes of all the El Niño events in this period are less than 5°C. Fig.5 shows the difference in atmospheric pressure between Easter Island and Darwin, Australia from 1949 to 1978 relative to a mean of 10.3 millibars. The period of the pressure shifts also has a preference of 3–4 years.

Rasmusson and Carpenter (1982) analyzed six El Niño episodes between 1950 and 1976. They found that the evolution of these six events was remarkably similar, although the amplitudes differed significantly. Fig.6 shows the sea surface temperature deviations from the normal seasonal cycle 100 kilometers off the coast of South America between 3°S and 12°N. The striking similarities between these six different El Niño events enabled Rasmusson and Carpenter to construct a "composite" El Niño episode. The following descriptions are from Philander (1990) who summarized the composite El Niño of Rasmusson and Carpenter.

Towards the end of the year before a warm event, the sea level pressures in the central and western Pacific ease, and the easterly trade weakens to the west of the dateline. The SST in the western Pacific becomes warmer than normal. During the early months of the next year the seasonal warming in the eastern Pacific amplifies and persists for several months. The warm SST slowly moves westward with a speed of about 50-100cm/s. Then the convective zone over the western Pacific moves eastward in the month of April, so that rainfall decreases and sea level increases in the western Pacific. By the month of July, anomalous conditions in the eastern Pacific have peaked although a secondary maximum could appear late in the year or early in the next year. Fig.7 shows the evolution of the composite El Niño.

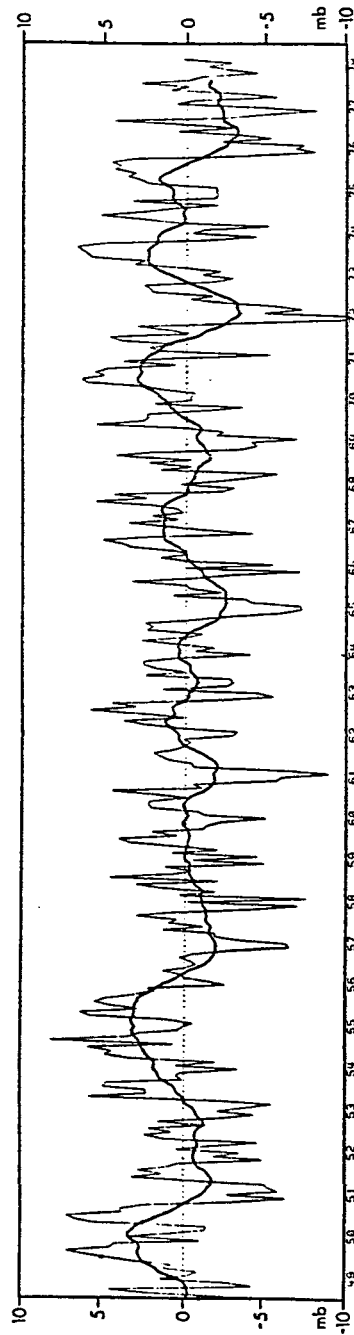


Fig.5: The difference of atmospheric pressure between Easter Island and Darwin, Australia from 1949 to 1978 relative to a mean of 10.3 millibars. The thin line gives monthly means, the heavy line gives the 12-month running mean (from Wyrski, 1982).

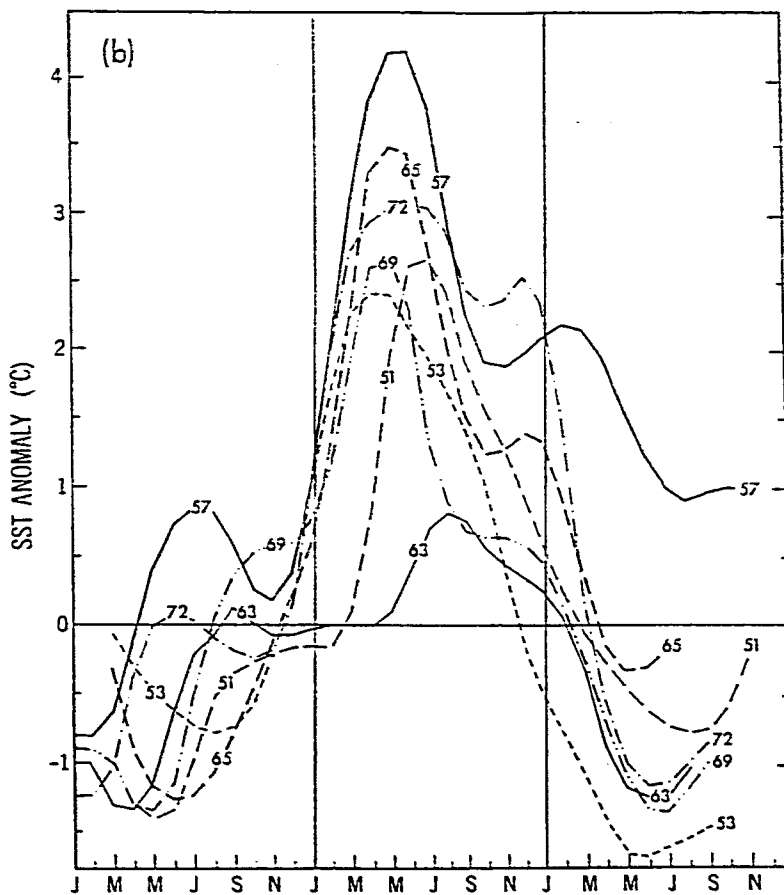


Fig.6: SST departures from the seasonal cycle, along the track 100 km off the coast of South America, during the El Nino in 1951, 1953, 1957, 1963, 1965, 1969 and 1972 (from Rasmusson and Carpenter, 1982).

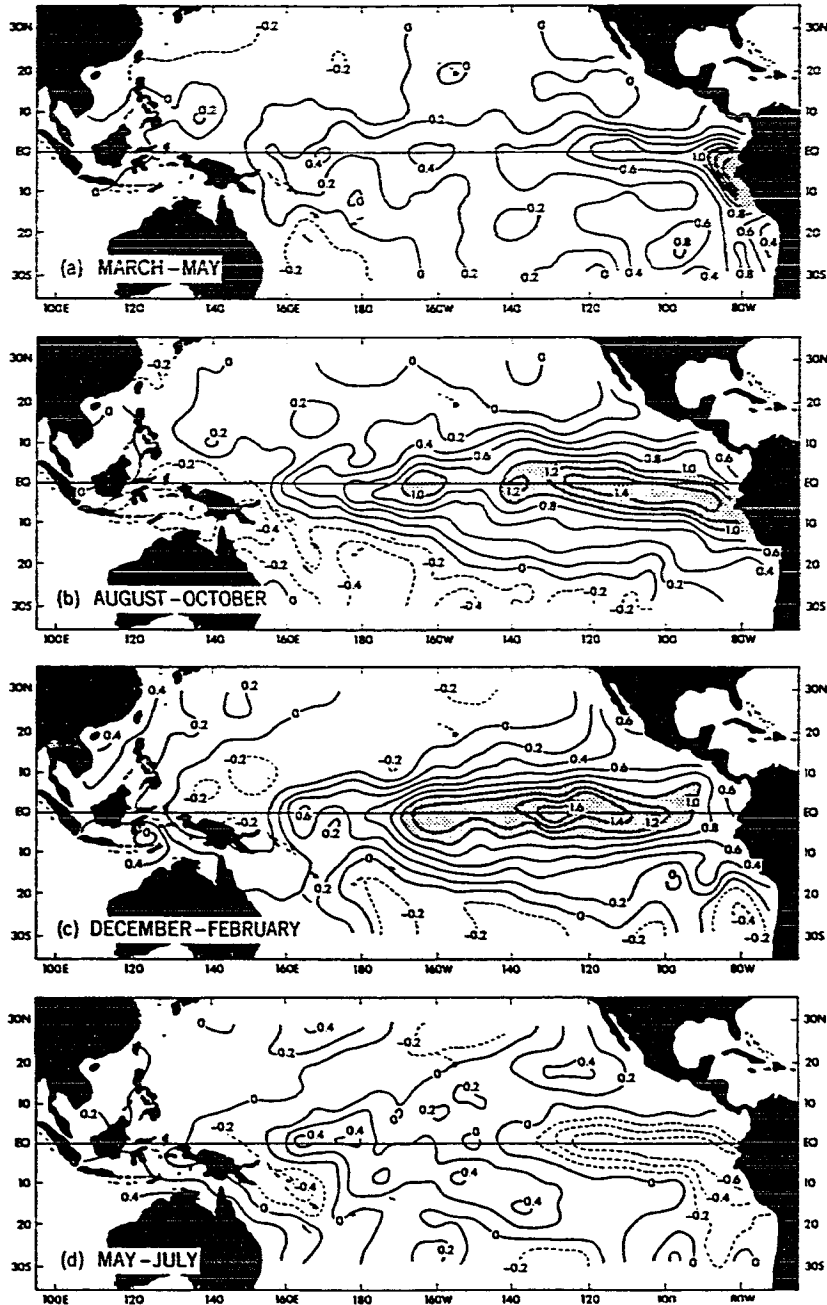


Fig.7: The evolution of the composite El Niño (from Rasmusson and Carpenter, 1982).

Although the six El Niño episodes between 1950 and 1973 evolved in a similar way, it is not necessary that all El Niño events behave like the composite El Niño. For example, the eastward movement of the convective zone in 1982/83 El Niño event was not preceded by warm and wet conditions in the eastern Pacific. Maybe due to its unusual evolution, it caught oceanographers by surprise when it occurred.

3. A simple coupled model with two equilibrium states

As we have discussed in the previous section, the interannual ENSO oscillations are attributable to the unstable air-sea interactions in the tropics. Most existing coupled models have been able to produce interannual variabilities which resemble ENSO in some aspects. However, many of these models were constructed in such a way that the model parameters and the climatological backgrounds were tuned to generate desired results. Few sensitivity tests have been conducted to compare the evolution of coupled oscillations when the climatological background has drifted from a normal state or when the various model parameters are changed. The strong dependence of model parameters was clearly shown by Neelin (1989) (hereafter N89). Fig.8 shows the different states of the ocean when different intensities of air-sea interaction are assumed. The same initial condition, which was created by a burst of a westerly wind in the western Pacific Ocean, was applied in all three tests in Fig.8. For a moderate strong coupling, the coupled model of N89 sustains an interannual oscillation which resembled ENSO in many aspects. A weak coupling parameter leads to a decaying of the initial disturbance. A secondary instability develops when a very strong air-sea interaction is assumed. The observation suggests that the real air-sea interaction in the equatorial Pacific is closer to that shown in Fig.8(b) in which the self-sustained oscillation is observed. The real processes of

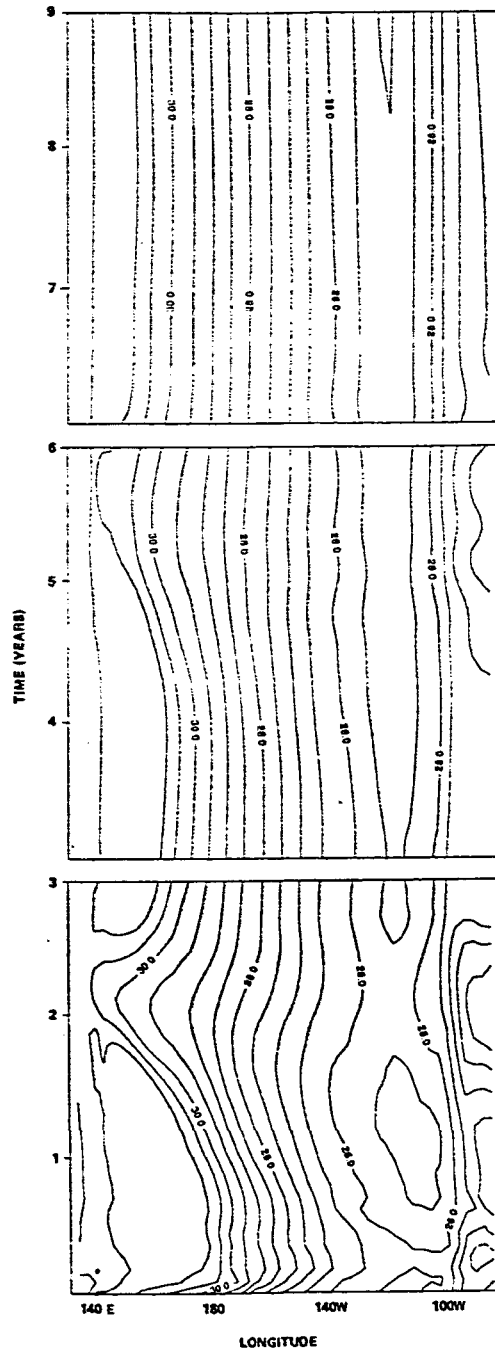


Fig.8(a): The fates of the coupled oscillations with weak coupling (from Neelin, 1989).

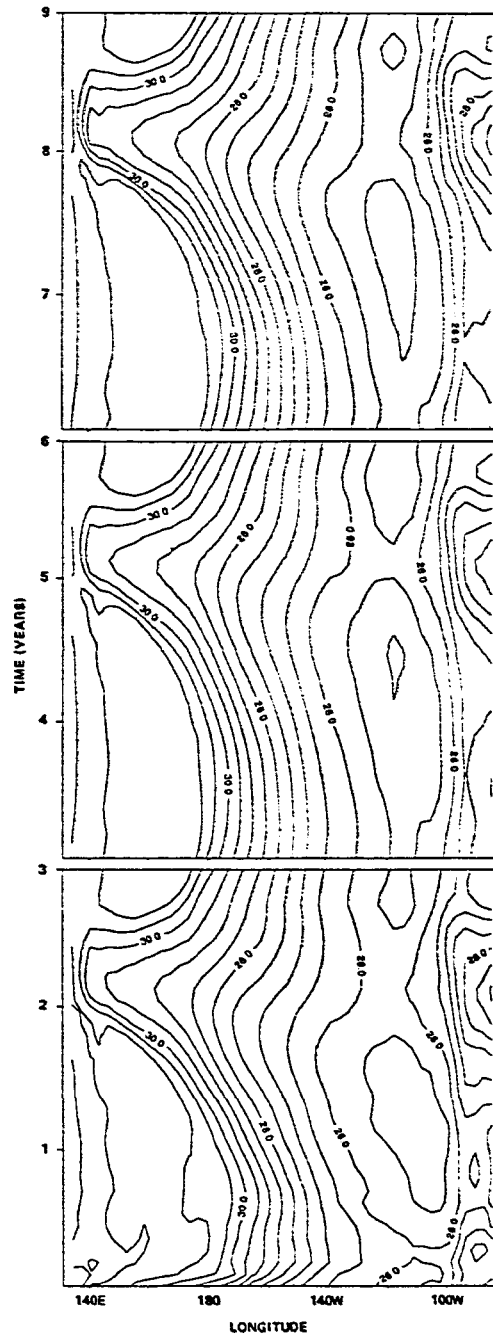


Fig.8(b): The fates of the coupled oscillations with moderate strong coupling (from Neelin, 1989).

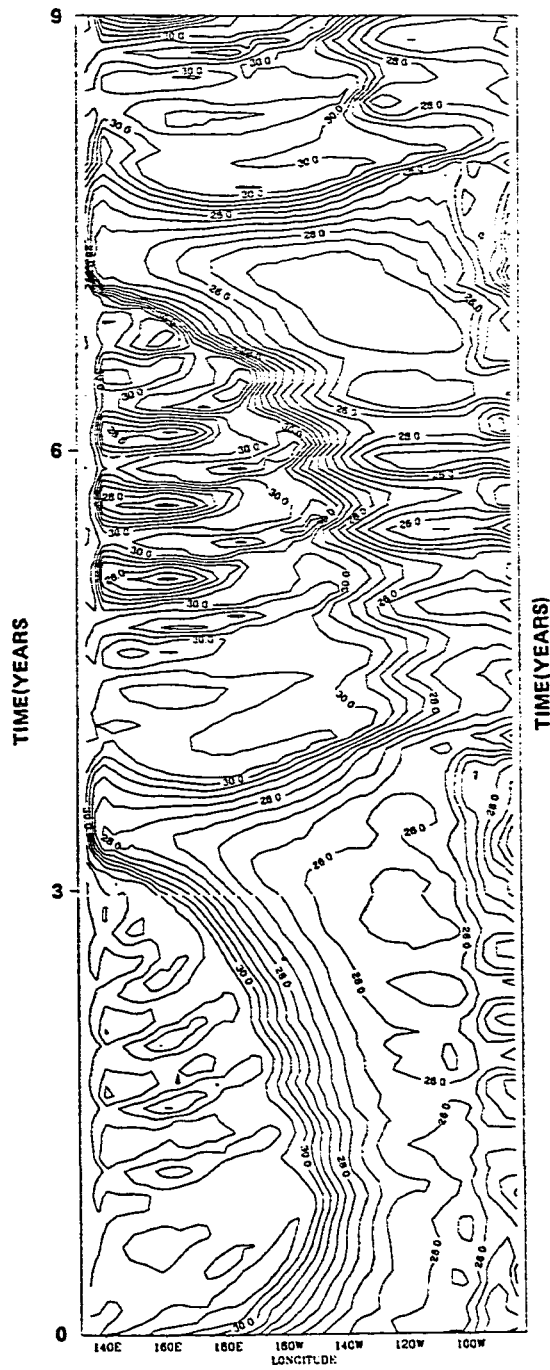


Fig.8(c): The fates of the coupled oscillations with strong coupling (from Neelin, 1989).

air-sea interaction are complicated and may be highly nonlinear. The coupling parameter strongly depends on the local environment, e.g., a warm SST background makes the lower atmospheric boundary layer less stable and a deep convection more likely to occur. Hence, a warm SST climatological background enhances the intensity of coupling while a cold SST state reduces the coupling. In fact, deep convective heating becomes especially intense when the SST approaches the critical value of about 28°C (Gadgil et al., 1984). The work of N89 implies that there are some favorable climatological conditions that make ENSO more likely to develop. In fact, N89 is one of the few works in this field to test the sensitivity of ENSO evolution to the shifts of the mean climatological backgrounds.

There are some other inhomogeneous climatological features that may be potentially important in determining the fate of ENSO. In this work, we will attempt to investigate how a zonally sloping thermocline affects the ENSO evolution. In order to tackle this problem, we must study the responses of each component of the coupling system to this prominent climatological feature. Then we will use a simple model to explain the dynamical consequences when a coupled system is considered.

3.1 The oceanic responses

The simplest interpretation of the existence of a zonally sloping thermocline is that the easterly trade wind stress is balanced by the zonal pressure gradient associated with the sea level slope. In a one-layer reduced-gravity model, the linear steady state equation is:

$$-f v = -g' H_x + \frac{\tau}{\rho_0 H_0} \quad (3.1)$$

where f is the Coriolis parameter, g' is the reduced gravity, τ is the zonal wind stress acting as a body force, ρ_0 is the water density, H is the layer thickness, and H_0 is the mean of H . At the equator, f vanishes and (3.1) yields:

$$H_x = \frac{\tau}{g'\rho_0 H_0} \quad (3.2)$$

For a given forcing, an integration of (3.2) gives a profile of H which, in many cases, can be viewed as the thermocline depth. Due to the forcing of the persistent easterly trade winds, an eastward shoaling thermocline is established and maintained. However, it must be pointed out that (3.2) is invalid away from the equator because the Coriolis force becomes important. A mean current must be included to balance the pressure gradient created by the thermocline slope. Fig.9 shows the mean profile of the observed main thermocline along the equator in the Pacific Ocean. It clearly shows the variations of the main thermocline depth along the equator. For example, the depth of the 20°C isotherm decreases from a depth of 200 meters at the western and central equatorial Pacific Ocean to less than 100 meters at the eastern equatorial Pacific Ocean. The strongest variation occurs at the central and eastern Pacific between 150°W to 110°W. The sloping thermocline is not unique in the Pacific Ocean. It also exists in the other two equatorial basins (Merle, 1980).

An eastward tilted thermocline has an important influence on both the dynamics and the thermodynamics of coupled atmosphere-ocean models. For example, the greater subsurface temperature gradient associated with the shallower main thermocline in the eastern equatorial Pacific Ocean is critical to localize the SST anomalies, while a deep

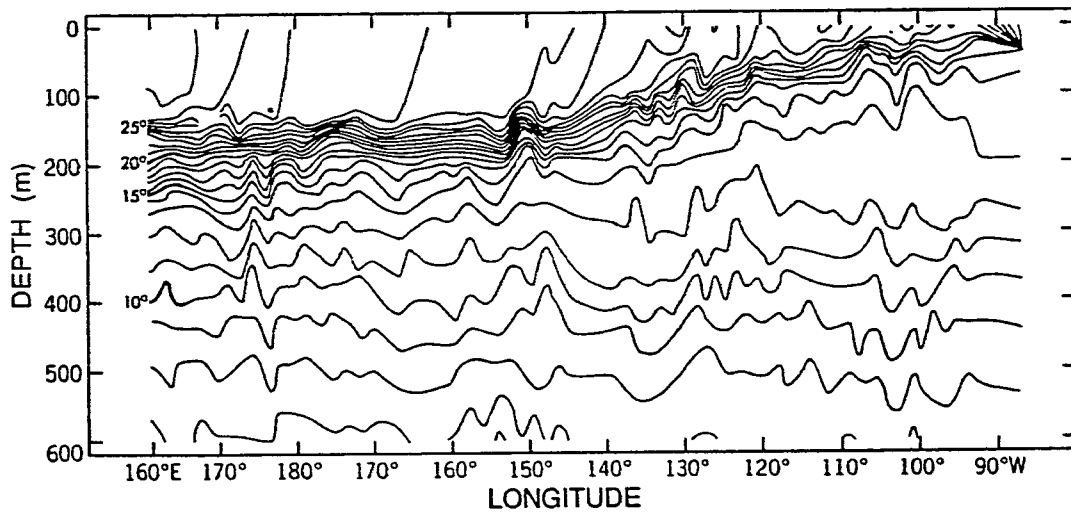


Fig.9: The mean thermocline depth along the equator of the Pacific Ocean as measured by Colin et al. (1971).

thermocline in the western equatorial Pacific Ocean enables long Rossby waves to propagate freely westward. These two factors, together with the reflection of long Rossby waves from the western boundary, constitute the so-called "delayed action oscillator".

The nondispersive character of the two most important classes of waves (i.e., Kelvin and long Rossby waves) and the relatively fast speeds of those waves make the remote forcing in the equatorial oceans very effective. For example, much of the variability observed in the eastern tropical oceans was originally generated in the western tropical oceans and transmitted to the east by Kelvin waves (O'Brien et al., 1978; Adamec and O'Brien, 1978; Yu et al., 1991). Some of the seasonal fluctuations in the western equatorial oceans, such as the semiannual reversal of the Somali Current in the Indian Ocean, are also attributable to the remotely generated long Rossby waves (Lighthill, 1969). Observations at the different positions along the equator (Knox and Halpern, 1982; Eriksen et al. 1983) have detected signals propagating eastward with a speed close to that of the first baroclinic mode Kelvin wave. From these observational evidences, one might think that the first vertical mode equatorially trapped Kelvin waves are dominant in the entire tropical Pacific Ocean. However, an analysis of bathythermograph records on the equator during 1971–1973 conducted by Gill (1982a) suggests a different conclusion. Gill's results show that the variation of isotherm displacement for the central equatorial Pacific Ocean is consistent with the first mode being dominant, but the variation found in the eastern Pacific is dominated by the second baroclinic mode. Some other works (e.g., Behringer, 1984) also indicate

that higher baroclinic modes are very important for describing variations in the equatorial eastern equatorial Pacific Ocean.

The question raised is, "does a first baroclinic mode Kelvin wave, generated in the western or central Pacific Ocean, undergo a significant change of the vertical structure when it encounters a changing density stratification during its propagation to the east?". More specifically, is the modal decomposition sufficiently effective to allow the higher vertical modes to become dominant before a first baroclinic mode Kelvin wave reaches the eastern Pacific Ocean? To answer this question, it is necessary to investigate the physical mechanism that determines the modal decomposition.

It was Lighthill (1969) who first solved analytically a linear, continuously stratified ocean model in the tropics. Lighthill's approach was to expand the vertical structure into a superposition of infinite modes which allowed him to separate the vertical dependence from the horizontal. Excellent reviews of this method are given in the papers of Moore and Philander (1978) and McCreary (1985). In a state of no motion the model ocean has stably stratified background $\rho_0(z)$ and an associated buoyancy frequency $N_0(z)$. Under suitable conditions it is possible to separate the vertical structure of the linear equations to an equation of the eigenfunctions ψ_n which satisfies

$$\frac{d}{dz} \left[\frac{c_n^2}{N_0^2} \frac{d\psi_n(z)}{dz} \right] + \psi_n(z) = 0 \quad (3.3)$$

The boundary conditions on (3.3) lead to

$$\frac{1}{c_n} \int_{-D}^0 \psi_n dz = 0 \quad (3.4)$$

where $z=0$, $-D$ represent the ocean surface and bottom respectively, and $\psi_n(z)$ is normalized so that $\psi_n(0)=1$.

The procedure that allows us to decompose the vertical and horizontal structures depends on the assumption that the mean background $\rho_0(z)$ does not depend on x , y and time. If the density $\rho_0(z)$ is x -dependent, the equation for eigenfunctions (3.3) does not hold uniformly across the basin. For example, if a Kelvin wave which has a vertical structure $\theta_0(z)$ propagates across a density discontinuity front where the stratification is different, it will induce a set of vertical modes $\eta_n(z)$ such that the sum of these new modes matches the structure of the incident Kelvin wave. Busalacchi and Cane (1988) have shown analytically that the modal energy exchanges occur when a wave travels across such a density jump. For a real ocean, the zonal variation of the density stratification is small over a wavelength for shorter waves. Thus these waves gradually adjust themselves to the new environment as they propagate along the equator. In this case, the WKBJ method is often useful to estimate the changes of wave amplitudes and wavelengths (e.g., Hughes, 1981; Yang and Yu, 1991). However, for such low-frequency and large scale variability associated with ENSO, the WKBJ method is no longer valid (Gill and King, 1985).

For very low frequency long waves, the shoaling region acts as a step as argued by Gill and King. Physically, it reduces to a problem of a long wave impinging on a step-like background change, similar to the

case studied by Busalacchi and Cane (1988). For example, when a first baroclinic mode long Kelvin wave propagates eastward and confronts such a change in the background, part of its energy penetrates through and continues its propagation to the east as a first mode Kelvin wave, while some of the incident Kelvin wave's energy is reflected back to the west as long Rossby waves. To dynamically match this discontinuity of the vertical background, higher baroclinic mode Kelvin and Rossby waves must be included. Fig.10 schematically shows the consequences of such a reflection process, which is consistent with the model results of Gill and King.

A natural question to be asked is, "how much of the incident Kelvin wave's energy will be reflected back as long Rossby waves?". Gill and King (1985) used a two-and-one-half-layer model with a sloping interface between the upper and lower layers to calculate the energy redistributions associated with an incident low frequency Kelvin wave. Their analytical results show that the energy loss due to the Rossby wave reflection is relatively small, i.e., the maximum proportion of incident energy that is reflected is about 25%. However the energy exchange between the first and second baroclinic modes is significant. They concluded that the structure of perturbations, such as El Niño, needs not be dominated by the first baroclinic mode even if it is generated by an incident Kelvin wave which has predominantly first mode structure in the central Pacific Ocean.

3.2 A simple coupled model

In this section we use a simple coupled model to elucidate some important physics associated with the positive and negative feedbacks

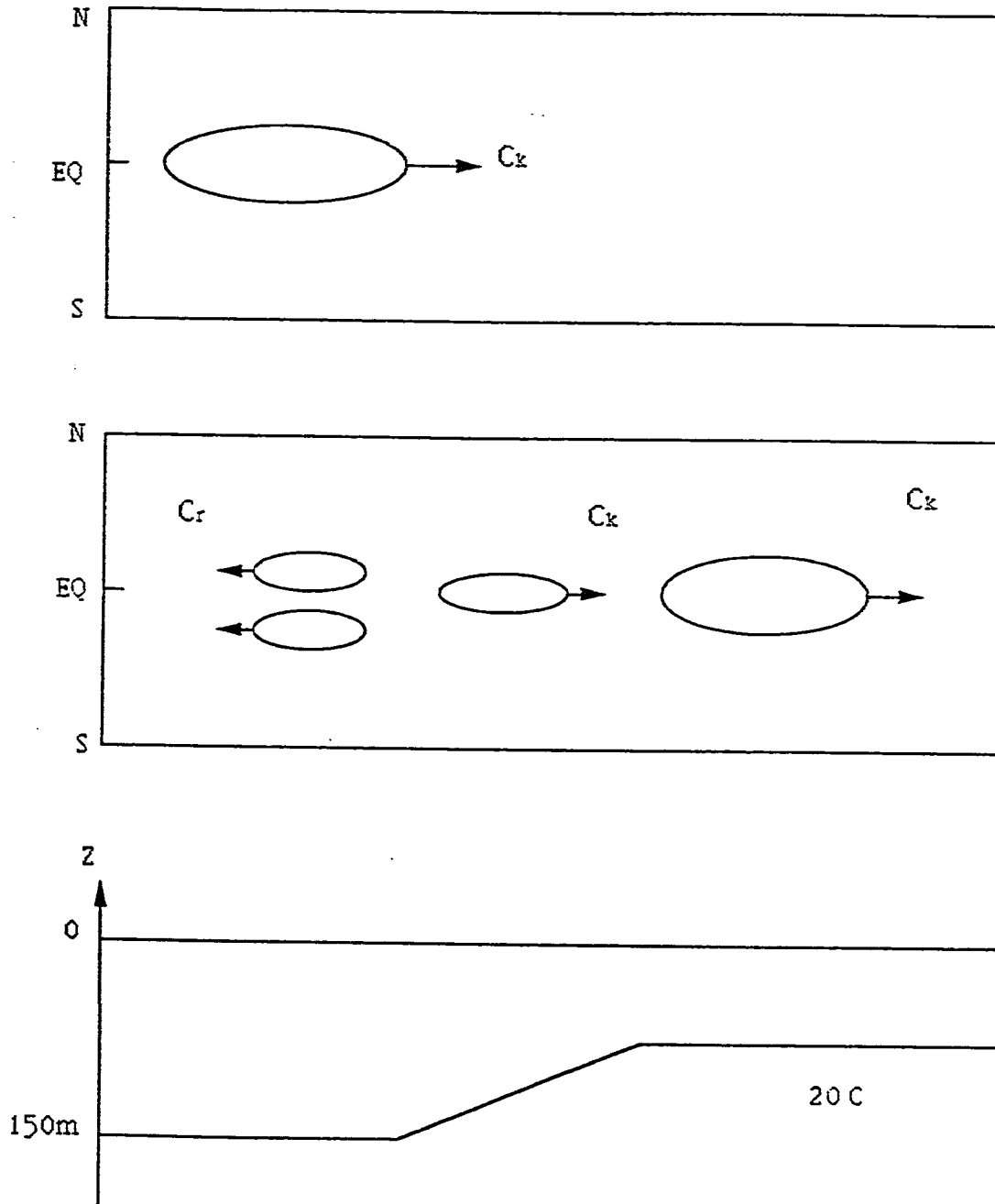


Fig.10: A schematic picture of wave reflection from a thermocline front.

between the ocean and the atmosphere. The atmosphere model is Gill's steady state model. The model of Hirst (1986) is used as our ocean model.

(A) The Oceanic Model

Hirst (1986) considered a surface mixed-layer governed by the full nonlinear equations. The base of the mixed layer is not a material surface. Waters are allowed to be entrained into the mixed layer from the lower layer or detrained from the mixed layer to the lower layer. The entrainment rate is estimated according to the Kraus-Turner formula calibrated by Garwood (1977). The SST is determined by the horizontal advection, the vertical entrainment, and the surface heat flux (longwave and shortwave radiations, sensible and latent heat fluxes etc.). The surface heat flux is calculated according to the formula of Paulson and Simpson (1977). The depth of the mixed layer is determined by the divergence/convergence of the mixed layer currents, and by the entrainment and detrainment. Hirst (1986) linearized the equations about a mean state of rest (the mean SST is not uniform horizontally) and simplified them to the following equations (see Appendix A for the derivations)

$$\frac{\partial u}{\partial t} - \beta y v + g \frac{\partial h}{\partial x} = -au + \tau^x / (\rho_0 H_0) \quad (3.5a)$$

$$\frac{\partial v}{\partial t} + \beta y u + g \frac{\partial h}{\partial y} = -av + \tau^y / (\rho_0 H_0) \quad (3.5b)$$

$$\frac{\partial h}{\partial t} + H_0 \left(\frac{\partial u}{\partial x} + \frac{\partial v}{\partial y} \right) = -bh \quad (3.5c)$$

$$T_t + uT_{0x} = \sigma h - \alpha T \quad (3.5d)$$

The mean currents are usually excluded in this type of model (e.g., Philander et al., 1984; Gill, 1985). The neglect of the mean current is not justified because the mean current plays one of the crucial roles in the total heat balance. The effects of the mean current in the momentum and continuity equations (3.5a-c) are measured by the ratio of mean current speed to the phase speed of waves (Philander, 1990). For free Kelvin waves or the lowest mode long Rossby waves, the phase speeds ($c \sim 2.4$ m/s for the first baroclinic mode Kelvin waves and $c \sim 0.8$ m/s for the lowest mode long Rossby waves) are usually greater than the current velocities. Hence the linearized advection terms are usually small. However, in the study of the low-frequency coupled modes, the mean current effects are not always negligible (see Appendix B). For the sake of simplicity, the effects of the mean currents are excluded in this work. The anomalous advection in the meridional direction is usually negligible (Appendix A). The values of the parameters b , σ and α are determined by the entrainment and the surface heat flux. In this model, a , b and α are all chosen to be $1/(100\text{days})$ which are the same as those estimated by Hirst (1986). The value of σ is determined by the mean mixed layer depth and the surface heat fluxes. In this model, σ is given as $5 \times 10^{-9} \text{ m}^{-1} \text{ }^\circ\text{K s}^{-1}$ compared with $3.5 \times 10^{-9} \text{ m}^{-1} \text{ }^\circ\text{K s}^{-1}$ in the central Pacific Ocean and $6.6 \times 10^{-9} \text{ m}^{-1} \text{ }^\circ\text{K s}^{-1}$ in the eastern Pacific Ocean as that estimated by Hirst (1986). H_0 is taken to be 200 meters. H_0 is much smaller than 200 meters in the central and eastern tropical Pacific Ocean. The value of the reduced gravity is chosen so that the Kelvin wave speed is 2 m/s. The meridionally averaged climatological mean SST (Shea et al., 1990) within 5° latitude in the Pacific Ocean is used to compute the mean zonal SST gradient T_{0x} . The wind stress forcing term

is calculated by $(\tau^x, \tau^y)/(\rho_0 H_0) = \gamma(U, V)$, where $\gamma = 8 \times 10^{-8} \text{ s}^{-1}$ is the same as that of Hirst (1986) which is obtained from the bulk aerodynamic formula. All the parameters are chosen so that the model sustains an oscillation with a reasonable amplitude and a period when a suitable initial condition is used to drive the coupled model. Xie et al. (1989) used a different version of the Kraus-Turner formula and derived a set of linear equations which are very similar to (3.5).

The equations (3.5a)-(3.5c) are solved numerically by using a staggered Arakawa C grid. A leapfrog scheme is used for the time integration, with a forward time difference scheme employed every 99th step to avoid the computational mode. The model resolutions are $\Delta x = 0.75^\circ$ and $\Delta y = 0.5^\circ$ and the time step is $\Delta t = 30$ minutes. The western and eastern boundaries are solid with the condition of no normal flow. The northern and southern boundaries are open and the method of Camerlengo and O'Brien (1980) is used to calculate the boundary values.

(B) The Atmospheric Model

The atmospheric fluctuations associated with the Southern Oscillation are closely correlated to the anomalous SST distributions associated with the El Niño events. Sophisticated atmospheric GCMs, heated by anomalous SST, have convincingly demonstrated that the Southern Oscillation is caused by the SST variations (e.g., Keshavamurty, 1982; Shukla and Wallace, 1983). However, an atmospheric GCM, like its counterpart in the ocean, is very expensive to run and sometimes difficult to diagnose. Simple atmospheric models (e.g., Gill, 1980) have been widely used in coupled atmosphere-ocean models. When forced with observed

oceanic boundary conditions, simple models (e.g., Zebiak, 1982; Zebiak, 1986) produce wind fields which resemble the observed winds remarkably well.

The most frequently used simple atmosphere model is Gill's steady state model (Gill, 1980). Modifications have been made in order to include more realistic features such as moisture convergence (e.g., Zebiak, 1986; Neelin, 1988). Gill's model is governed by the following equations (see Appendix C for derivation):

$$-\beta yV = -P_x - \gamma U \quad (3.6a)$$

$$\beta yU = -P_y - \gamma V \quad (3.6b)$$

$$C^2 (U_x + V_y) = -Q - \gamma P \quad (3.6c)$$

where Q is the forcing by the latent heat release associated with the anomalous SST, the last terms of (3.6a)–(3.6c) are Rayleigh friction and Newtonian cooling, and C is the internal gravity wave speed. In (3.6c) a positive (heating) Q acts like a sink of mass in the lower atmosphere, or like a source if it is cooled. This parameterization ensures that heating will induce a convergence in the boundary layer. The underlying idea is that a warm SST anomaly locally enhances evaporations. The positive anomalous evaporation increases moisture in boundary layer. The associated enhancement of conditional instability gives rise to the increased cumulus convection and the atmosphere heating.

Several assumptions are used in this model. First, it assumes that the atmospheric adjustment time scale is much shorter than that of the ocean, hence the atmosphere is always in equilibrium with the evolving

ocean. Second, the atmosphere is only forced by the latent heat release associated with SST.

The value of the internal gravity wave speed C used by other studies ranges from 15 m/s (Lau, 1981) to 63 m/s Philander et al. (1984). In this study, we choose $C = 60$ m/s which is the same as that used in Zebiak and Cane (1987). The damping time scale is chosen as 5 days, i.e., $\gamma = 1/(5\text{days})$, which is the same as in Philander et al. (1984). The heating is directly related to the SST anomalies by

$$Q = K_q T \quad (3.7)$$

where $K_q = 5 \times 10^{-3} \text{ m}^2 \text{ s}^{-3} \text{ }^\circ\text{K}^{-1}$ is used, which is estimated by using the Clausius-Clapeyron equation (see equation (4.11) in the next section). K_q varies from $3 \times 10^{-3} \text{ m}^2 \text{ s}^{-3} \text{ }^\circ\text{K}^{-1}$ at 26.5°C to $11 \times 10^{-3} \text{ m}^2 \text{ s}^{-3} \text{ }^\circ\text{K}^{-1}$ at 29°C (Hirst, 1986). In this model the atmosphere and the ocean communicate to each other once every day, i.e., the wind fields are updated once a day, due to the fact that the motion in the ocean is slow.

Equations (3.6a) - (3.6c) are solved numerically as described by Zebiak (1982). The fast Fourier transform (FFT) is used in x , and then the system is reduced to a single ordinary differential equation in y (with the transform of V as the dependent variable). This ODE equation is solved by a finite-difference method with $V=0$ at both the northern and the southern boundaries. The boundary condition in x direction is cyclic with a global extent (the zonal length of the atmosphere model is 360° in longitude). Once the solution of V is obtained, U and P are readily calculated. A more detailed description of the numerical scheme is given by Zebiak (1982).

(C) Coupled modelling

With the coupled model described above, two experiments are conducted to compare the model responses to different initial conditions. In the first experiment, the initial condition is: $(u,v,h) = 0$, and a patch of positive SST anomaly is given, as shown in Fig.11(a), to alter the atmosphere and therefore drive the whole coupled system. Fig.11(a) shows low level winds converging to the region of heating with westerly winds considerably stronger than easterly winds. In this experiment the initial condition is slowly amplified due to the positive feedback from the atmosphere, and the patterns of SST anomalies move slowly to the east. The period of oscillation is about 3 years. Fig.11(b) shows the model condition at the 1450th day when the temperature at the eastern Pacific Ocean is higher and the temperature at the western Pacific is lower. This is the typical year of the warm phase of ENSO. The wind anomalies are dominated by westerly winds in the central and eastern equatorial Pacific Ocean, which realistically resemble the meteorological conditions when a warm event occurs. Roughly one and a half years later at the 1950th day, an opposite condition is observed when cooler water appears off the eastern boundary (Fig.11(c)). At this time the low level winds are dominated by easterly winds in the central and eastern equatorial Ocean.

Fig.12 shows the time-longitude plot of SST anomalies. The sloping contours clearly show the SST traveling slowly to the east similar to the results of Philander et al. (1984) and Wakata and Yamagata (1989).

In the second experiment we run the model with the same parameterization as the first experiment, but a different initial condition is used. Again, we assume that there is no motion in the ocean initially,

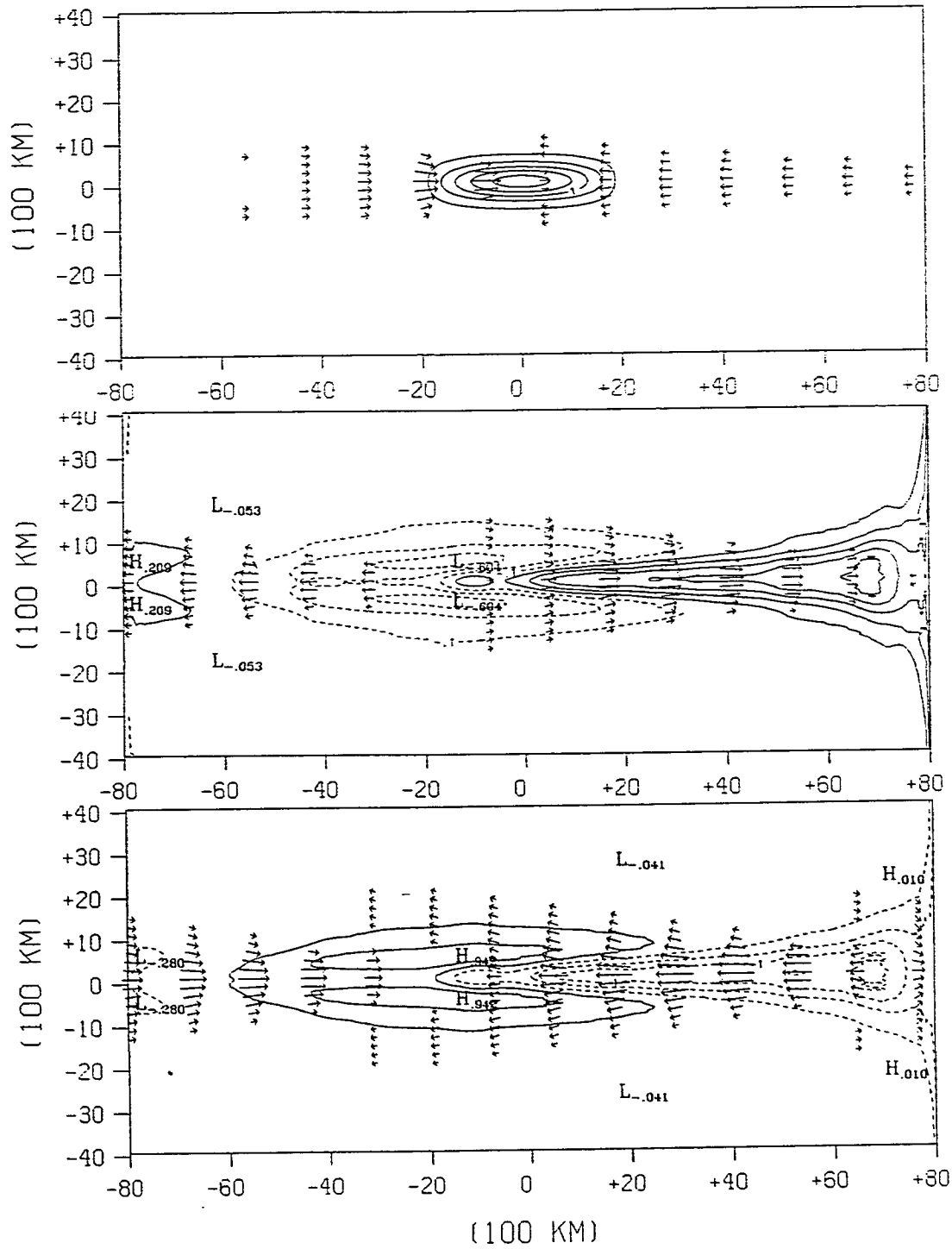


Fig.11: (a) The initial anomalous SST and its induced winds of the first run; (b) the anomalous SST and winds at 1450th day; (c) the anomalous SST and winds at 1950th day.

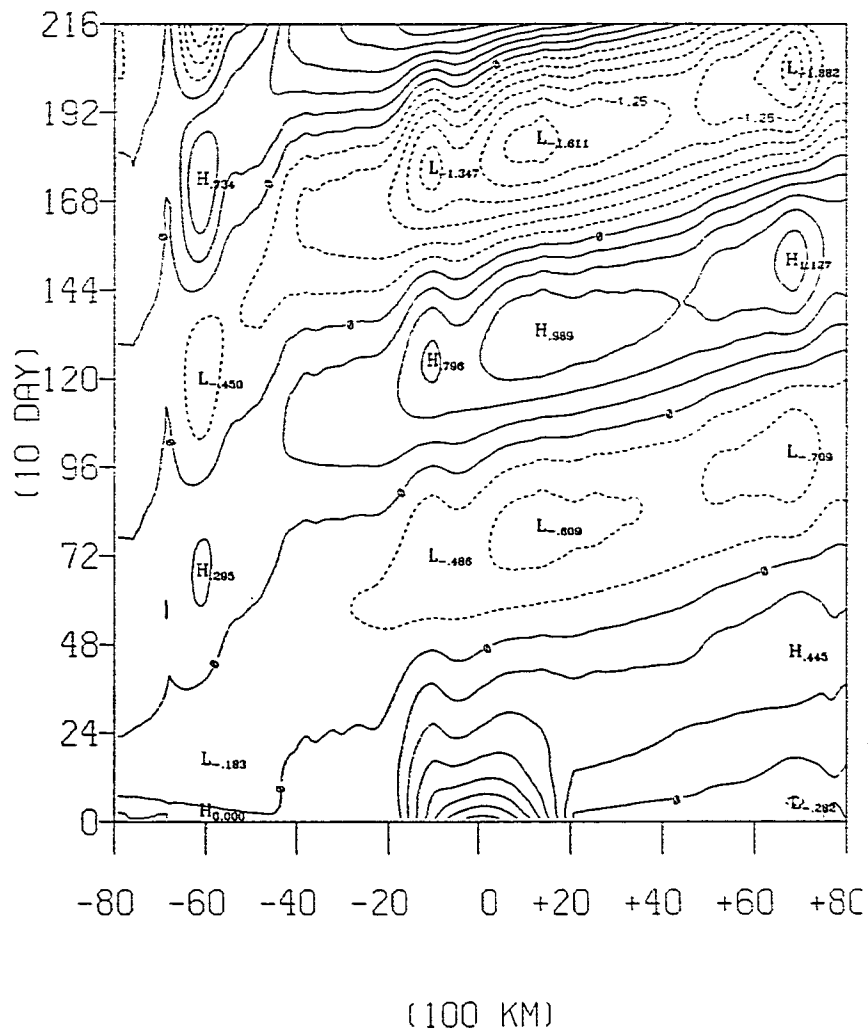


Fig.12: The lonitude-time plot of the SST anomalies along the equator for the first run.

i.e., $(u,v,h)=0$. The initial distribution of the SST anomaly is shown in Fig.13, i.e., two patches of positive SST anomalies are located in the equator. The total heat content of this initial SST field is the same as the first experiment. Fig.13 also shows the response of the atmosphere to this SST heating. Both positive SST patches induce low level convergent winds. It is interesting to note that the wind fields between these two SST patches are very weak, because the winds induced by the two SST patches have opposite signs in this region. However, the wind anomaly, especially the westerly wind, is critical to amplify a downwelling warm event. The weakening of the winds reduces the coupling intensity and the necessary atmospheric feedback. Fig.14 shows the evolution of SST anomalies in this run. The initial disturbances slowly decay eastward, and the system finally comes back to the equilibrium state of rest.

These two experiments demonstrate that there are two equilibrium states in this simple coupled system, namely the equilibrium state of rest and the equilibrium state of oscillation. In the first experiment, the initial condition is able to alter the coupled system so that the positive feedback continues to maintain regular oscillations. In the second experiment, the intensity of coupling is significantly weakened due to the damping effects by the winds induced by two SST anomaly patches. Therefore, an initial disturbance is unable to lead to a final oscillatory state.

Two competing factors are critical in determining the resulting state. One is the positive feedback that tends to amplify the initial disturbance; the other factor involves damping processes, like Newtonian cooling, which attempt to bring the initial disturbance back to the state of rest. The magnitudes of both forces increase with the amplitude of

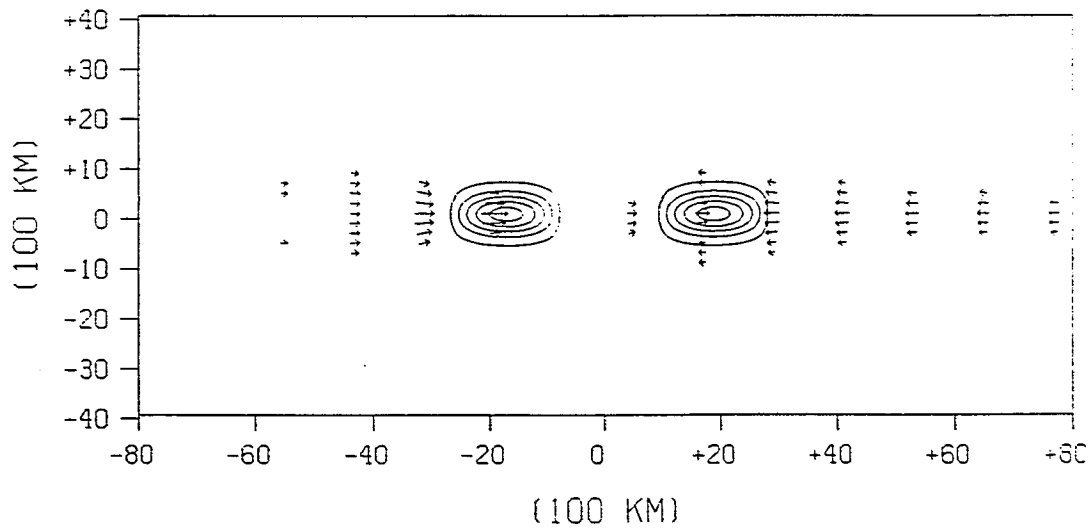


Fig.13: The initial SST and its induced winds of the second run.

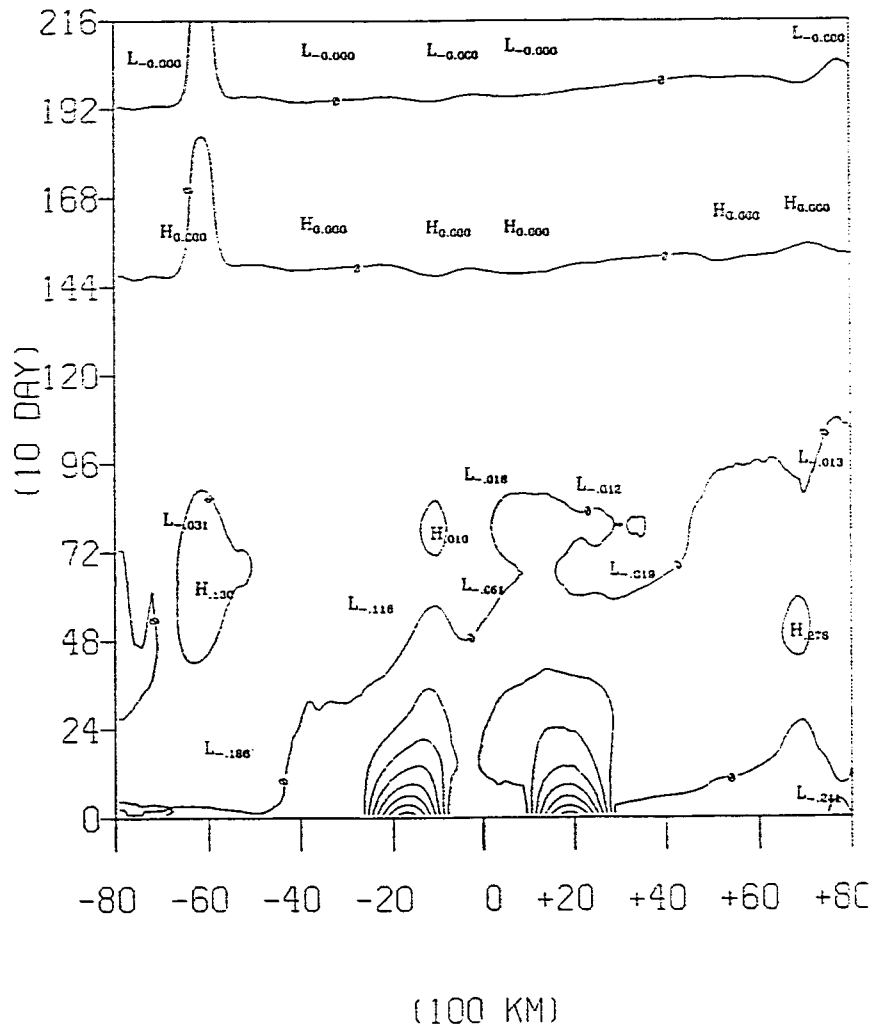


Fig.14: The longitude-time plot of the SST anomalies along the equator for the second run.

disturbances. If there were no damping in the coupled system, then any disturbance would lead to an unstable state. In the first experiment the system is altered in such a way that the atmospheric response immediately drives the ocean to produce greater SST anomalies (depressing the thermocline by the westerly winds) and enhances the coupling. Therefore the intensity of coupling (positive feedback) prevails over the damping effects, and the initial SST anomaly is able to reach the oscillatory state. In the second experiment, the wind fields induced by the initial oceanic heating attempt to damp the initial SST fields. The Newtonian cooling process becomes dominant before the coupled system adjusts itself to a more favorable condition. Hence the initial condition leads to a final equilibrium state of rest.

Now let's look at the implications of these two experiments when a nonuniform climatological background is considered. As we discussed earlier, a single baroclinic mode Kelvin wave is unable to preserve its identity when it confronts a sloping thermocline jump at the central Pacific Ocean. For example, if an initial oceanic disturbance were created in the western or central equatorial Pacific Ocean by some unusual meteorological condition, such as relaxation of easterly trade winds, this initial disturbance would propagate eastward as a Kelvin mode, similar to the mode in Philander et al. (1984). After this Kelvin mode propagates through the shoaling thermocline region, the original wave energy is redistributed as westward Rossby waves, and the first and the second baroclinic mode Kelvin waves (and higher modes if a continuously stratified ocean is considered). This condition is very similar to the initial condition used in the second experiment. Therefore the question becomes

"can a thermocline front terminate an initial disturbance through the atmospheric feedbacks?".

In the next section, we will use an intermediate coupled model which includes many realistic climatological features. The model will be used to investigate the sensitivity of the model to the drift of mean climatological conditions. The simple model discussed in this section is very useful to help us to diagnose the results of the more complicated model.

4. An intermediate coupled model with a sloping thermocline

In the previous two sections we have briefly discussed the physics that govern the several types of coupled instabilities. The dynamical framework of the proposed research is also outlined in Section 3. A simple idealized coupled model is used to elucidate the positive feedbacks and the negative feedbacks existing in the coupled system. However, as we have already pointed out in Section 1, the ocean needs at least two internal modes when a nonuniform background is considered. A condition, which is similar to the initial SST field of experiment#2 in Section 3, is likely to be created by Rossby wave reflections and vertical modal decompositions. In order to simplify the problem, but without losing the basic physics, we will use the simplest possible ocean model and couple it to Gill's steady state atmosphere model whose state is determined diagnostically. Hence we only retain two baroclinic modes and assume all the modal energy exchanges in the vertical direction occur only between the first and second baroclinic modes. The thermodynamics are also included in a surface mixed layer. The formulation of the model is given in the following section.

4.1 The Model Formulation

(A) The Ocean Model

The ocean model is a $2\frac{1}{2}$ reduced-gravity model. By assuming that

the deep layer is at rest, we actually filter out the fast travelling barotropic modes. The mean depth of the interface of the two upper layers is not uniform in the zonal direction but shoaling eastward as the 20°C isotherm in the equatorial Pacific Ocean. The interface between the second active layer and the motionless deep ocean, which represents the 10°C isotherm in the equatorial Pacific Ocean, is flat. This assumption is justified because the 10°C isotherm is fairly flat in the real ocean (Fig.9). We assume that the water densities remain constant in both layers. This assumption is reasonable since it introduces rather small errors due to the strong mean vertical temperature gradients in the upper equatorial oceans (see Appendix D). The effects of the mean flow are neglected though the magnitude of the linearized advection terms is not always small as Appendix B shows. The thermocline slope needs a mean current off the equator to balance the pressure gradient. Hence the exclusion of the mean currents can not be rigorously justified. Since the purpose of this work is not to simulate the ENSO events with all realistic features, we exclude the mean-flow effects in our model for the sake of simplicity.

The equations that govern the two layers are:

$$u_{1t} - \beta y v_1 = -p_{1x} - \gamma u_1 + \tau^x / (H\rho_1) \quad (4.1a)$$

$$v_{1t} + \beta y u_1 = -p_{1y} - \gamma v_1 + \tau^y / (H\rho_1) \quad (4.1b)$$

$$h_{1t} + (H u_1)_x + (H v_1)_y = 0 \quad (4.1c)$$

$$u_{2t} - \beta y v_2 = -p_{2x} - \gamma u_2 \quad (4.2a)$$

$$v_{2t} + \beta y u_2 = -p_{2y} - \gamma v_2 \quad (4.2b)$$

$$h_{2t} + (H_2 u_2)_x + (H_2 v_2)_y = 0 \quad (4.2c)$$

where (u_1, v_1) and (u_2, v_2) are the velocities in the upper and lower layers, $-\gamma(u_1, v_1)$ and $-\gamma(u_2, v_2)$ are Rayleigh frictions, h_1 and h_2 are the deviations of the layer thicknesses in the upper and lower layers, $H = H_1 + H_m$ is the mean upper layer thickness (including the mixed layer), and H_2 is the mean layer thickness of the lower active layer. The wind stress is estimated by the aerodynamic bulk formula

$$(\tau^x, \tau^y) = \rho_a C_D |U| (U, V)$$

where ρ_a is the density of air, C_D is the wind stress drag coefficient. In this work, $\rho_a C_D = 3.2 \times 10^{-3} \text{ kg m}^{-3}$ is used (same as Zebiak, 1984), \mathbf{U} is the wind speed vector, and (U, V) are wind speed components in x and y directions respectively.

The pressure gradients in the two upper layers are given by

$$\nabla p_1 = \left(\frac{\rho_3 - \rho_1}{\rho_3}\right) g \nabla h_1 + \left(\frac{\rho_3 - \rho_2}{\rho_3}\right) g \nabla h_2$$

$$\nabla p_2 = \left(\frac{\rho_3 - \rho_2}{\rho_3}\right) g \nabla h_1 + \left(\frac{\rho_3 - \rho_2}{\rho_3}\right) g \nabla h_2$$

where ρ_1, ρ_2 and ρ_3 are the water densities in the upper, lower and deep layers respectively, g is the gravitational acceleration rate. The density differences between layers are chosen as $(\rho_2 - \rho_1) = \alpha \rho_0 \Delta T_1$ and $(\rho_3 - \rho_2) = \alpha \rho_0 \Delta T_2$, where $\alpha = 0.00025 \text{ } ^\circ\text{C}^{-1}$ is the thermal expansion coefficient, $\Delta T_1 = \Delta T_2 = 10^\circ\text{C}$ are the temperature differences between the layers, and $\rho_0 = 1020 \text{ kg m}^{-3}$ is the mean water density.

As argued by Zebiak (1984), a reduced-gravity layer model should not be expected to give a good estimate for the three dimensional current fields near the ocean surface. The assumption that the entire upper layer is homogeneous is likely to be violated because we expect there to be a turbulent well-mixed layer at the surface. To overcome this deficiency, the upper layer is divided into two parts. The surface part is a linear, homogeneous, frictional mixed layer with a constant depth. The formulation of this constant depth mixed layer is the same as Zebiak (1984). The adoption of this mixed layer is motivated by the following considerations (Zebiak, 1984). The effective friction of the mixed layer is assumed to be much greater than that below. Hence, nearly all of the frictionally induced (or Ekman) transport in the upper ocean should occur in this region alone. The thermodynamics are only included in the mixed layer. Fig.15 schematically shows the model formulation.

Following Zebiak (1984) and Zebiak and Cane (1987), the equations for a homogeneous mixed layer are

$$r_s u_s - \beta y v_s = \tau^x / (\rho_0 H_m) \quad (4.3a)$$

$$r_s v_s + \beta y u_s = \tau^y / (\rho_0 H_m) \quad (4.3b)$$

where (u_s, v_s) are the frictional velocity components, τ is the wind stress, H_m is the depth of the mixed layer and r_s is the friction coefficient (interfacial friction, entrainment friction, etc.). The wind stress is distributed uniformly in the mixed layer as a body force.

With the adoption of the mixed layer, (4.1a,b) can be interpreted as the equations of the averaged velocities of the mixed layer and the

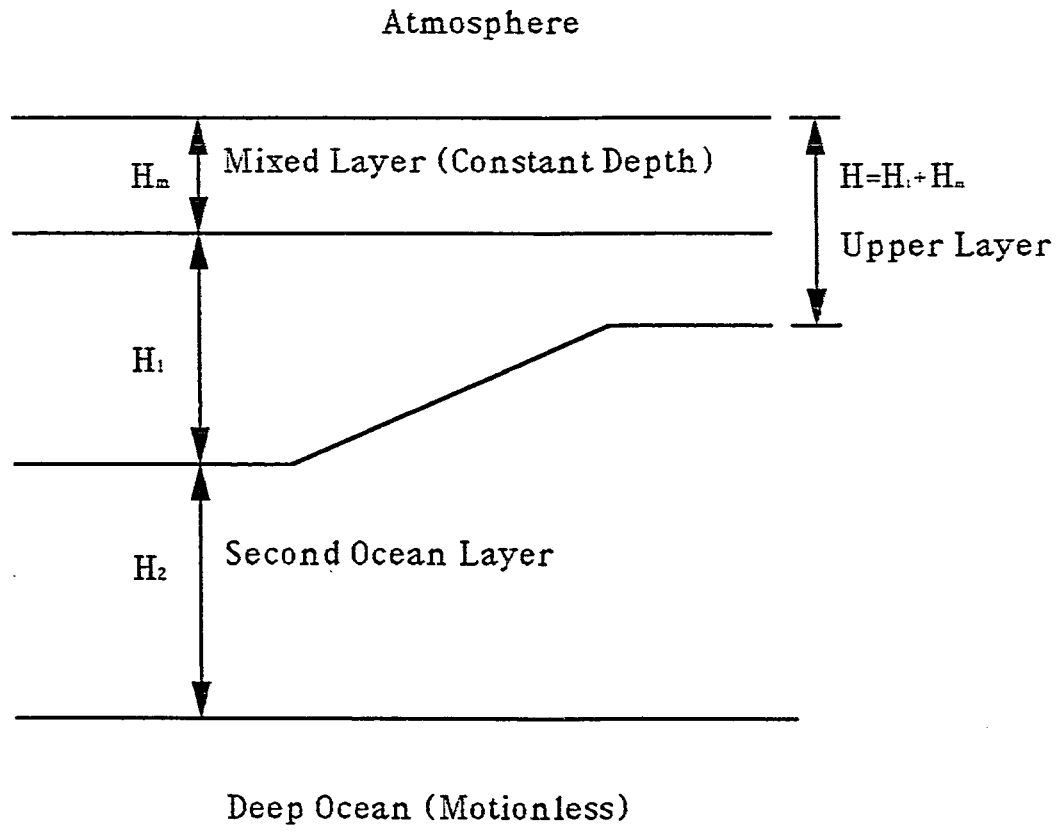


Fig.15: The schematic model formulation.

remainder of the upper layer. Hence, the solution of (4.1) contains the frictional (Ekman) component that should be concentrated in the mixed layer, and the component of the flow which is related to the pressure gradient, i.e.,

$$(u_1, v_1) = (u_E, v_E) + (u_p, v_p) \quad (4.4a)$$

where (u_E, v_E) and (u_p, v_p) are the components related to the Ekman transport in the mixed layer and the pressure gradients in the entire upper layer. Since the total Ekman transport obtained from (4.1) is the same as that given by (4.3), (u_E, v_E) is related to (u_s, v_s) by

$$(u_E, v_E) = H_m(u_s, v_s)/H \quad (4.4b)$$

The total mixed-layer velocity (u_m, v_m) contains the frictional part (u_s, v_s) and the part driven by the pressure gradient (u_p, v_p) . By using (4.4a,b), (u_m, v_m) can be expressed as

$$u_m = u_s + u_1 - u_s H_m/H \quad (4.5a)$$

$$v_m = v_s + v_1 - v_s H_m/H \quad (4.5b)$$

More detailed discussions about this mixed layer formulation can be found in Zebiak (1984).

Since the mixed layer depth H_m is taken as a constant, the vertical entrainment rate is determined by the divergence of the mixed-layer transports,

$$w_e = \frac{\partial}{\partial x}(H_m u_m) + \frac{\partial}{\partial y}(H_m v_m) \quad (4.6)$$

For example an easterly wind produces a Ekman drift poleward, and the divergence along the equator is compensated by the upward entrainment of subsurface water.

In this model, we choose $H_m = 50$ meters, and $H_0 = H_m + H_1 + H_2 = 350$ meters. The profile of $H(x) = H_1(x) + H_m$ varies for different simulations and will be discussed separately. The coefficient of the Rayleigh friction γ ranges from $1/(100 \text{ days})$ in Hirst (1986) to $1/(2.5 \text{ years})$ in Battisti (1988). In this work, we choose γ to be $1/(250 \text{ days})$. The effective damping time scale of the mixed layer is chosen to be 2 days, i.e., $r_s = 1/(2 \text{ days})$ which is the same as that used in the model of Zebiak (1984) and Zebiak and Cane (1987). Zebiak (1984) argued that the choice of $r_s = 1/(2 \text{ days})$ is to give model upwelling velocities of the order of 10^{-3} cm/s , comparable to what can be inferred from observations.

Because the SST plays a crucial role in determining the atmospheric feedback, its treatment deserves special attentions. The SST evolution is determined by horizontal advections, vertical entrainment and surface fluxes. The SST equation used by Zebiak (1984) and Zebiak and Cane (1987) is

$$T_t = -\mathbf{u}_m \nabla(T_0 + T) - \mathbf{u}_0 \nabla T - \\ - \{M(W_0 + w) - M(W_0)\} \frac{T_0 - T_{\text{sub}}}{H_m} - \mu M(W_0 + w) \frac{T - T_e}{H_m} - \alpha T \quad (4.7)$$

where $M(x) = \begin{cases} x & \text{if } x > 0 \\ 0 & \text{if } x < 0 \end{cases}$ is the Heaviside step function, T_{sub} is the mean subsurface water temperature, T_e is the anomalous subsurface water temperature, μ is the efficiency coefficient ($\mu=0.75$ in Zebiak and Cane's

model), and $-\alpha T$ is the Newtonian cooling which represents all one-dimensional vertical processes (mixing, surface sensible and latent heat fluxes, long and short wave radiations etc.). Because the entrainment (upward) brings the colder subsurface water to the surface, it cools the surface mixed layer. The detrainment, however, warms up the subsurface water but does not change the temperature in the surface directly. Hence, the vertical advectons in (4.7) are turned on only when entrainments occur. There are four distinct cases to consider (Zebiak, 1984). If the mean field is downwelling and the total field is also downwelling, there is no effect on the surface temperature anomaly. If the mean field is downwelling but the total field is upwelling, then the SST anomaly is affected by the total upwelling. If the mean field is upwelling but the total field is downwelling, then the SST anomaly is affected, but only in proportion to the strength of the mean upwelling. If the mean field is upwelling and the total field is also upwelling, then the SST anomaly is affected according to the sign and magnitude of the anomalous vertical velocity. Anomalous upwelling produces anomalous cooling and anomalous downwelling produces anomalous warming.

The cooling mechanism in (4.7) is clear because the upward entrainment brings cooler subsurface water to the mixed layer. The warming mechanism is not very obvious. The existence of a mean upwelling field (i.e., $W_0 > 0$) is essential for the anomalous warming. For example, an anomalous downwelling reduces the climatological cooling and therefore produces anomalous warming, i.e., $-\{M(W_0+w) - M(W_0)\} (T_0 - T_{sub})/H_m > 0$ if $w < 0$. Positive SST anomaly can also be produced by total upwelling of anomalous temperature $-M(W_0+w) (T - T_e)/H_m$. For example,

a depression of the thermocline induces a higher subsurface water temperature. When the warm subsurface water is entrained into the upper layer, it produces a positive SST anomaly.

The SST equation (4.7) is used in our calculations except that the mean current advection $\mathbf{u}_0 \nabla T$ is neglected. This advection term is small compare to anomalous current advection term $\mathbf{u} \nabla T_0$ (Appendix E). $\mathbf{u}_0 \nabla T$ is excluded in many previous studies (e.g., Hirst, 1986; Gill, 1985; Neelin, 1991). Hirst (1991) diagnosed all terms in (4.7) and concluded that $\mathbf{u}_0 T_x$ was small. In fact, Battisti (1988) did a sensitivity test by dropping $\mathbf{u}_0 T_x$ from (4.7) and found that the model oscillation was not significantly altered. Neelin (1991) did a scaling analysis and found that $\mathbf{u}_0 T_x$ was considerably smaller than $\mathbf{u} T_{0x}$ (a factor of 3 to 5). The magnitude of the meridional advection $\mathbf{v}_0 T_y$ is not always small especially near the edge of the SST anomalies in the eastern Pacific. Strictly, it can not be neglected especially near the eastern boundary. However, its main role is to spread the SST anomalies meridionally and is not crucial in producing SST anomalies (Hirst, 1991).

In (4.7) ∇T_0 is estimated by using the annual mean SST of Shea et al. (1990) and $\alpha = 1/(200 \text{ days})$ is used as the coefficient of Newtonian cooling. The values of Newtonian cooling and Rayleigh frictions are chosen that the model produces an oscillation with the reasonable amplitudes when a realistic thermocline profile is used. A uniform value of the mean equatorial upwelling rate $W_0 = 1.15 \times 10^{-5} \text{ m/s}$ or 1 m/day, as estimated by Wyrtki (1981), is used in this model. It must be pointed out that the value of the mean upwelling rate varies considerably in the zonal direction. Bryden and Brady (1985) used a diagnostic model of the three-

dimensional circulation in the upper equatorial Pacific Ocean to study the mass budgets. By integrating the horizontal divergence vertically, they estimated the mean upwelling rate between 110°W and 150°W was about 2×10^{-5} m/s at 50 meters below the sea surface. The maximum upwelling rate in this region occurs at a depth of 65 meters with a value of 3×10^{-5} m/s. A greater mean upwelling field in the equatorial oceans will result in a greater correlation between the sea level anomalies (or the thermocline depth anomalies) and the SST anomalies, as we will discuss later.

Zebiak and Cane (1987) parameterized the anomalous temperature T_e as:

$$T_e = \theta(h) [\tanh(\lambda((H+1.5|h|))) - \tanh(\lambda H)] \quad (4.9)$$

where $\theta = 28$ °K and $\lambda^{-1} = 80$ m for $h > 0$, and $\theta = -40$ °K and $\lambda^{-1} = 80$ for $h < 0$. In this model, we use a different formula derived from the observations by Seager et al. (1988). Seager et al. (1988) used the climatological data of Levitus (1982) and a cubic spline interpolation to derive a relationship between the subsurface temperature at 50 meters below the sea surface and the depth of the 20°C isotherm. This formula $T_s(H)$ is plotted and shown in Fig.16. The anomalous temperature is estimated as

$$T_e(x,y,t) = T_s[h(x,y,t)+H(x)] - T_s[H(x)] \quad (4.10)$$

Fig.16 clearly shows that the subsurface temperature increases rapidly as the main thermocline deepens. For the same magnitude of vertical thermocline displacement, it induces much greater subsurface temperature variation in an area with shallower thermocline than it does in the deep thermocline area.

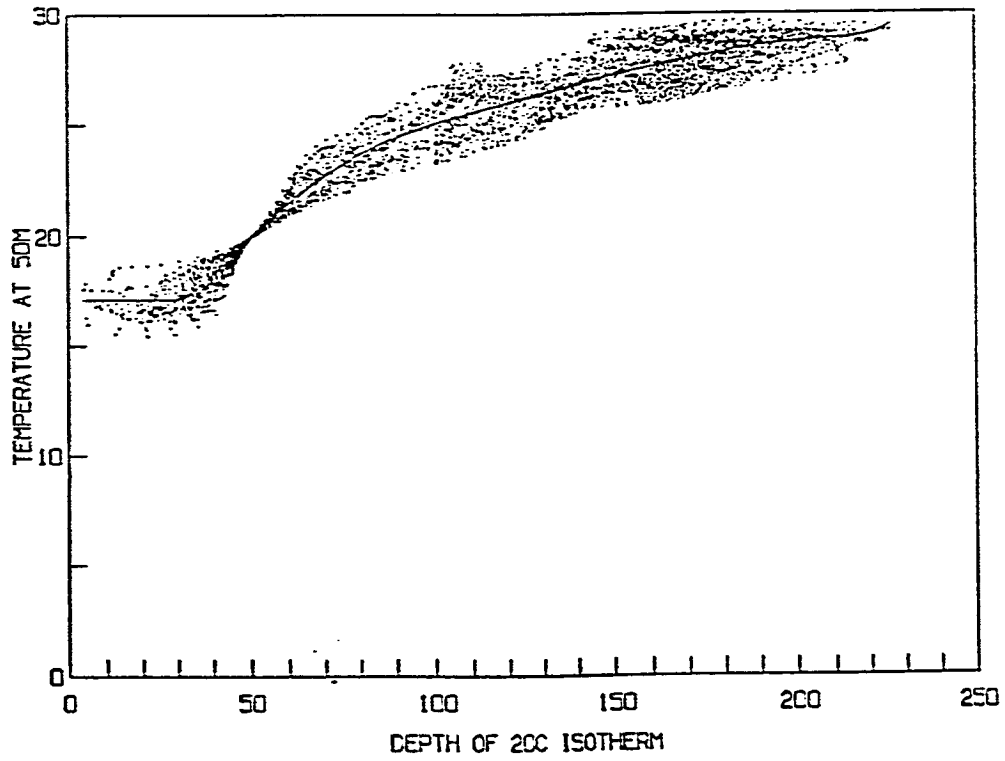


Fig.16: The relation between the depth of the 20°C isotherm and the temperature at 50 meters (from Seager et al., 1988).

In Zebiak (1984) and Zebiak and Cane (1987), the anomalous entrainment by the mean upwelling was parameterized as

$$- \{M(W_0 + w) - M(W_0)\} \frac{T_0 - T_{\text{sub}}}{H_m} = - \{M(W_0 + w) - M(W_0)\} T_{0z}$$

where T_{0z} is the vertical gradient of the mean temperature. In our model, a different parameterization is used, i.e.,

$$- \{M(W_0 + w) - M(W_0)\} \frac{T_0 - T_{\text{sub}}}{H_m} = - \{M(W_0 + w) - M(W_0)\} \frac{T_0 - T_s(H)}{H_m}$$

where $T_s(H)$ is the water temperature at the base of the mixed layer and H is the mean depth of the thermocline. $T_s(H)$ is estimated from the formula of Seager et al. (1988).

There are several processes by which an internal wave can affect the SST fields. For example, a downwelling Kelvin wave can induce a positive SST anomaly by: (1) advecting warmer water by anomalous currents from the western equatorial ocean to the east; (2) reducing the climatological cooling associated with the mean upwelling W_0 by creating a relative detrainment w ; (3) raising the temperature of the subsurface water, which is to be entrained to the surface, by depressing the thermocline depth. An upwelling wave cools the SST in an opposite way. These three factors explain why the SST anomalies are highly correlated to the thermocline depth anomalies. In fact, Busalacchi and O'Brien (1981) used a reduced-gravity shallow water model without explicit thermodynamics and successfully modeled the interannual variability in the Pacific Ocean. However, this high correlation between the thermocline depth and the SST is not always warranted. In the western equatorial Pacific Ocean the horizontal SST gradients and the vertical temperature

gradients are small. The advections in both the horizontal and vertical directions induce less SST change. In many models, e.g. Philander et al. (1984), the SST anomalies are made proportional to the vertical displacement of the thermocline depth. This relation works quite well for the climatological mean state and, to a less extent, for the seasonal and interannual variabilities. The basis for this relationship is the dominance of the upwelling near the equator, and this condition is likely to be invalid away from the equator (Zebiak, 1990).

(B) The atmosphere model

The atmosphere model is the widely used Gill's steady state model described by equation (3.6). The parameterization is basically the same as that in Section 3 except the heating is treated differently here. The anomalous diabatic heating term Q in (3.6c) is given, as in Battisti (1988), by the Clausius-Clapeyron equation:

$$Q = \phi C^2 \left(\frac{2\beta}{C} \right)^{\frac{1}{2}} \left[\frac{T_{\text{ref}}}{T_0} \right]^2 \exp(b(1/T_{\text{ref}} - 1/T_0)) T \quad (4.11)$$

where $\phi = 1.6 \text{ m } ^\circ\text{K} / \text{s}$ and $b = 5400 \text{ } ^\circ\text{K}$ are constants. $C = 60 \text{ m/s}$ is the phase speed of internal gravity waves in the atmosphere. $T_{\text{ref}} = 303 \text{ } ^\circ\text{K}$ is the reference temperature. The values of all these parameters are chosen the same as those in Battisti (1988). The mean temperature T_0 is from the annual mean SST of Shea et al. (1990). The Clausius-Clapeyron equation (4.11) states that the diabatic heating is more effective in a background of warmer SST. Indeed, deep convective heating becomes especially intense when the total SST approaches a critical temperature of about 28°C

(Gadgil et al., 1984). Neelin and Held (1987) argued that the temperature dependence of the Clausius-Clapeyron equation was much too weak. Various modifications have been made to include the low level moisture convergence (e.g., Neelin and Held, 1987; Zebiak, 1986) in order to improve the atmosphere model.

4.2 The model results and discussion

In order to test our ocean model, we spin up the model ocean from a state of rest by an easterly wind stress of the form:

$$\begin{aligned}\tau^x &= \tau_0 \sin\left(\frac{\pi x}{L_x}\right) \cos\left(\frac{\pi y}{2L_y}\right) \\ \tau^y &= 0\end{aligned}\tag{4.12}$$

where (τ^x, τ^y) are the zonal and meridional components of the wind stress respectively, $x = 0, L_x$ are the positions of the solid boundaries, and $y = \pm L_y$ are the northern and southern boundaries. In (4.12), $\tau_0 = 0.0225 \text{ Nm}^{-2}$ is used.

The numerical resolutions are $\Delta x = 1.5^\circ$, $\Delta y = 0.5^\circ$ and the time step $\Delta t = 30$ minutes. The model zonal width is taken as 16,000 kilometers, and the model meridional boundaries extend to 4000 kilometers from the equator. The numerical scheme is the same as that described in Section 3.

The model is spun up from a state of rest with initial conditions: $H_1 = 150$ meters, $H_2 = 150$ meters, and $(T_1, u_1, v_1, h_1, u_2, v_2, h_2) = 0$. The initial sea surface temperature is $T_0 = 28^\circ\text{C}$. The model takes only several months to be fully spun up, and the model results change very little after one year.

Fig.17(a) shows the depth of the interface between the upper and

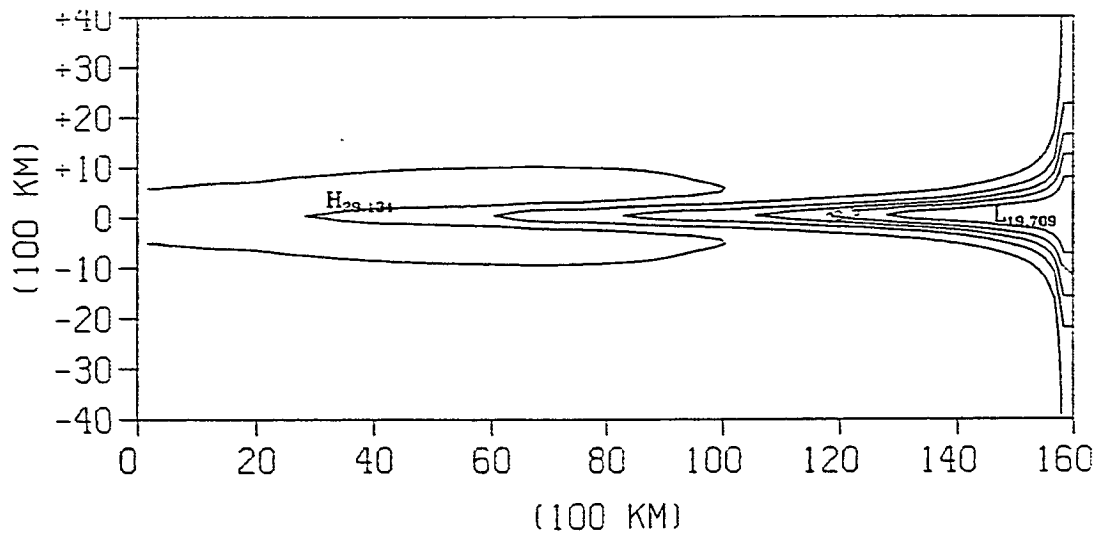
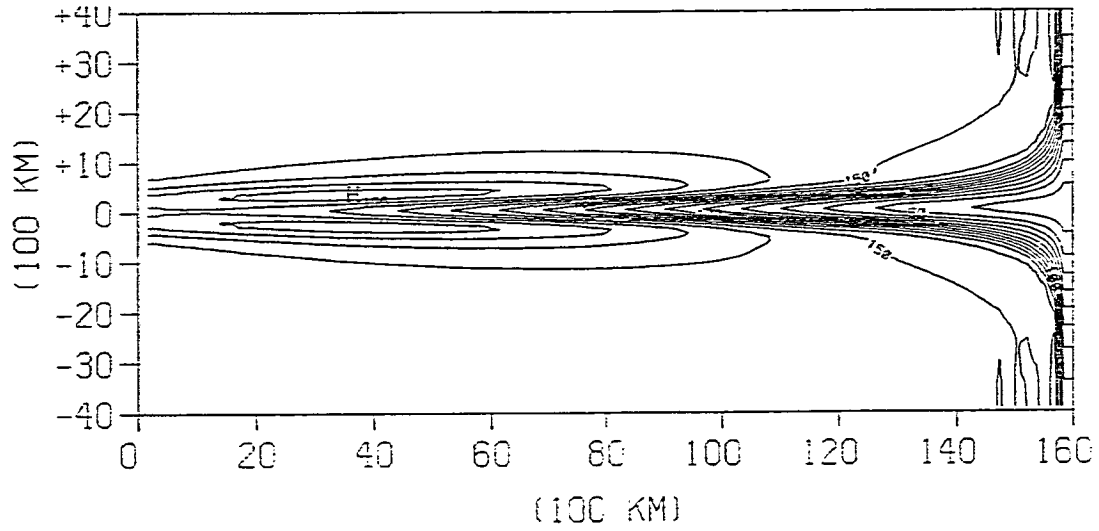


Fig.17: (a) the thermocline depth; (b) the SST, produced by the model when it was forced by a steady wind.

lower active layers, which represents the depth of the main thermocline. The model climatology resembles the main feature of the zonal profile of the main thermocline depth. Fig.17(a) shows that the depth of the main thermocline is about 200 meters in the western equatorial ocean and 50 meters in the eastern equatorial ocean. The most rapid change occurs at the central equatorial ocean between $x = 7000$ km and $x = 12,000$ km. The depth of the thermocline is shallower near the equator and gradually increases poleward. The shallowness of the main thermocline along the equator is due to the Ekman pumping along the equator resulting from the forcing of the easterly winds. These features reasonably resemble the climatology observed in the equatorial Pacific Ocean (Fig.9).

Fig.17(b) is the model SST field. In the western and central equatorial ocean from $x = 0$ to 10,000 kilometers there is a warm pool of water located within 10° in latitudes. The temperature in this warm region varies from 28°C to 30°C . A cold tongue of water is observed along the eastern boundary and in a narrow area along the equator from $x = 7,000$ km to $x = 16,000$ km at the eastern boundary. This cold tongue results from the intense upwelling along the eastern boundary in the eastern equatorial Pacific Ocean. The locations of the warm pool in the central and western equatorial Pacific Ocean and the cold tongue in the eastern Pacific Ocean are consistent with the observations. In fact Seager et al. (1988) used a very similar model to simulate the climatological SST. Their results show that the model works remarkably well. The differences of their simulated results and the observed SST were less than 0.1°C in most area in the tropical Pacific Ocean, except near the western boundary where about 1°C difference was observed.

Next four numerical experiments will be performed and the results of the different experiments will be compared and interpreted. The same model parameterization and the same initial condition will be applied to all experiments in order to allow direct comparisons. In the first experiment the realistic thermocline profile (the depth of the interface between the two active upper layers) is used. The profile of the main thermocline depth is plotted in Fig.18 (the solid line). In this experiment the depth of the thermocline in the western and central Pacific Ocean from 120°E to 160°W is at 175 meters below the sea surface. It decreases linearly from 175 meters at 160°W to 75 meters near the eastern boundary at 100°W , and is constant east of 100°W . This mean condition is considered as the "standard condition" or the "normal condition". All the model parameters are tuned to allow this "normal Pacific Ocean" to exhibit an interannual oscillation when a suitable initial disturbance is introduced. In the second experiment the depth of the main thermocline is plotted in Fig.18 where a very steep thermocline slope is confined in a small area from 120°W to 100°W . The deviation of the climatology in this state is possibly induced by the strong easterly trade winds in the eastern Pacific Ocean. The third experiment is conducted by using a smoother thermocline profile. The depth of the thermocline is plotted in Fig.18 where it increases from 200 meters at 160°E to 75 meters at 100°W . The drift of the climatological condition from the "normal condition" could be caused by continually weakening easterly winds over a period of time. In the fourth experiment we will test the role of the western boundary reflection of the long Rossby waves. The normal climatological condition as specified in the first experiment is used in this run. However the

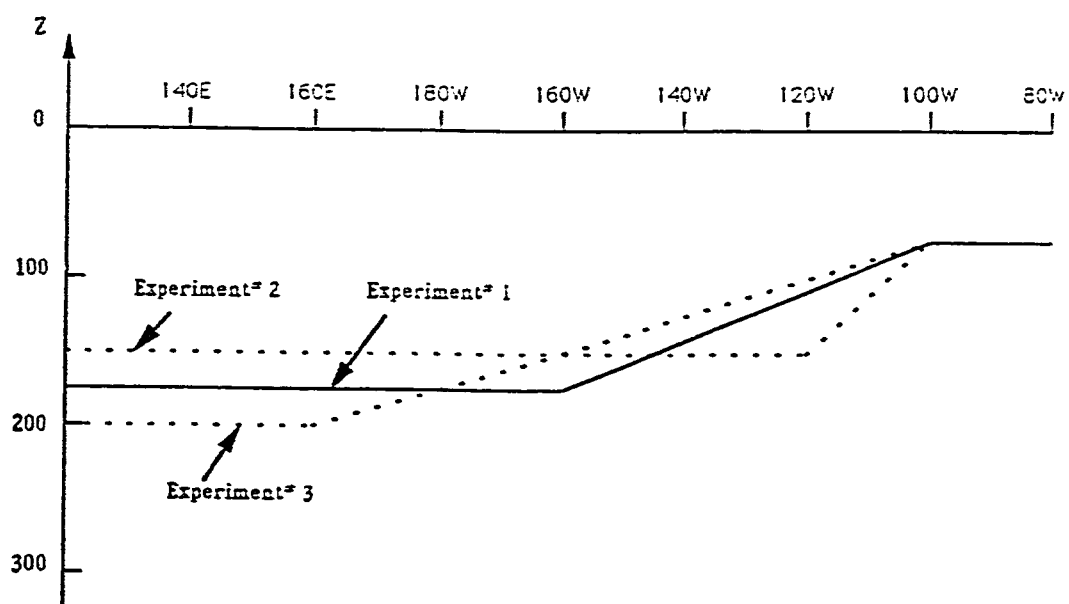


Fig.18: The model thermocline profiles.

western boundary is open, which allows long Rossby waves generated by the wind anomalies in the central and eastern Pacific Ocean to propagate freely out of the computational domain. Again the radiational open boundary condition of Camerlengo and O'Brien (1980) is used to compute all variables along the western boundary.

The initial condition in all the four experiments is created by forcing the model with a westerly wind anomaly patch in the western Pacific Ocean for 20 days. The westerly wind stress locally creates Ekman drift toward the equator and depresses the thermocline. The convergence of the surface currents induces detrainment which causes the warming of the local SST by reducing the mean equatorial upwelling field. The westerly wind stress also generates downwelling Kelvin waves and upwelling long Rossby waves. The downwelling process associated with the Kelvin waves warms up the surface ocean east of the forcing region, while the upwelling long Rossby waves cause the cooling in the western ocean. Fig.19(a) shows the anomalous depth of the main thermocline after a 20 day burst of the westerly wind stress. Fig.19(b) depicts the anomalous SST fields. The initial condition of the atmosphere model is created by using the initial oceanic SST distribution in the forcing term Q as described in (4.12). In all the experiments the ocean and the atmosphere communicate with each other once every model day, i.e., the anomalous wind stress is updated every one model day and remains the same between the model days.

Fig.20(a) shows the anomalous SST evolution at the equator off the eastern boundary over a period of ten years for the first experiment. A regular interannual oscillation with a period of about 2~3 years is self-

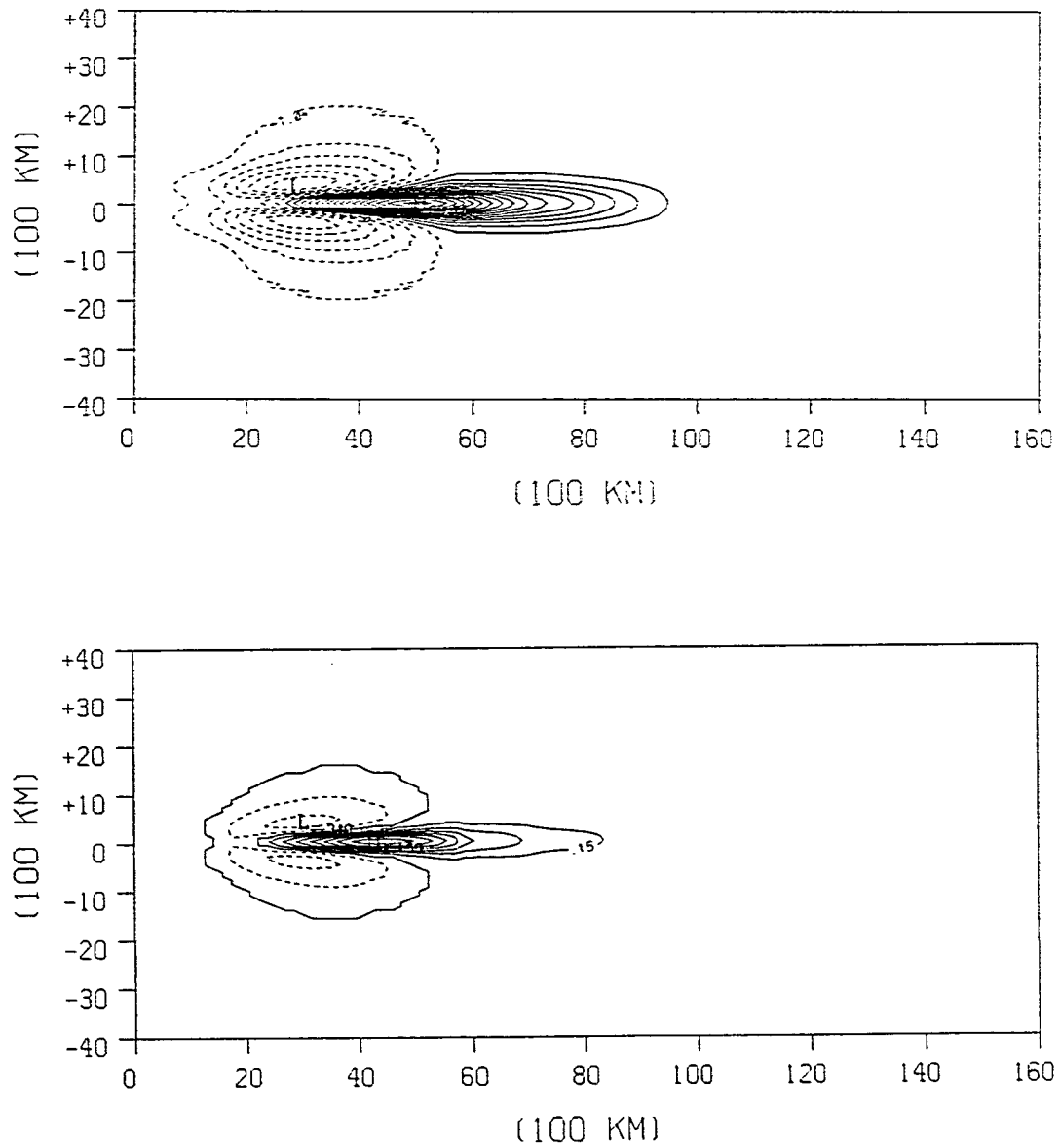


Fig.19: The initial conditions of the model, (a) the thermocline depth anomalies; (b) the SST anomalies.

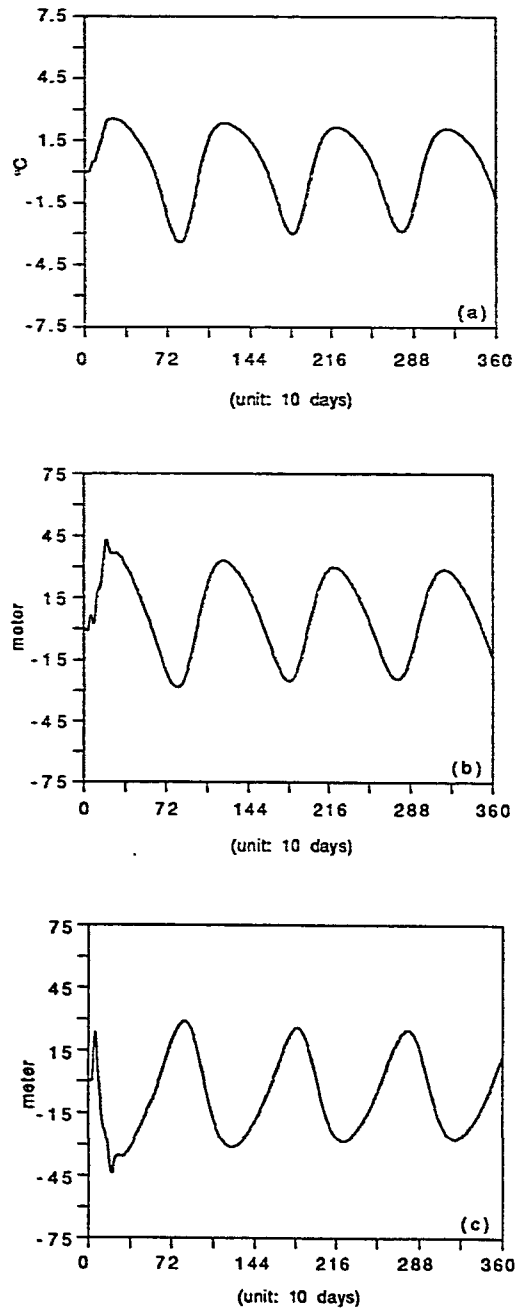


Fig.20: The evolution of the model variables in the eastern boundary at the equator. (a) SST anomalies; (b) the thermocline depth anomalies; (c) the second layer thickness anomalies (run 1).

sustained. The maximum SST anomaly in the eastern equatorial Pacific Ocean, in this run, is about 3°C. The anomalous depth of the main thermocline is depicted in Fig.20(b). The anomalous thermocline depth also oscillates with the same period as the anomalous SST. The maximum deviation of the thermocline depth is about 35 meters except for the first peak associated with the initial conditions. It is obvious that the anomalous SST and the thermocline deviation are closely correlated in phase in the eastern Pacific. This close correlation can be easily explained because the shallow thermocline depth in the eastern tropical Pacific makes the vertical advection dominate over the other thermodynamic processes. The second layer thickness anomaly oscillates with the same frequency as the SST but in the opposite phase (Fig.20(c)).

The eastward propagation of the oscillatory mode can be easily seen in the plot of the anomalous SST along the equator versus the time evolution as shown in Fig.21(a). The initial anomalous SST propagates eastward with increasing amplitude due to the amplification of the winds. The SST warms up rapidly near the eastern boundary between 110°W and 70°W. At about the 200th day the warm event begins to decay while a negative anomalous SST starts to develop west of the warm event. The cooler water slowly intrudes eastward and cools the previously existing warm SST in the eastern ocean. At the 500th day the warm SST anomaly completely vanishes and the eastern Pacific Ocean starts to develop the cold phase of the SST oscillation. It is interesting to note that a positive SST anomaly starts to develop and slowly migrate eastward when the cold event begins to amplify in the eastern Pacific. This weak warm signal amplifies quickly in the eastern ocean at 110°W. At about the 1000th day

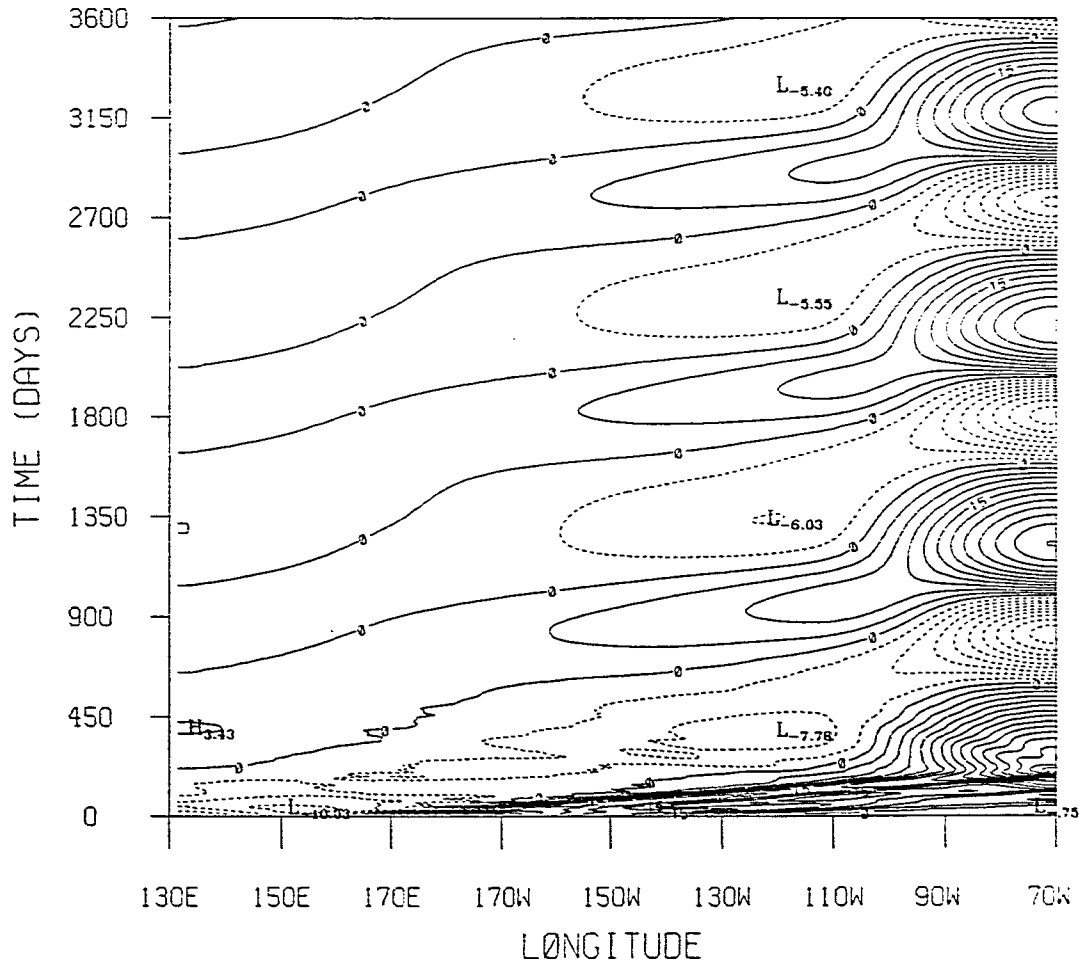


Fig.21(a): The longitude-time plot of the SST anomalies (run 1).

this warm event completely dominates over the entire eastern equatorial Pacific Ocean. The model ocean continues to oscillate in a similar manner in the remaining time. Fig.21(a) shows that the model experiences four warm events and three cold events in a period of ten years.

The development of the anomalous thermocline depth (the interface between the two active upper layers) is shown in Fig.21(b). The evolution of the anomalous thermocline depth in the eastern equatorial Pacific is very similar to the anomalous SST fields. However the origins of the warm and cold events in the western and central equatorial Pacific Ocean are more evident in the contours of the anomalous thermocline depths. For example during the early stage of the first warm event, an upwelling signal associated with a cold event is clearly detected in the western Pacific between 130°E and 170°E . The upward thermocline depth deviation of this potential cold event has an amplitude of over ten meters. When this upwelling signal moves eastward to the central equatorial Pacific Ocean, a downwelling wave has already formed near the western boundary. An upwelling Kelvin wave is also detected during the opposite phase of the oscillation between the 900th and the 1400th day. The model equatorial Pacific Ocean always experiences two conditions along the equator. When an El Niño develops near the eastern boundary, upwelling processes are dominated in the western and central Pacific and slowly intrude eastward to terminate the El Niño. This weak signal will be amplified during its way to the east and will finally terminate the warm phase of the oscillation. Fig.21(c) shows the evolution of the second layer thickness anomalies. As we have already noted, the second layer thickness anomaly oscillates with the same frequency and travels to the east. The SST

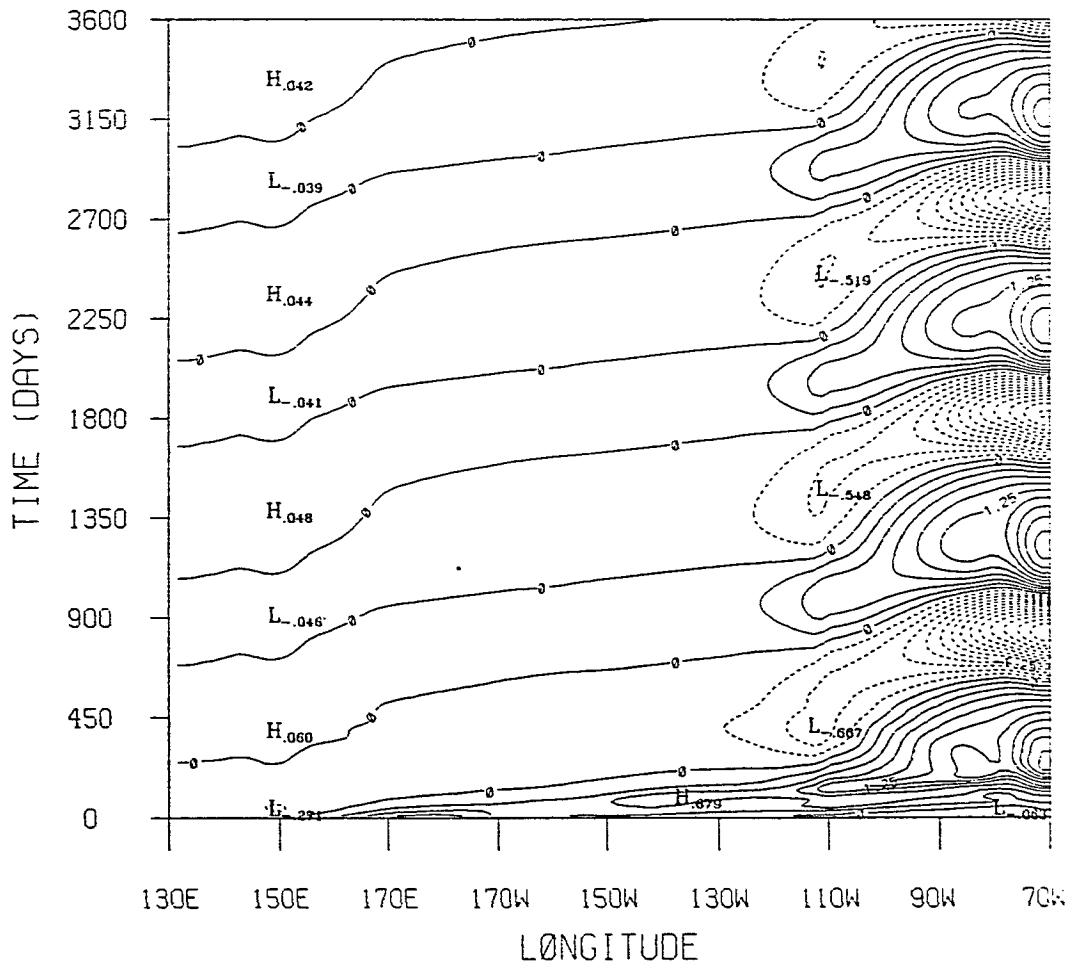


Fig.21(b): The longitude-time plot of the anomalous thermocline depth (run 1).

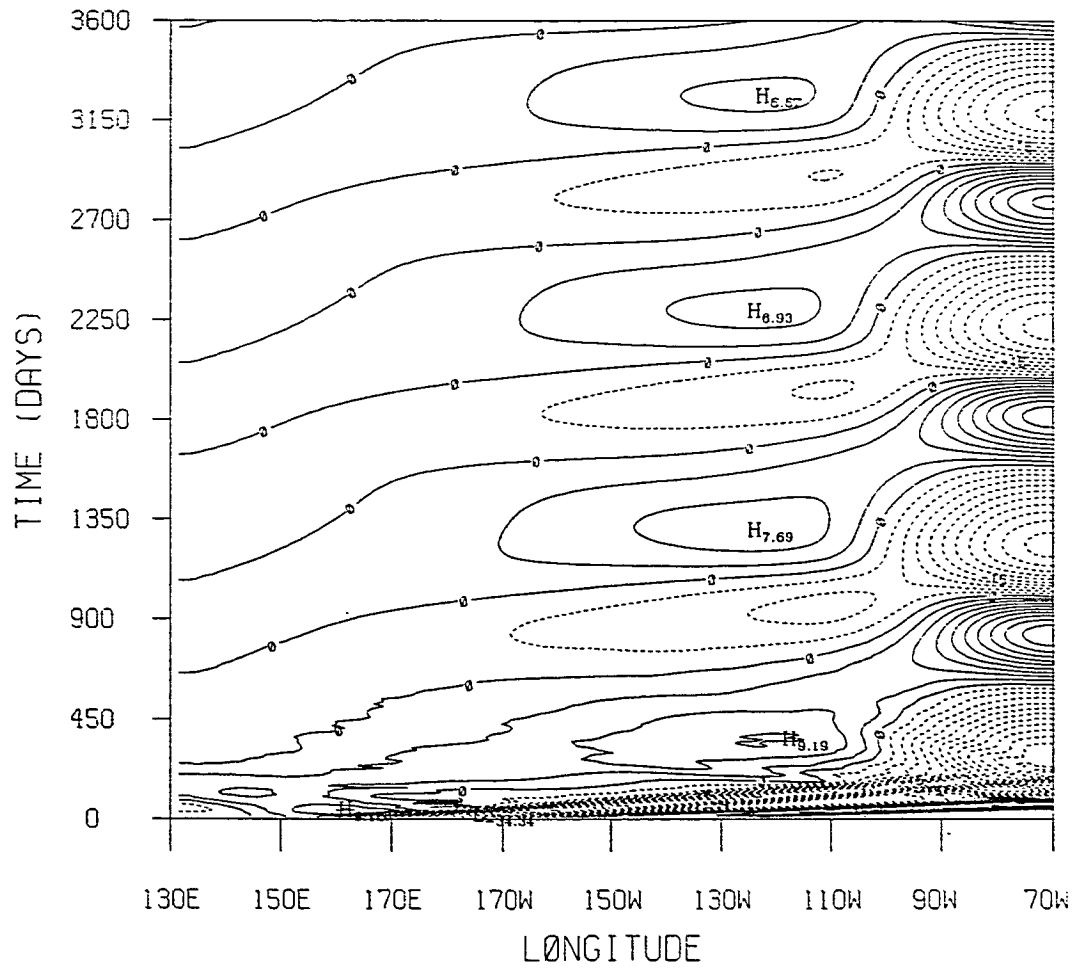


Fig.21(c): The longitude-time plot of the second layer thickness anomalies (run 1).

anomalies of this oscillatory mode are mainly localized in the eastern Pacific Ocean. This feature is very similar to the results of Zebiak and Cane (1987) and Battisti (1988). The physical reason for this SST localization is due to the inhomogeneous mean background in the zonal direction. In the western Pacific Ocean, only small SST anomalies will be induced by finite amplitude waves because of the small temperature gradients in the vertical and horizontal directions. Hence the oceanic thermodynamics are less influenced by those disturbances in the western Pacific. The eastern Pacific is also a weakly coupling zone because the mean SST is low. However, as we have discussed earlier, the dependence on the mean SST in the Clausius-Clapeyron equation is too weak. Hence the model still experiences relatively strong coupling in the eastern Pacific Ocean.

The anomalous heat content in the mixed layer can be calculated as

$$H_Q = \rho_m C_p H_m \iint T \, dx dy$$

where T is the anomalous SST, ρ_m is water density in the mixed layer, H_m is the mixed layer depth and C_p is the heat capacity of sea water.

In this calculation, the density ρ_m is 1000 kg m^{-3} and the sea water heat capacity C_p is $3998 \text{ J (kg } ^\circ\text{C)}^{-1}$. Fig.21(d) shows the evolution of the heat content. The anomalous heat content oscillates with the ENSO cycles. During an El Niño event, the surface mixed layer of the tropical Pacific Ocean is heating and the total heat content is higher than normal. During a cold event, the surface layer is cooling and the total heat content is lower. The heating of the upper layer mainly results from reductions of the climatological cooling associated with the mean upwelling. The cooling is from the strengthening of the cooling effects associated with upwelling.

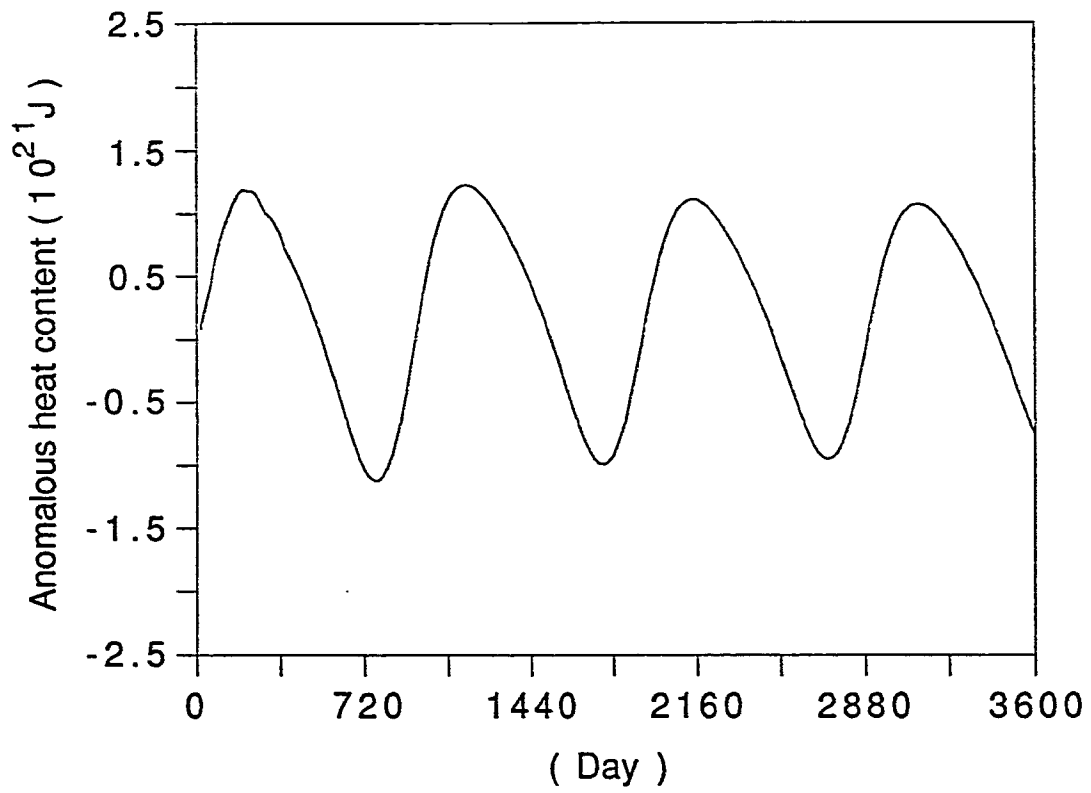


Fig.21(d): The anomalous heat content in the mixed layer.

From the total anomalous heat content, we can also calculate the anomalous heat fluxes during warm and cold events. First, we compute the anomalous heat flux when the model ocean evolved from a cold event to a warm event. The first peak of a cold event occurred at $t = 760$ days when $H_q = -1.1241 \times 10^{21}$ J. The following peak of a warm event occurred at $t = 1160$ days when $H_q = 1.2233 \times 10^{21}$ J. If we assume all the heating processes take place within 15° latitude, then the heat flux during this period is $F = 1.414 \text{ Wm}^{-2}$. Similarly, we compute the negative heat flux during a cooling period from 1160th day to 1760th day. The heat flux in this period is $F = -0.8915 \text{ Wm}^{-2}$.

Now let's consider a situation when the mean climatological background has shifted away from the "normal condition". The thermocline slope in the central equatorial Pacific Ocean in this experiment is steeper, as we have introduced in the beginning of this section and shown in Fig.18. Fig.22(a) shows the anomalous SST evolution just off the eastern boundary at the equator. The initial disturbance does reach the eastern boundary and causes the local warming there. The SST oscillation, however, is damped, and the model returns to the equilibrium state of rest after six years. Although the steep thermocline does not terminate the initial development of the warming in the eastern Pacific Ocean, the amplitude of the the anomalous condition is reduced to about 2.3°C compared with the initial peak of 3°C in the first experiment. The initial reduction is caused by the greater Rossby wave reflections from the steeper thermocline. It is possible that the reduction of the oscillation amplitude in the first cycle strongly influences the further evolution. The maximum SST anomaly of the following cold event is further reduced.

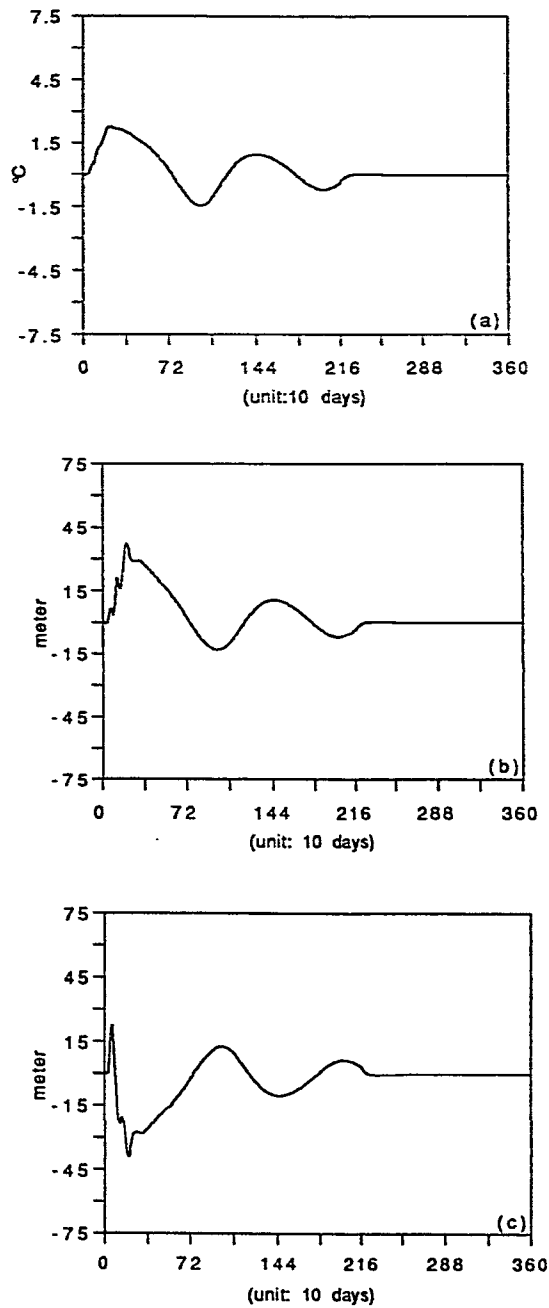


Fig.22: The evolution of the model variables in the eastern boundary at the equator. (a) SST anomalies; (b) the thermocline depth anomalies; (c) the second layer thickness anomalies (run 2).

Fig.22(a) shows that the SST in the eastern ocean is about 1.5°C below the mean condition, which is smaller than 3.85°C in the first experiment (Fig.20(a)). The model, under this condition, experiences two weak warmings and two very weak coolings before it returns to the state of rest. The deviation of the thermocline depth and the second layer thickness anomalies also damp in the same time scale. The fate of this damped oscillation is more clearly seen in Fig.23(a) which depicts the anomalous SST along the equator as a function of time. The initial condition is able to reach the eastern boundary and is locally amplified. However, the negative SST anomalies in the eastern and central equatorial region are weak, possibly caused by the warming of downwelling long Rossby waves reflected from the thermocline front. The warm SST event lasts about 650 day in comparison with the shorter duration time of the same event observed in the first experiment. This time delay is probably due to the weakening of the upwelling fields in the central Pacific Ocean. The oscillatory decay of the initial condition is also evident in the plot of the anomalous thermocline depth as shown in Fig.23(b). The reflection process can be detected in this plot where the thermocline deviation associated with the upwelling in the central Pacific Ocean dramatically reduces its amplitude after it propagates through the thermocline front. The contour of the second layer thickness anomalies is shown in Fig.23(c). The decayed oscillation, similar to the SST and the thermocline depth deviations, is also observed. This experiment suggests that the mean background specified in this experiment is unfavorable for the development of the self-sustained oscillatory mode. In other words, if the Pacific Ocean has a mean climatological background like this, each El

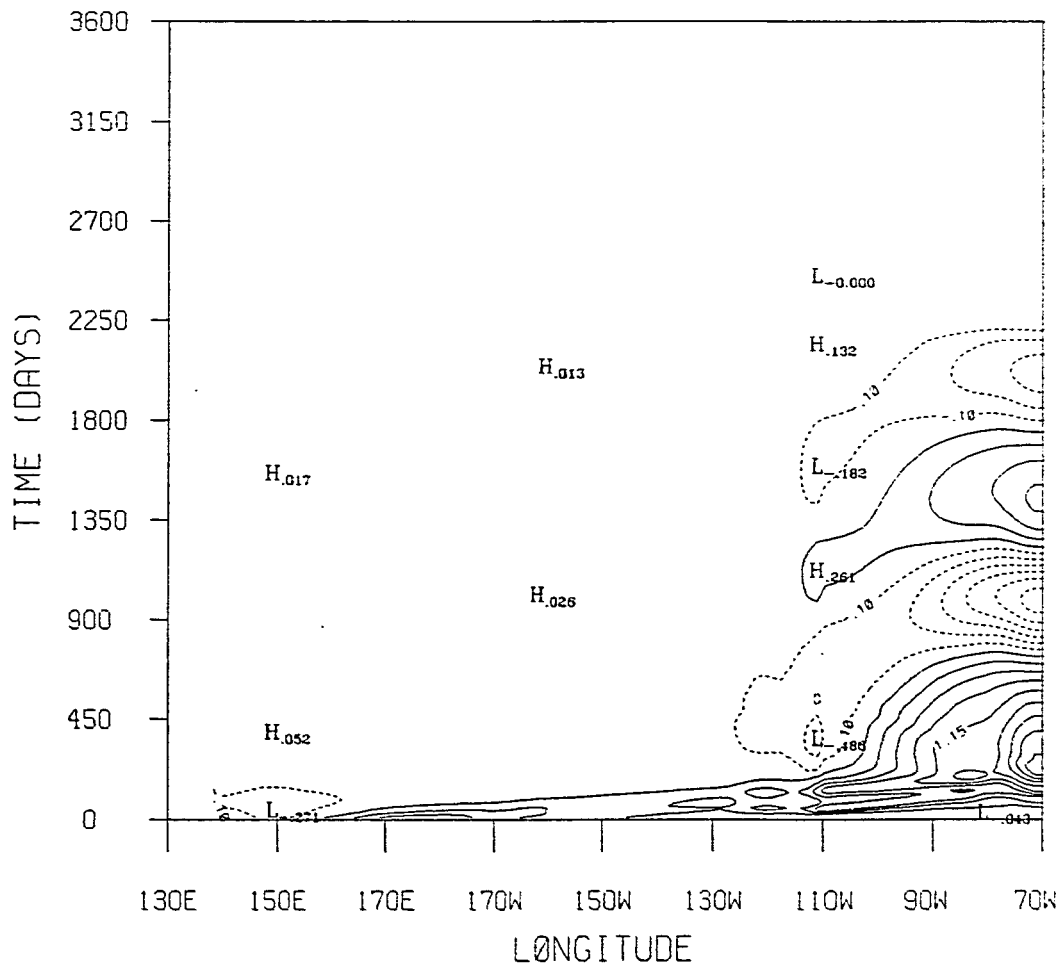


Fig.23(a): The longitude-time plot of the SST anomalies (run 2).

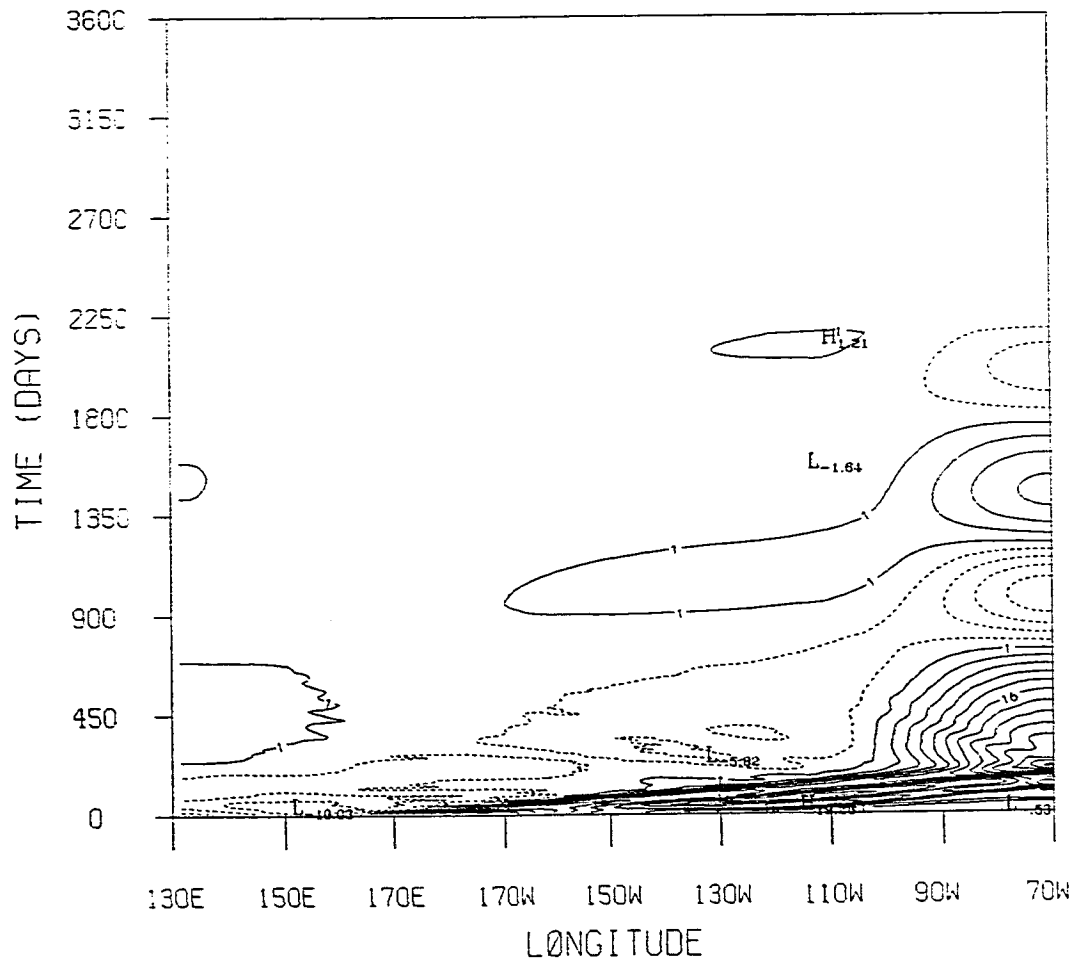


Fig.23(b): The longitude-time plot of the anomalous thermocline depth (run 2).

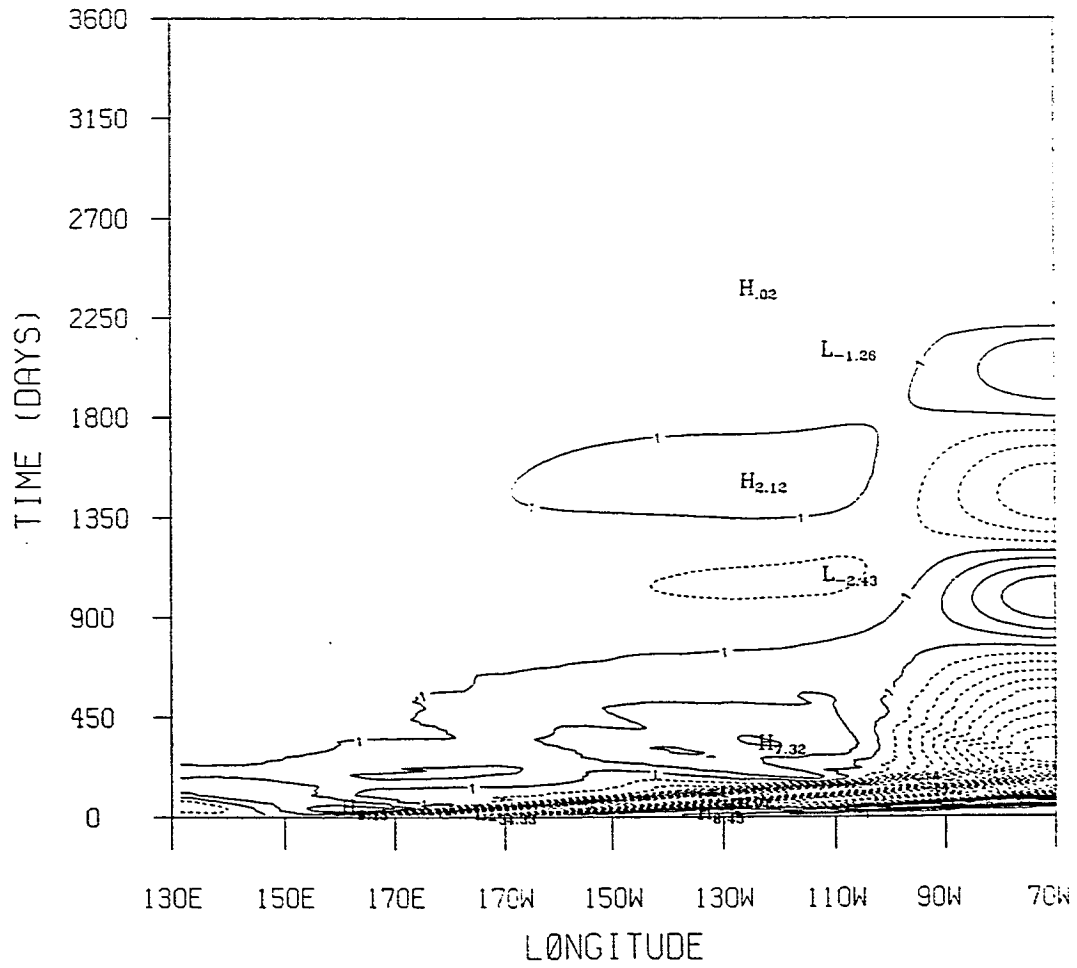


Fig.23(c): The longitude-time plot of the second layer thickness anomalies (run 2).

Niño phenomenon must be triggered by some suitable initial disturbances before it develops.

Next we will discuss the model results when the thermocline profile is flatter than the "normal condition". The thermocline profile is shown in Fig.18 and described in the beginning of this section. Again the same initial condition is used in the numerical run. The flatter thermocline slope in this experiment reduced the reflection of long Rossby waves and the degree of the vertical modal decompositions.

Fig.24(a) shows anomalous SST versus time. The amplitude of the SST anomaly gradually increases from 3.15°C in the peak of the first warm event to 4.5°C in the peak of the second warming. The model develops the numerical instability at the beginning of the 9th model year. The numerical instability is due to the surfacing of the interface between the two active layers in the shallow area in the eastern Pacific Ocean. This can be seen in Fig.24(b) which shows the anomalous depth of the interface. During the peak of the cold event, the upward deviation of the main thermocline is about 75 meters, which is about the mean thermocline depth specified in the eastern ocean. Strictly speaking, the formulation of the mixed layer, during the peak of the cold phase of ENSO in a small area near the eastern boundary, does not hold because the thermocline has almost surfaced, and the mixed layer should be very shallow or even vanish locally. However, we still adopt this model formulation in this special case for the purpose of allowing direct comparison with the results of the "normal case" (experiment one). The second layer thickness anomaly evolution is plotted in Fig.24(c). The period of the oscillation is slightly shorter than that of the first experiment. Fig.25(a,b,c) shows the

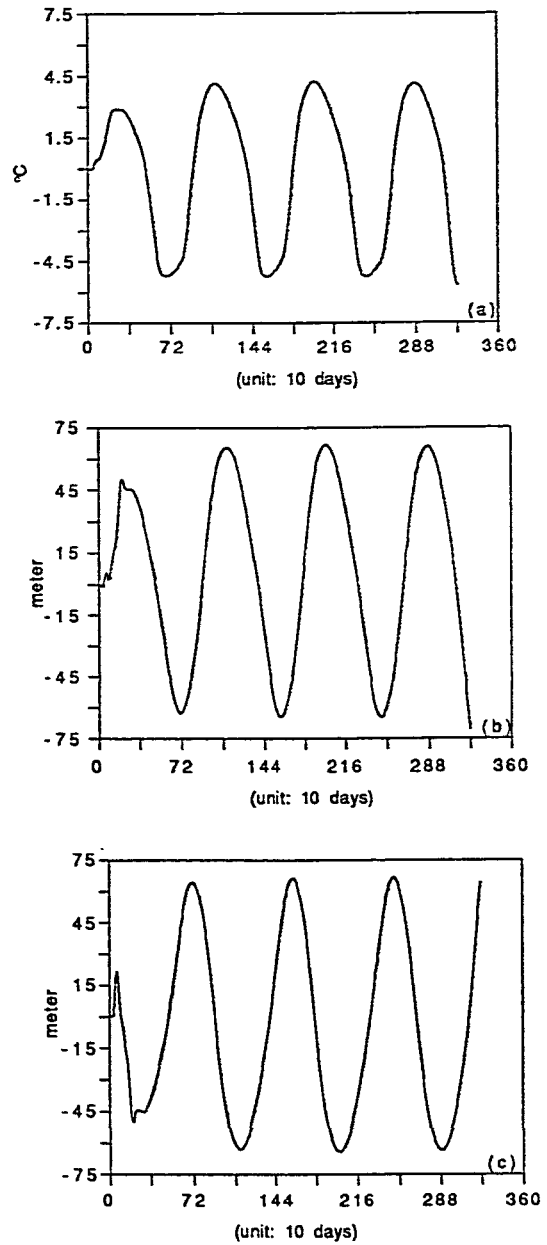


Fig.24: The evolution of the model variables in the eastern boundary at the equator. (a) SST anomalies; (b) the thermocline depth anomalies; (c) the second layer thickness anomalies (run 3).

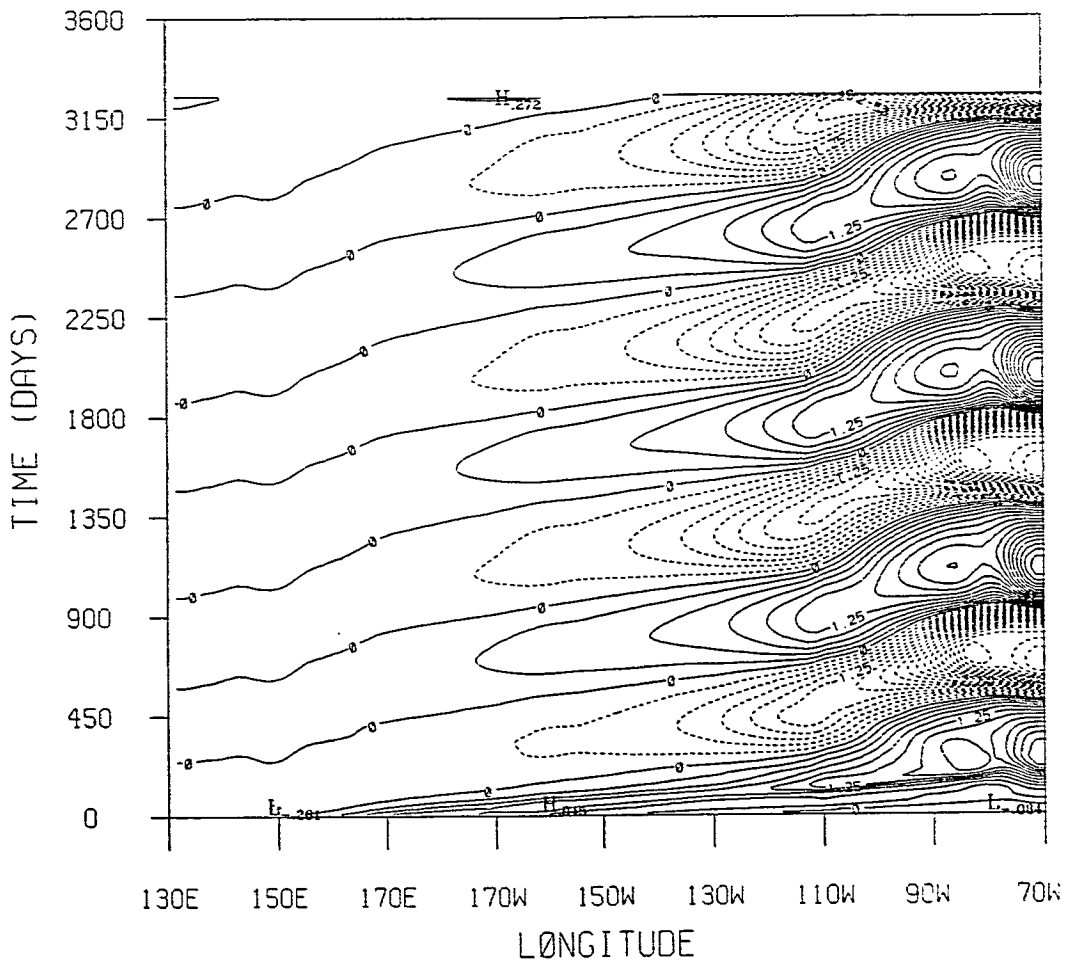


Fig.25(a): The longitude-time plot of the SST anomalies (run 3).

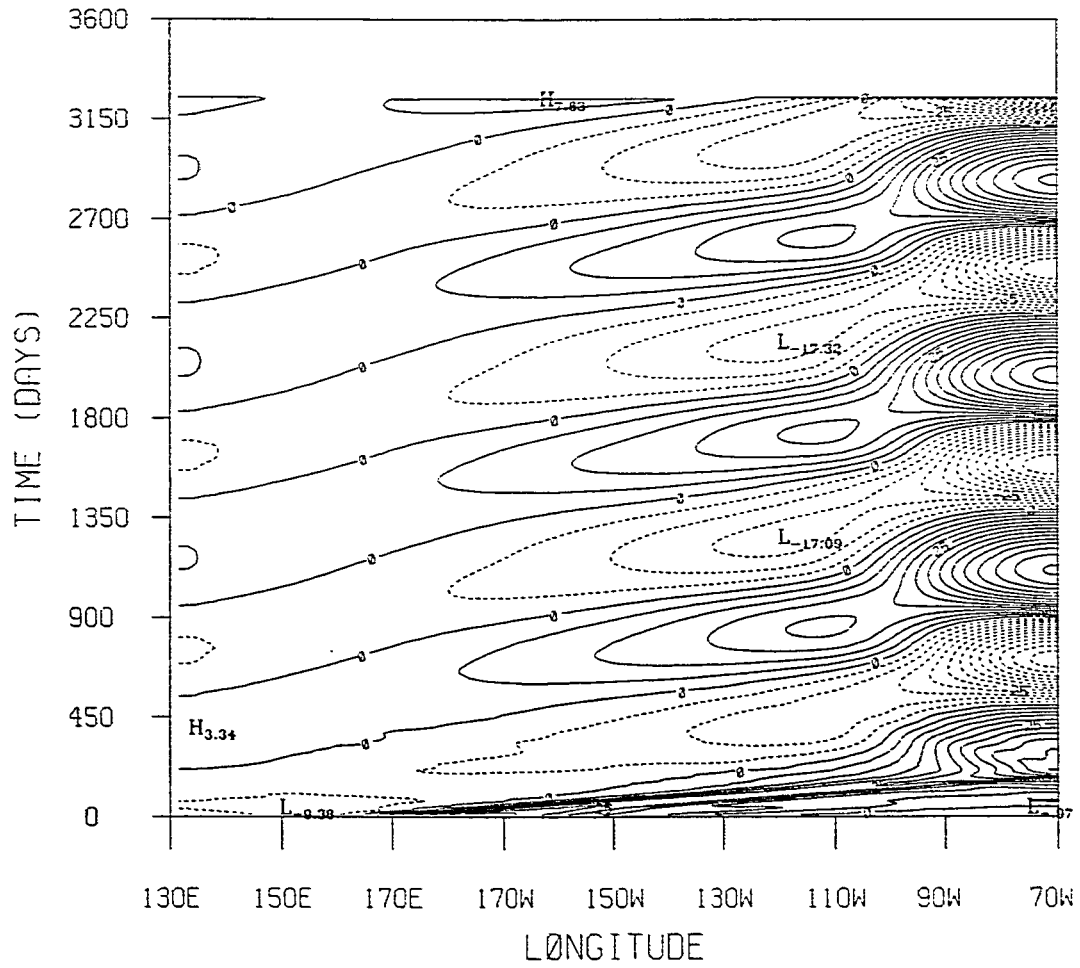


Fig.25(b): The longitude-time plot of the anomalous thermocline depth (run 3).

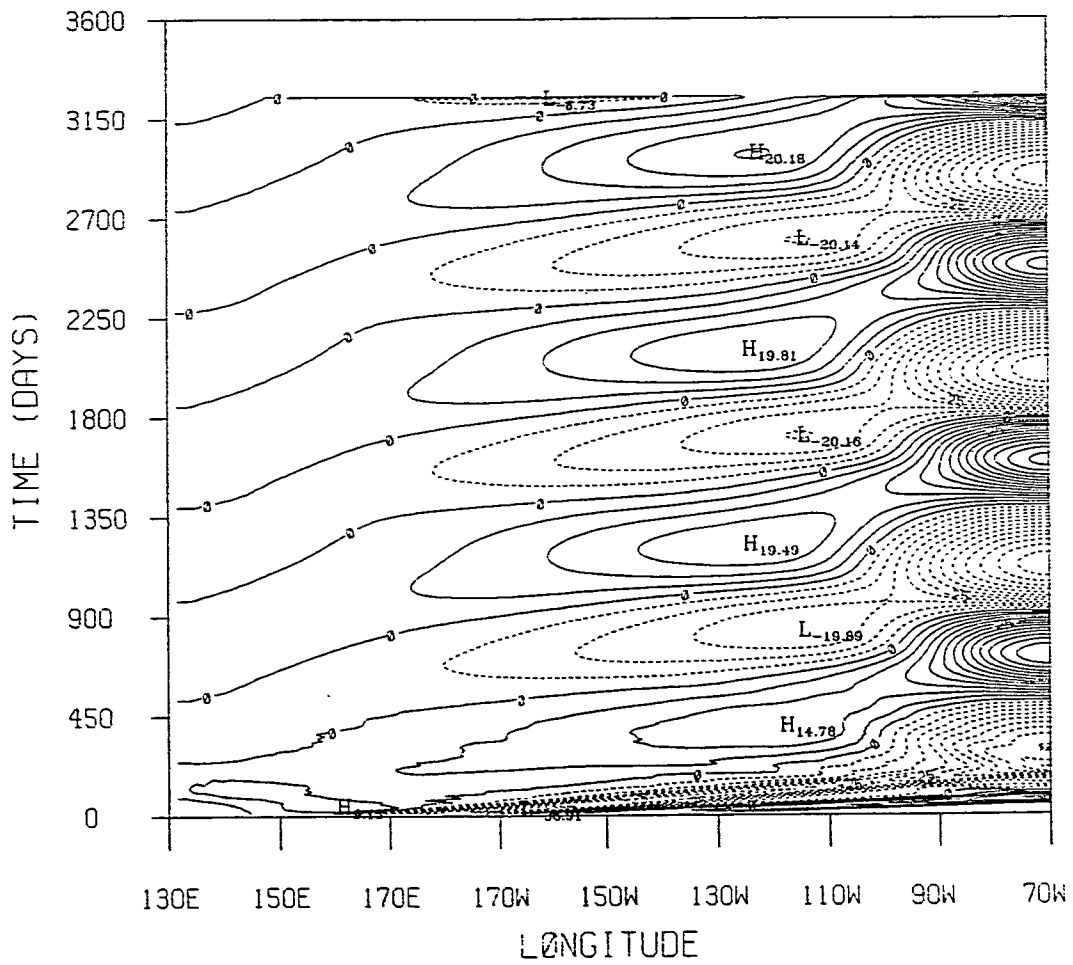


Fig.25(c): The longitude-time plot of the second layer thickness anomalies (run 3).

time-longitude plots of the anomalous SST, the thermocline depth deviation, and the second layer thickness anomaly along the equator. The origin of the model warm and cold events can be clearly traced back to the western Pacific Ocean in the plot of the thermocline depth anomaly in Fig.25(b). For example, a downward depression of the thermocline depth of 3.34 meters just off the western boundary is detected during the peak of the upwelling cold event in the eastern tropical Pacific Ocean. The eastward amplification is also clearly seen in all three contours. Slight reductions of the SST and the thermocline depth anomalies east of the sloping thermocline are due to the energy loss associated with the long Rossby wave reflections. The strongest deviations of both the SST and the thermocline depth occur just off the eastern boundary. From the previous three experiments, we have seen the different behaviors of the ENSO-like oscillations. It is very clear that the small upwelling (downwelling) signals appearing in the western Pacific Ocean during the peak of the downwelling (upwelling) event in the eastern ocean will be amplified during their movement to the east. It seems that those small signals play an important role in the termination of the anomalous conditions near the eastern boundary. Do these small amplitude waves result from the long Rossby wave reflections from the western boundary, or are they part of the unstable propagating waves, like those in Philander et al. (1984), in their early stages? Is reflection from the western boundary critical to determine the period of the oscillation as those reflected Kelvin waves in the delayed action oscillator discussed by Battisti (1988) and Schopf and Suarez (1988)? To explore these questions we decided to conduct one more experiment. In this numerical run, the parameterization and the profile of the

thermocline slope of the "normal run" (i.e., the first experiment) are used. The initial condition is the same as those previous experiments. The only difference is that the western boundary is now open. Battisti (1988) conducted a similar experiment and found that the SST anomaly in the eastern ocean continues growing, and he concluded that the delayed negative feedback from the reflected Kelvin waves is critical to sustain the oscillation and to determine the oscillatory period.

Fig.26(a) shows the evolution of the SST anomaly in the equator off the eastern boundary. The oscillatory solution still exists in this experiment but with much greater amplitude. The maximum deviation of the SST is about 4.5°C after the first peak, compared with the 3°C SST anomaly observed in the first experiment. The period of the oscillation is about 2~3 years and is exactly the same as that in the first experiment. The anomalous thermocline depth is plotted in Fig.26(b), and the second layer thickness anomaly is shown in Fig.26(c). The maximum deviation of the thermocline depth is 75 meters which is the mean thermocline depth we prescribed locally in the eastern ocean. Again the formulation of the constant depth mixed layer is not valid during the peak of upwelling when the thermocline surfaces. The assumption that the interface between the two active upper layers is a material surface is violated. Physically, a very shallow mixed layer is still maintained by deepening effects of the turbulent mixing. Since this experiment serves as a sensitivity test, we still adopt this model formulation.

Fig.27(a) shows the longitude-time plot of the anomalous SST along the equator. The pattern is very similar to the first experiment except the SST anomalies extend far more westward. The thermocline depth and the

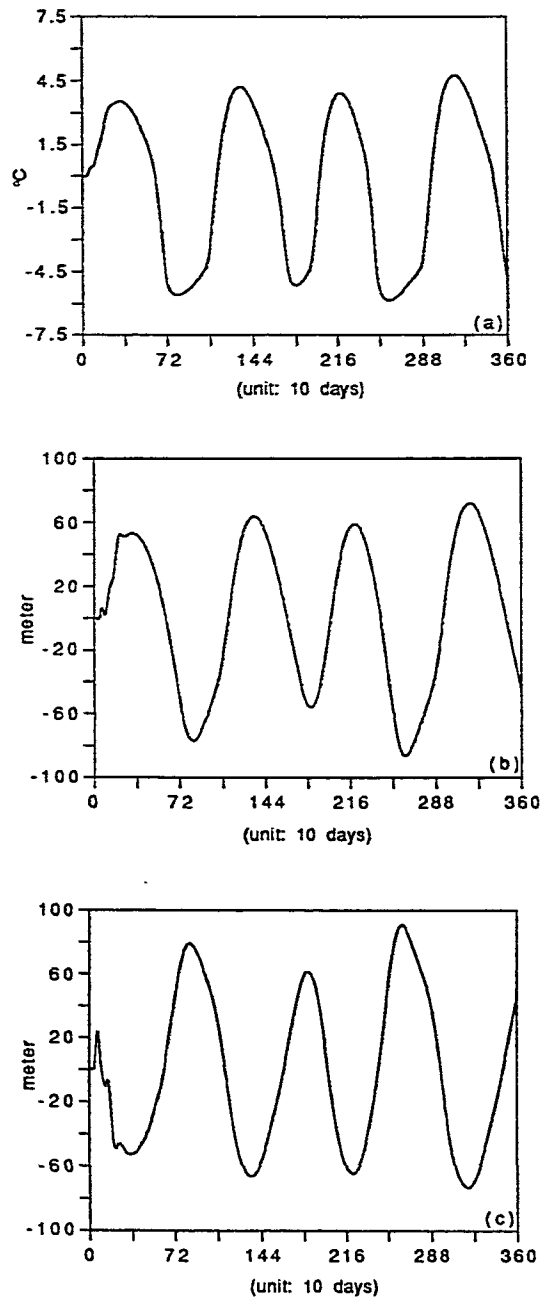


Fig.26: The evolution of the model variables in the eastern boundary at the equator. (a) SST anomalies; (b) the thermocline depth anomalies; (c) the second layer thickness anomalies (run 4).

second layer thickness anomalies are plotted in Fig.27(b) and Fig.27(c) respectively. They are all similar to the evolution of the same fields observed in the first experiment except the amplitudes are much greater.

It is obvious that the period of this oscillation is not determined by the delayed period of the negative feedbacks associated with the reflected Kelvin waves. However, the amplitude of the oscillation is strongly related to the reflections of long Rossby waves from the western boundary. The reflected Kelvin waves intensify the eastward moving anomalous conditions in the central and western Pacific Ocean and help to reduce the amplitude of the warm or cold events in the eastern Pacific Ocean. Hence this oscillatory mode is not the delayed-action oscillator in the sense that the delayed feedback does not set the period of the oscillation. However, it is similar to the delayed-action oscillator in the sense that the reflected Kelvin waves from the western boundary strongly reduce the oscillation amplitudes. It is obvious that the internal processes of the coupled system determine the frequency of the oscillation.

The fundamental question is "why does the model select the propagating mode rather than the nonpropagating mode (delayed mode)?" As we already discussed in the previous sections, the three necessary conditions for the delayed mode are (1) reflections of long Rossby waves from the western boundary, (2) a large basin which provides a long delay time, and (3) western part of ocean is free from interacting with the atmosphere (hence long Rossby waves are able to propagate freely westward). The first two conditions are satisfied in our model (in the first three numerical runs). Now we must examine the validity of condition (3) in this model. The connection of the ocean and the atmosphere in this

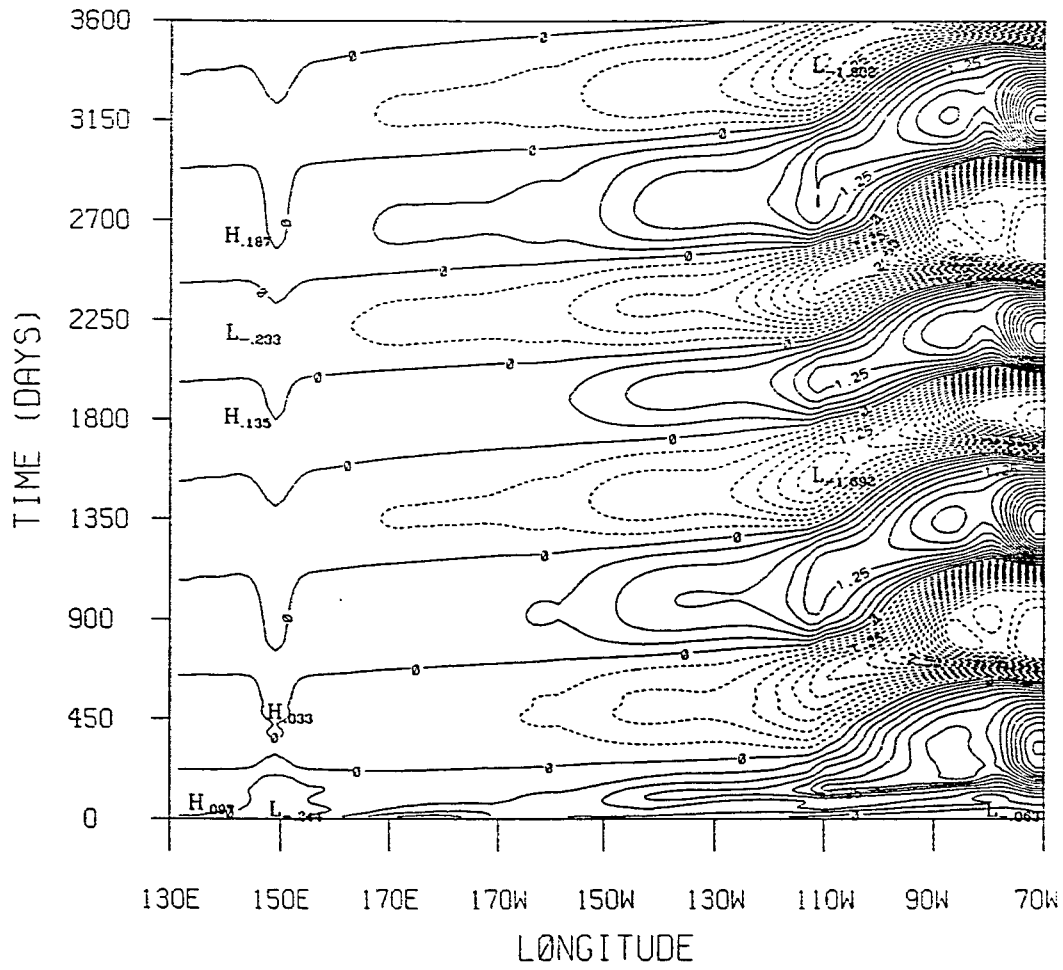


Fig.27(a): The longitude-time plot of the SST anomalies (run 4).

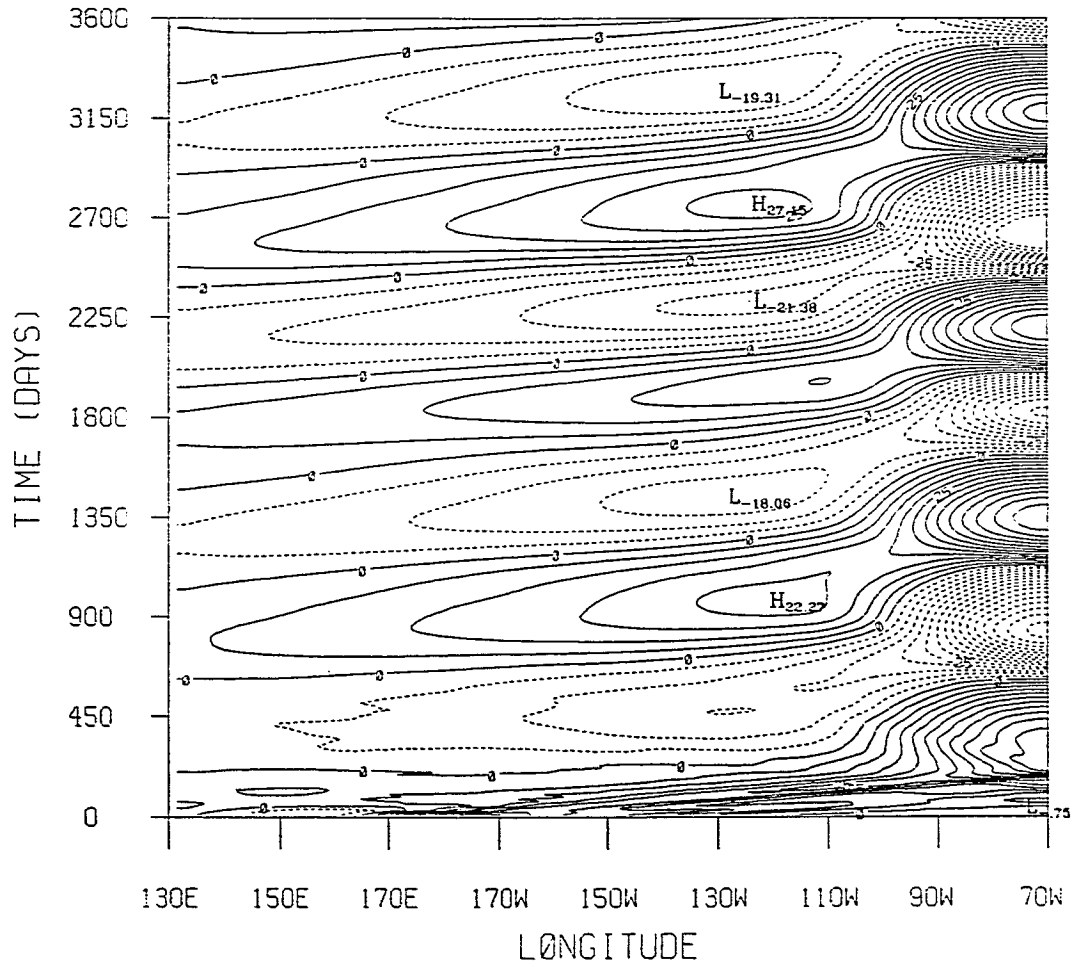


Fig.27(b): The longitude-time plot of the anomalous thermocline depth (run 4).

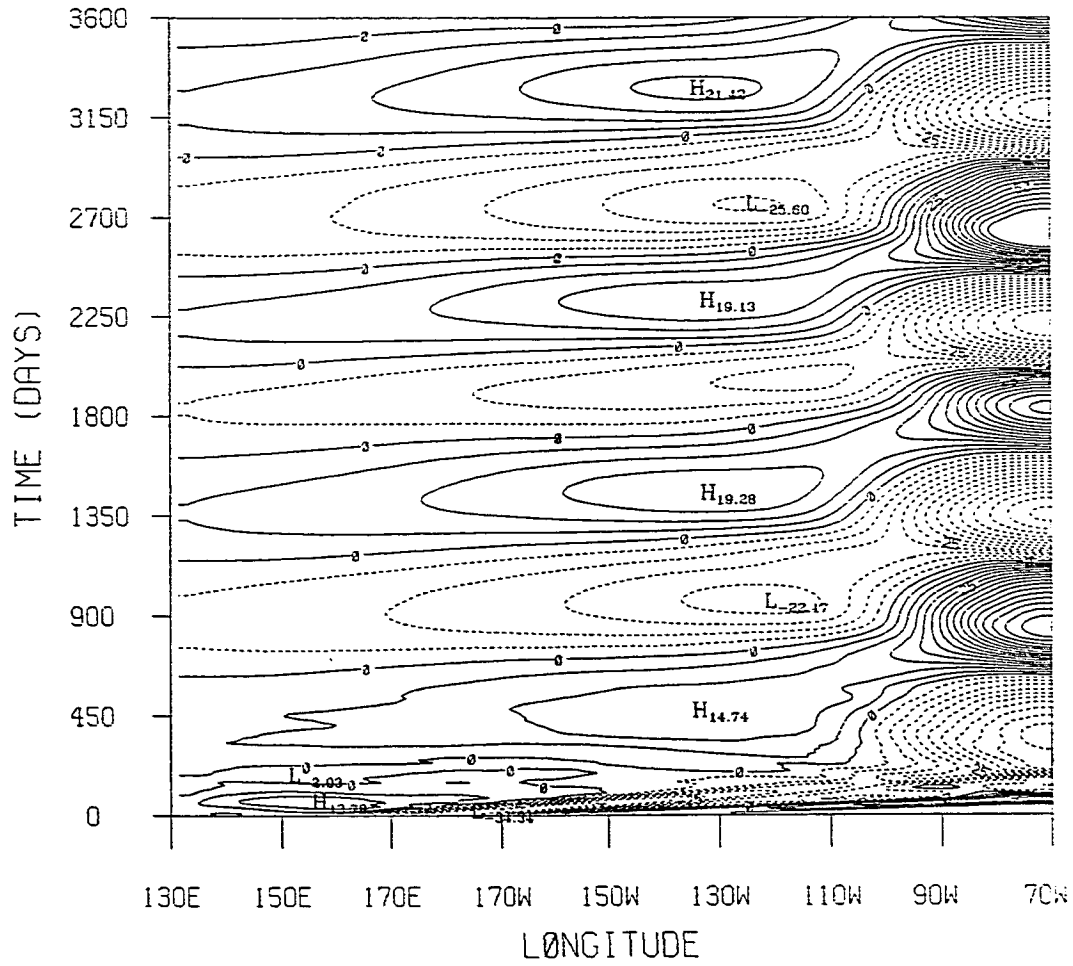


Fig.27(c): The longitude-time plot of the second layer thickness anomalies (run 4).

model is through the latent heat release associated with the SST anomaly and the wind stress induced by anomalous heating. Hence the condition (3) becomes that the oceanic thermodynamics are decoupled from the oceanic dynamics in the western ocean.

Let's consider the linearized version of the SST equation (4.7) ,

$$T_t = -\mathbf{u}_m \nabla T_0 - w \frac{T_0 - T_{\text{sub}}}{H_m} - \frac{\mu W_0}{H_m} (T - T_e) - \alpha T \quad (4.13)$$

Assumption that W_0 is upward and $w < W_0$ is made in deriving (4.13). The effects of the mean horizontal currents are neglected as we discussed in the model formulation. In the model of Zebiak and Cane (1987) (also as Battisti, 1988), the subsurface temperature T_e was parameterized as (4.9), i.e.,

$$T_e = \theta(h) [\tanh(\lambda((H+1.5|h|)) - \tanh(\lambda H)]$$

where $\theta = 28$ °K and $\lambda^{-1} = 80$ m for $h > 0$, and $\theta = -40$ °K and $\lambda^{-1} = 80$ for $h < 0$. If we linearize (4.9), (4.13) becomes

$$T_t = -\mathbf{u}_m \nabla T_0 - w \frac{T_0 - T_{\text{sub}}}{H_m} - \alpha^* T + \sigma(H) h \quad (4.14)$$

where $\alpha^* = (\alpha + \mu \frac{W_0}{H_m})$, $\sigma = \mu \frac{W_0}{H_m} \frac{\theta \lambda}{\cosh^2(\lambda H)}$, and h is the deviation of the thermocline depth. In (4.14), $-\alpha^* T$ represents the effective damping and $\sigma(H)h$ measures the effects of the vertical thermocline movement on SST changes. Fig.28 (dashed line) shows $\sigma(H)$ (averaged between $\sigma(H)|_{h>0}$ and $\sigma(H)|_{h<0}$) as function of the mean thermocline depth. As we can see, the value of σ decreases very rapidly when H increases.

In our model, the subsurface temperature T_e is estimated by using the formula derived by Seager et al. (1988). We can also calculate the

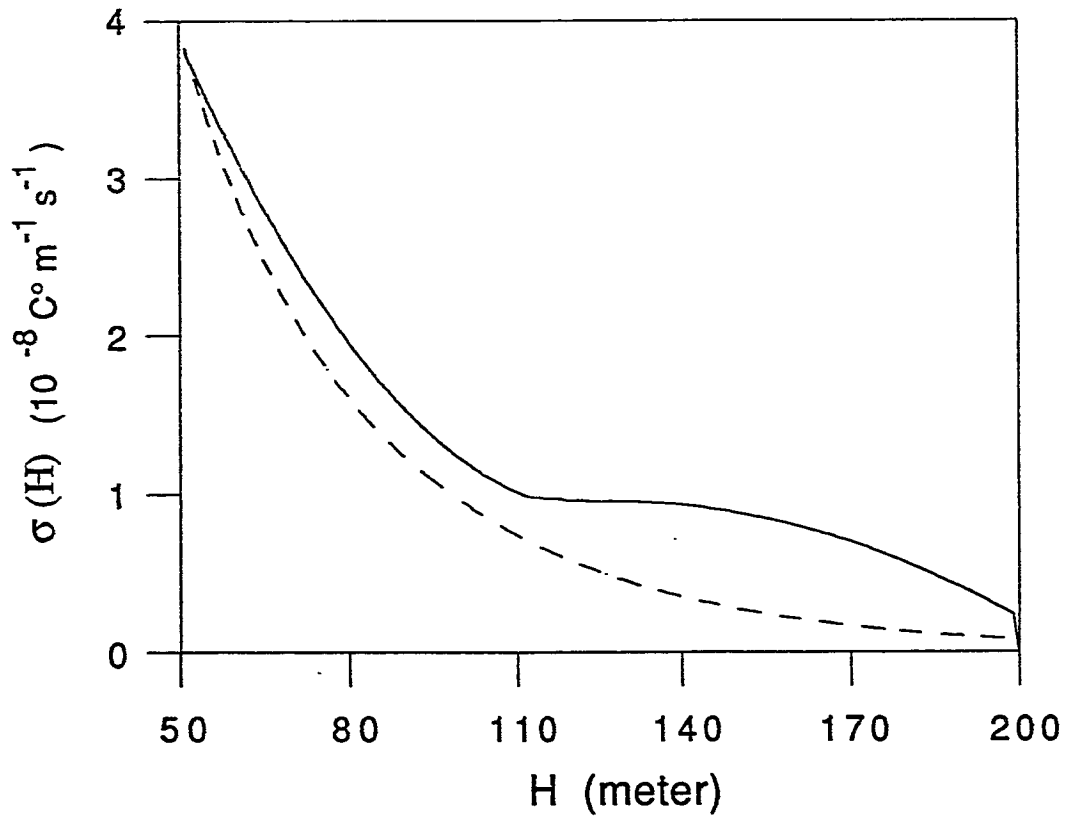


Fig.28: The entrainment coefficient σ as function of mean thermocline depth (the dashed line is from Zebiak and Cane's formula; the solid line is from Seager et al.'s formula which is used in this work).

coefficient $\sigma(H)$ (solid line in Fig. 28) from Seager et al.'s formula. The value of $\sigma(H)$ used in Zebiak and Cane's model and that used in our model are very close when H is small but differ significantly when the thermocline becomes deeper. For example, when $H = 150$ meters, Zebiak and Cane's model gives $\sigma(H) = 0.27 \times 10^{-8} \text{ } ^\circ\text{C m}^{-1} \text{ s}^{-1}$ while our model uses $\sigma(H) = 0.88 \times 10^{-8} \text{ } ^\circ\text{C m}^{-1} \text{ s}^{-1}$, a factor of three.

As many previous studies (e.g., Wakata and Sarachik, 1989; Hirst, 1986 and 1988) indicate, the term $\sigma(H)h$ is one of the important processes that connect oceanic dynamics to the SST field. In fact, Battisti (1988) concluded that the growth of instabilities in his model is governed by the simplified equation of (4.14), i.e.,

$$T_t = -\alpha^* T + \sigma(H) h \quad (4.15)$$

According to Hirst (1986), the instability mechanism in the model of Anderson and McCreary (1985) can also be described by (4.15). Fig.28 shows that the relation between the thermocline movement and SST fluctuations is much stronger in our model than that in Zebiak and Cane's model, especially in the western Pacific Ocean. As a consequence, the air-sea coupling in the western Pacific is stronger in our model. Hence, condition (3) of the delayed mode is not satisfied in our model.

What is the mechanism that determines the oscillation in our model? During an El Niño event, SST is high in the eastern Pacific Ocean. The positive SST anomaly induces westerly winds in the central and western Pacific. The westerly winds further intensify the anomalous SST condition in the eastern Pacific. At the same time, the westerly winds generate upwelling long Rossby waves on the western side. Those upwelling long Rossby waves tend to cool the local SST and produce small

negative SST anomalies. The atmosphere then responds to the SST cooling by producing an easterly wind. This easterly wind, in turn, generates upwelling Kelvin waves which also cools the local SST. The upwelling Kelvin modes are amplified by the atmosphere feedbacks when they propagate eastward. Those initially generated long Rossby waves travel westward. Based on this analysis, the period of the oscillation is determined by the internal parameters of the propagating modes, such as the coupling coefficient, and the shallow water gravity wave speed c . If the western boundary is reflective, the upwelling Kelvin waves, which result from long Rossby wave reflections, travel eastward and strengthen the cooling process. This explains why the reflection of long Rossby waves can only affect oscillatory amplitude but does not change the oscillatory period.

This mechanism can be identified in the model. Fig.29 (a) shows the anomalous SST field and the wind anomalies at the 1090th model day obtained from experiment#4. At this time, a warm El Niño is developing in the central and eastern Pacific Ocean and a cold event is decaying along the eastern boundary. Westerly winds are dominated in the central and western Pacific Ocean and easterly winds associated with the decaying cold event are still evident near the eastern boundary. Fig.29(b) shows the anomalous thermocline depth. As we can see, small amplitude upwelling long Rossby waves have already formed in the western Pacific Ocean. The upwelling long Rossby waves induce local cooling (dashed line contours) in the western Pacific (Fig.29(a)). The cooling process intensifies due to the atmosphere feedback. At the 1250th day, the entire western and central tropical Pacific Ocean experiences upwelling processes (Fig.30(b)). The

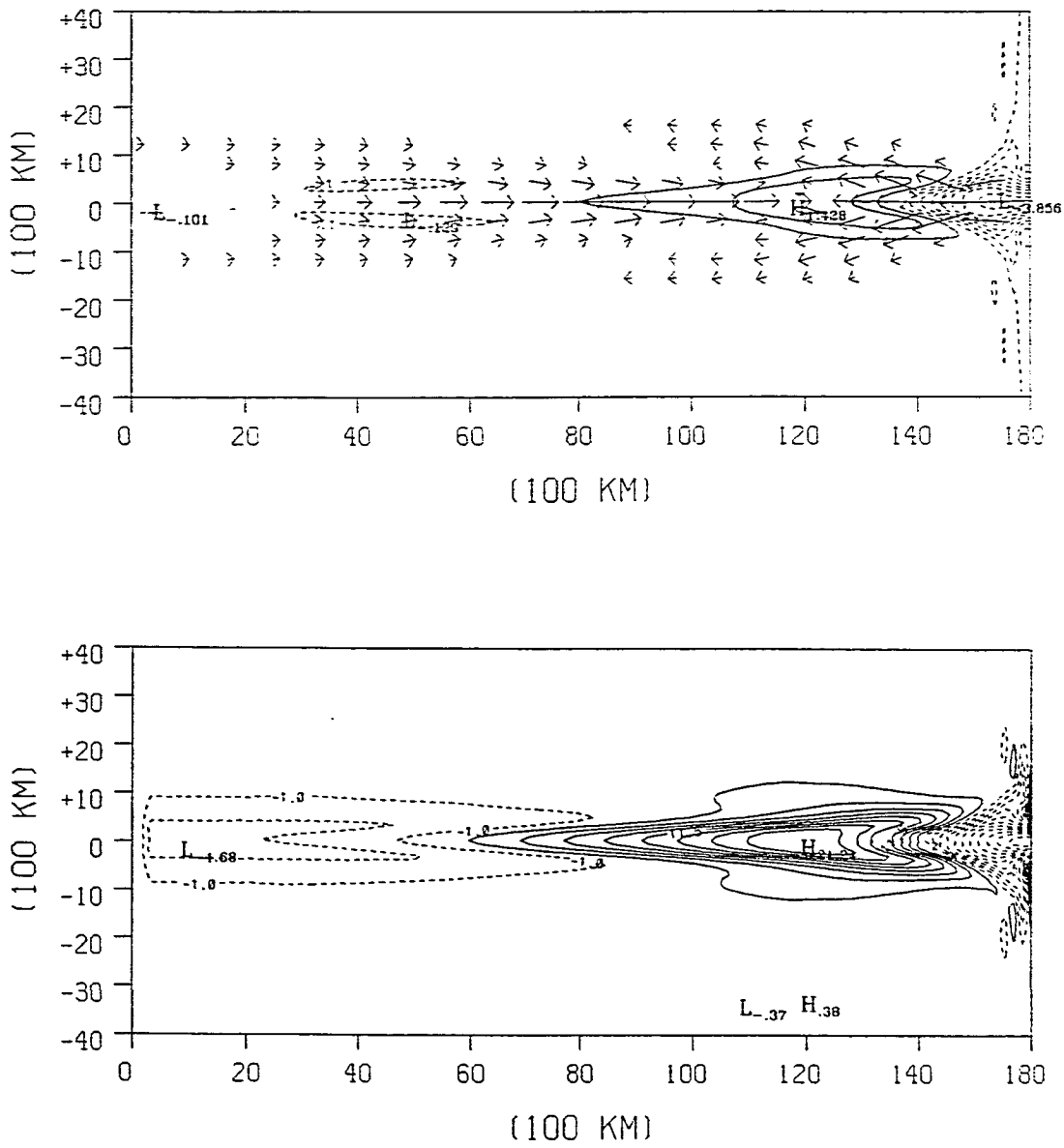


Fig.29: (a) Anomalous SST and wind fields at the 1090th day in experiment#4; (b) anomalous depth of thermocline.

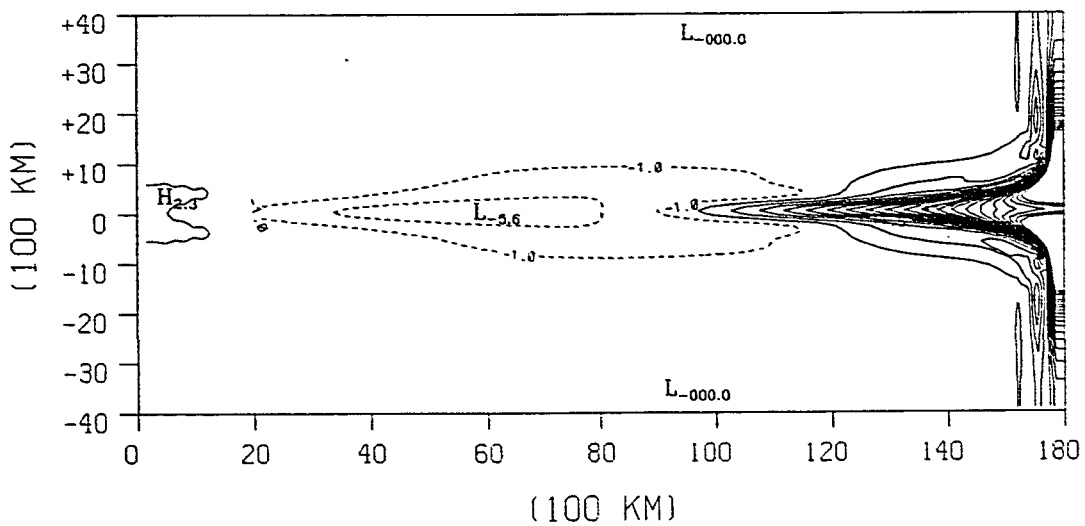
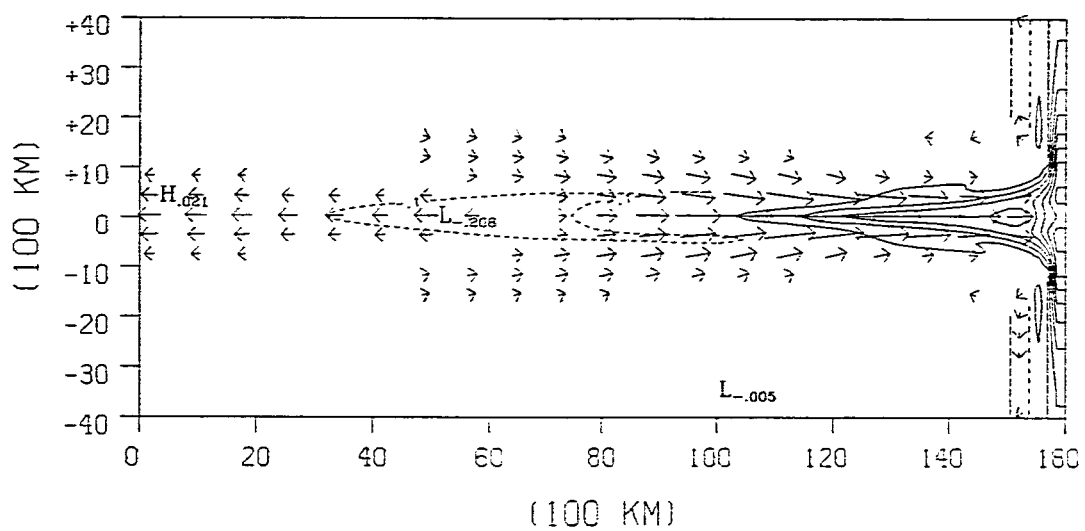


Fig.30: (a) Anomalous SST and wind fields at 1250th day in experiment#4;
 (b) anomalous depth of thermocline.

SST is lower and the easterly winds start to dominate over the western ocean (Fig.30(a)).

The oscillation in this model is set by the following processes: warm SST in the eastern Pacific Ocean ==> westerly winds in the central Pacific ==> upwelling long Rossby waves ==> local cooling ==> easterly winds ==> upwelling Kelvin waves ==> cooling mechanism intensifies and propagates eastward ==> terminating warm SST and developing cold event ==> easterly winds in the central Pacific ==> downwelling long Rossby waves ==> local warming ==> westerly winds ==> downwelling Kelvin waves ==> warming intensifies and propagates eastward ==> warming in the eastern Pacific. These processes describe an oscillation cycle.

By comparing the first three experiments, the condition of the first experiment is regarded as the normal condition of the Pacific Ocean where the interannual oscillation is believed to be self-sustained. If the mean thermal structure remains unchanged, the model suggests that the ocean should experience an oscillation with approximately the same amplitude unless other processes are introduced. If the Pacific Ocean possessed the same mean climatological condition as that in the second experiment, the self-sustained oscillation could then be impossible. Each El Niño episode requires a suitable initial condition to trigger it. If the thermocline slope barrier is weaker, as in the third experiment, exceptionally strong oscillations will be sustained unless some limiting factors, such as nonlinearity, are included. The ocean condition in the Pacific is varying. Some of these variations are in part due to the ENSO variations, and some are attributable to the extra-equatorial influences. If

the oceanic condition just before the onset of an El Niño event has drifted from the normal condition (such as the mean seasonal cycle) to the condition of experiment#2, it is unfavorable for the further development of ENSO. Under this condition, one might expect a small El Niño or an aborted El Niño. If the oceanic condition deviated from its seasonal cycle toward a favorable condition, as in the third experiment, the oscillation within this cycle might have a greater amplitude.

Do the wave reflection and modal decomposition mechanisms play a crucial role in determining the evolution of these oscillatory modes? In experiment 2, a steep thermocline enhances this damping mechanism. To detect this damping effect, we take a snapshot of the model state at the 90th day in the second experiment. Fig.31(a) shows the anomalous SST and wind fields. Two separate warm SST patches are observed in the eastern ocean along the equator. These two warm SST patches are induced by the first and second mode Kelvin waves after the original incident Kelvin wave propagated through the thermocline front. This process is clearly shown in the contours of the anomalous thermocline depth (Fig.31(b)). The amplitude of the second Kelvin mode is about 20 meters and the amplitude of the first Kelvin mode is smaller. This agrees with the results of Gill and King (1985) who showed that modal decomposition could be so effective that the second mode Kelvin wave might have greater amplitude than the first mode Kelvin wave in the eastern ocean. However, the amplitude of the anomalous SST associated with the first Kelvin mode is greater than that of the second Kelvin mode. The anomalous winds are weaker between these two warm SST patches (Fig.31(a)). If there was no such damping mechanism, the anomalous wind would have its maximum amplitude

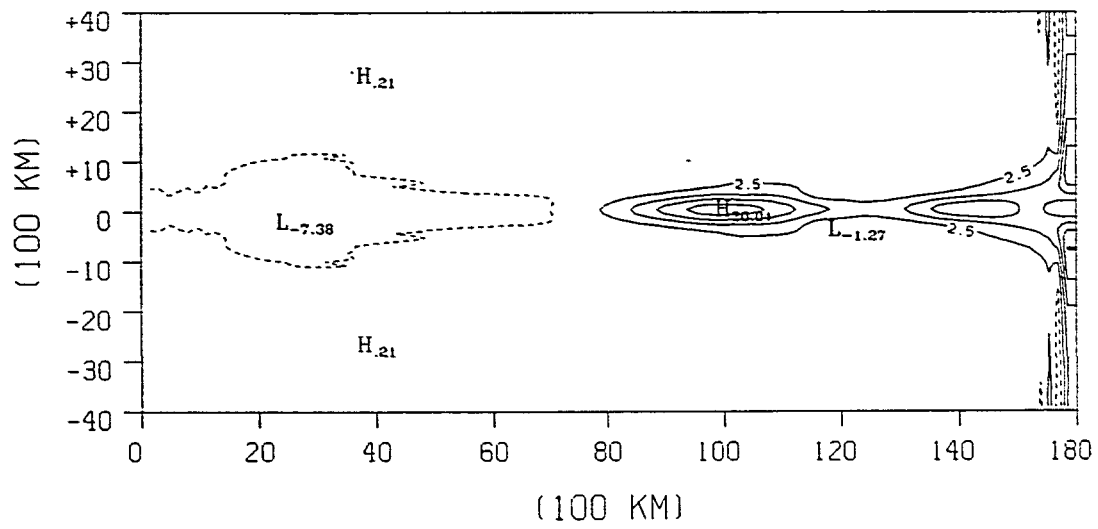
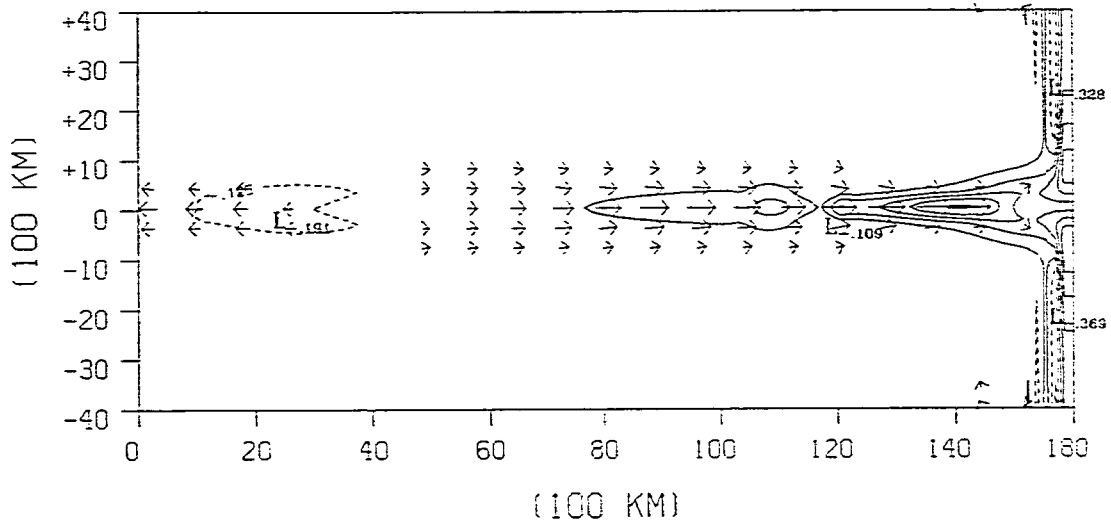


Fig.31: (a) Anomalous SST and wind fields at 90th day in experiment#2;
 (b) anomalous depth of thermocline.

near the center of the SST anomaly (see Fig.11(a)). The weakening of the winds over the warm SST associated with the first baroclinic mode reduces the intensity of the air-sea coupling. The SST field in Fig.31(a) is similar to the second initial condition used in the simple model (Fig.13).

The condition shown in Fig.31 is taken from the early stage of the model evolution. In fact, the modal decomposition is resulted from the initial disturbance propagating through the thermocline slope. Does this damping mechanism play an important role in the later development of the model oscillation? The modal decomposition and wave reflection are not easy to be detected in the longitude-time plot, such as Fig.21(a) of the first experiment. In order to examine this mechanism, we plot the model conditions at the 670th day of the first experiment and at the 760th day of the second experiment when the unstable waves have just propagated through the thermocline slope. The eastern Pacific Ocean, in the first experiment, is dominated by the upwelling process. The thermocline is shallow (Fig.32(b)) and the temperature is lower (Fig.32(a)). There is a small amplitude Rossby wave located between $x=12,000\text{km}$ and $x=14,000\text{km}$. The easterly anomalous winds are dominant in the eastern/central Pacific. The easterly winds further intensify the cold event in the eastern ocean. The condition in the second experiment is different. Fig.33(b) shows the anomalous thermocline depth observed in the second experiment which has a steeper thermocline profile. Like the first experiment, the upwelling process is dominant in the eastern ocean. However, the amplitudes of the reflected Rossby waves are greater (Fig.33(b)). The anomalous SST field is plotted in Fig.33(b). The negative SST is divided into two patches. The easterly winds are absent between

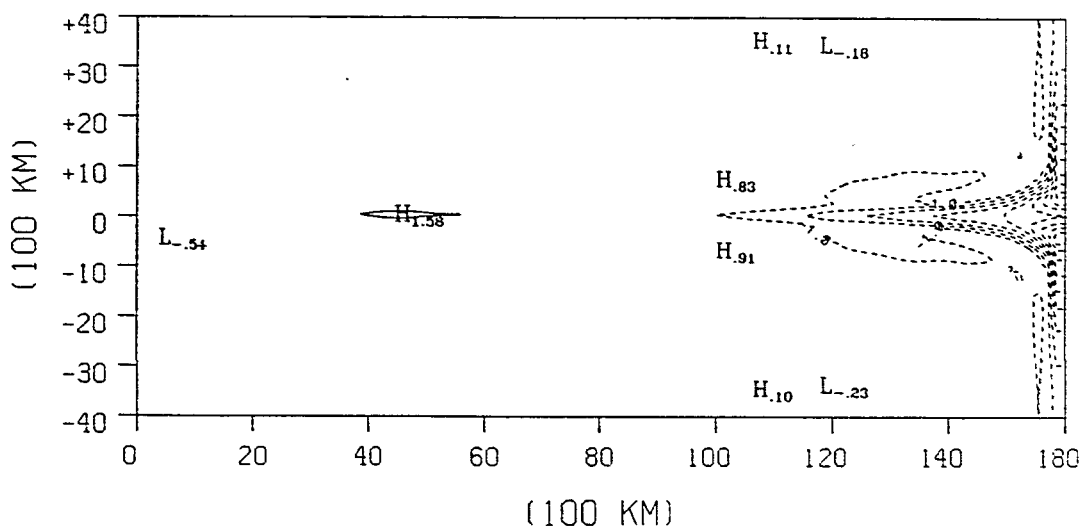
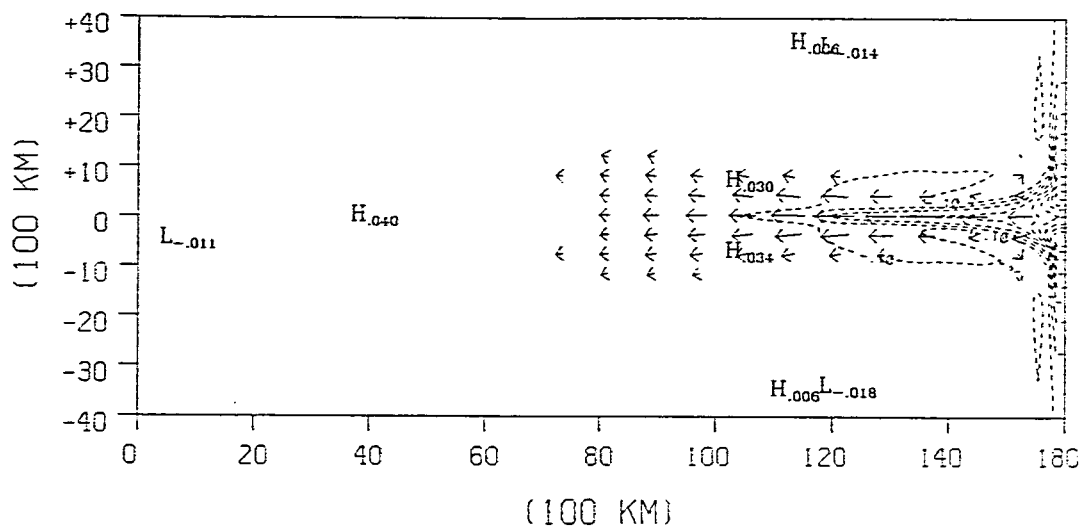


Fig32: The model conditions of experiment#1 at the 670th day, (a) the anomalous SST and winds; (b) the anomalous thermocline depth.

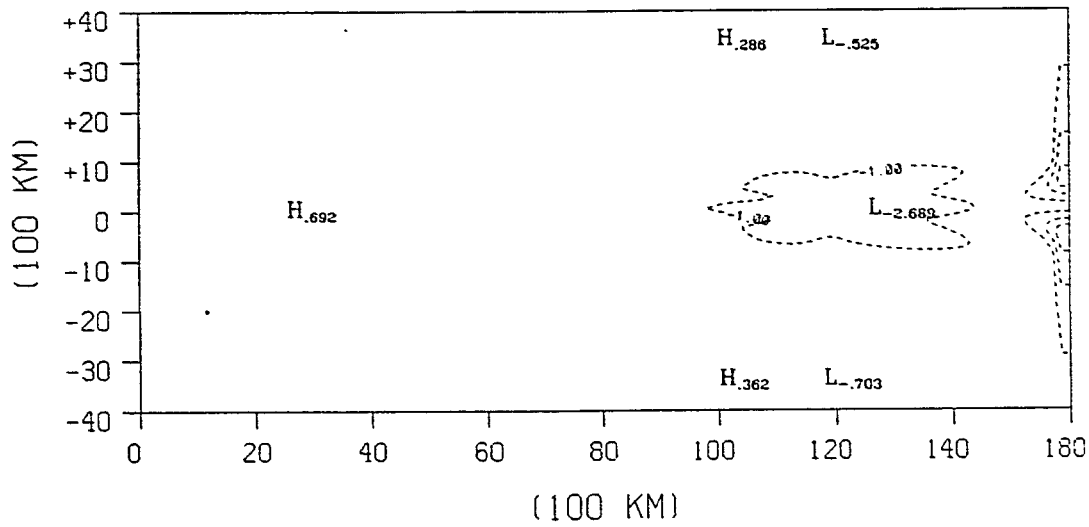
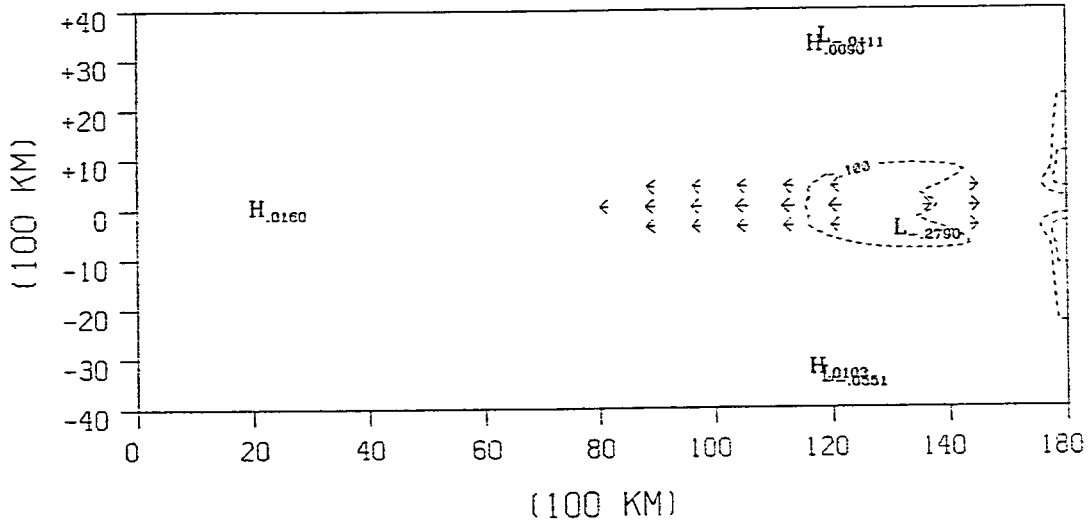


Fig33: The model conditions of experiment#2 at the 760th day, (a) the anomalous SST and winds; (b) the anomalous thermocline depth.

these two patches (Fig.33(a)). Hence the model continues to decay in this experiment.

As we discussed in Section 3, there are two mechanisms which determine the oscillations. The positive feedbacks between the ocean and the atmosphere tend to enhance the anomalous conditions. The damping mechanism (Newtonian cooling, Rayleigh friction, etc.) tends to terminate the disturbances and brings the system back to the state of equilibrium. The oscillation is resulted from the competition between these two opposite mechanisms. Hence the result of the simple model can be used to explain the decayed oscillations in experiment#2 of the intermediate model.

There are some small amplitude disturbances observed off the eastern boundary in Fig.29-31. These disturbances are probably due to the distorted physics caused by the coarse model resolution. The model resolution is $\Delta x = 1.5^\circ$ in longitude. The trapping scale in the eastern boundary is in the order of the Rossby deformation radius which is about 30 kilometers in the mid-latitude. Hence the coastally trapped variabilities are distorted. Fortunately the model behaves well within the equatorial zone.

There are very few continuous long time observations of the vertical thermal structures along the equatorial Pacific Ocean. Fortunately, the 1982/83 El Niño event, which was exceptionally strong, was documented and studied. Fig.34 shows the low-pass filtered isotherm fluctuations at $109^\circ 30' W$ and $95^\circ W$ from June, 1981 to May, 1983. During a normal year, the thermocline in the central and eastern tropical Pacific is steep and shallow. However, when the thermocline slope relaxes, the slope becomes less steep and the thermocline becomes deeper in the eastern equatorial

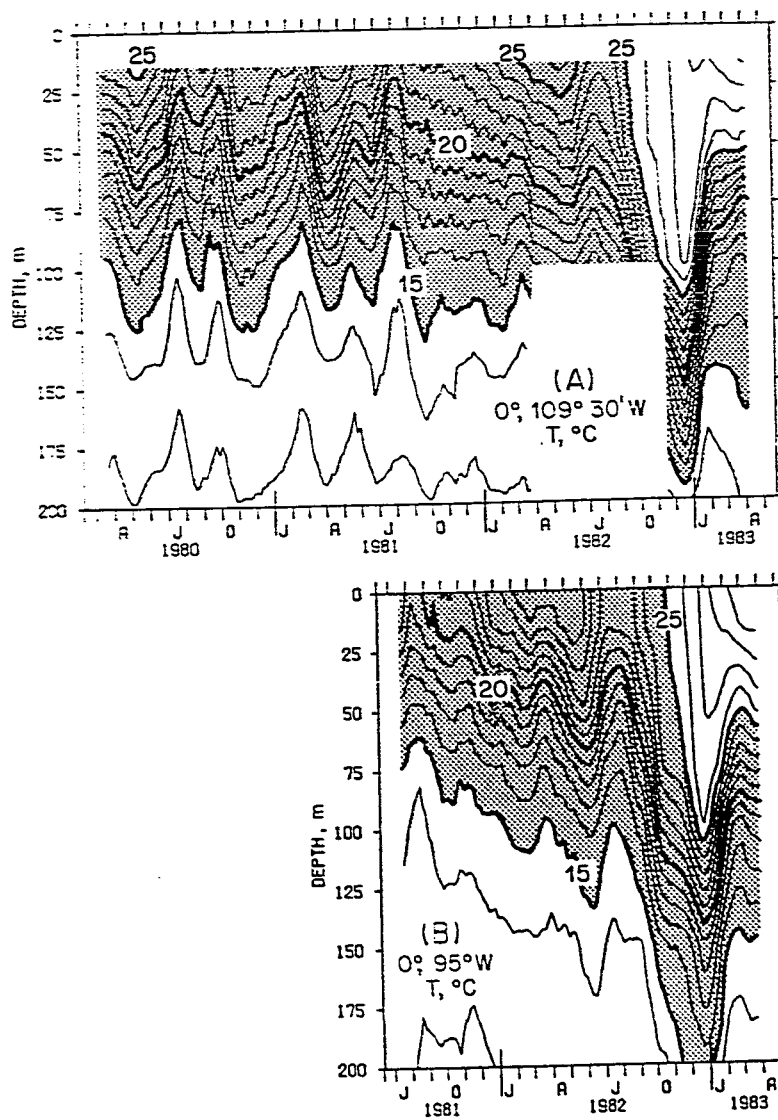


Fig.34: Low pass (31 day running mean) filtered isotherm fluctuations at (a) $109^{\circ}30'W$ and (b) $95^{\circ} W$ from 1981 to 1983 (from Halpern, 1984).

Pacific Ocean. For example, when an El Niño occurs, the zonal variation of the thermocline depth is small. When a cold event develops, the thermocline becomes shallow in the central Pacific Ocean and surfaces in the eastern tropical Pacific Ocean. As Fig.34 clearly shows, the thermocline started to depress from the month of June, 1981. The depression of the thermocline in the eastern and central Pacific Ocean indicates a relaxation of the thermocline slope. Hence it created a favorable condition for the development of El Niño. By the month of July, 1982 just about the onset of the 1982/83 El Niño, the isotherm of 20°C depth at 109°30'W reached 75 meters compared with 25 meters one year before at the same season. The measurement shows that about one year before the 1982/83 El Niño, the thermocline slope in the central and eastern equatorial Pacific Ocean already started to relax. This relaxation of the thermocline slope helped the subsequent development of the El Niño event. If the thermocline slope remained normal in 1981 and 1982 before the onset of the 1982/83 El Niño, the amplitude of the anomalous SST could be smaller. In the experiment#2, the sloping area of the thermocline is located near the eastern boundary. We also fix the mean thermocline depth near the eastern boundary. In the real ocean, the thermocline surfaces in the central and eastern Pacific Ocean when it becomes steeper. If we adopted such a thermocline profile, numerical instabilities would immediately develop. The adoption of the thermocline profile in experiment#2 is to avoid such undesired numerical instabilities.

V. Summary

A tropical atmosphere-ocean coupled model is used to investigate some important effects of a zonally sloping thermocline on the coupled instabilities in the tropical Pacific. The atmospheric component of the model is Gill's (1980) steady state model, and the oceanic model consists of a constant-depth mixed-layer and two active upper ocean layers overlying a motionless deep ocean. The thermodynamics are included in the mixed layer. The SST is determined by the advectations and the vertical entrainments. The temperature anomaly of the entrained water (at the base of the mixed layer) is determined by the vertical movement of the main thermocline. The relationship between the entrained water temperature (at 50 meters) and the depth of the 20°C isotherm derived by Seager et al. (1988) is used in this model. The interface of the two upper layers is sloping and prescribed as the observed 20°C isotherm in the Pacific Ocean.

The unstable waves behave like the propagating modes with greater SST anomalies observed in the eastern Pacific Ocean. It is found that the coupled instabilities are very sensitive to the steepness of the tilted thermocline in the central Pacific Ocean. The effects of the sloping thermocline on the thermodynamics have been studied in several previous works (such as Zebiak and Cane, 1987; Battisti, 1988). Our model also shows that the sloping thermocline is also very important in the coupled dynamics. When a first baroclinic mode Kelvin wave-like warm (cold)

event propagates through the steep sloping thermocline in the central equatorial Pacific Ocean, it undergoes an energy exchange with higher baroclinic modes. As a result of modal exchange, warm (cold) Rossby waves are formed as reflected waves, and the remaining energy forms first baroclinic mode and second baroclinic mode Kelvin waves. The reflected Rossby waves not only reduce the amplitude of the unstable Kelvin waves by removing part of their energy, but also induce convergent (divergent) winds. The induced wind anomaly further reduces the amplitudes of the unstable Kelvin waves. The first mode Kelvin wave and the second mode Kelvin wave damp each other through their induced winds. A series of numerical experiments with different thermocline profiles have been performed.

A simple coupled model is also used to explain the physics. Gill's atmosphere model and Hirst's (1986) ocean model are coupled. By using two different initial conditions, this simple model produces two equilibrium states. When the initial condition is favorable for the positive feedbacks between the atmosphere and the ocean, an interannual oscillation is sustained with a period of 3 years. When the initial condition is unfavorable for the coupled system, the initial disturbance damps and the system comes back to the equilibrium state of rest. The simple model is used to help us explain the model results obtained from a more complicated model.

Appendix A: Derivation of linearized equations

The following is the derivation of the linearized equations for an ocean mixed-layer from Hirst (1986). By assuming there is no motion below the mixed layer, the equations are

$$u_t + uu_x + vu_y - \beta yv = -g'H_x + \frac{\tau^x}{\rho_0 H} - \frac{w_e u}{H} + \nu \nabla_H^2 u \quad (\text{A1})$$

$$v_t + uv_x + vv_y + \beta yu = -g'H_y + \frac{\tau^y}{\rho_0 H} - \frac{w_e v}{H} + \nu \nabla_H^2 v \quad (\text{A2})$$

$$H_t + (Hu)_x + (Hv)_y = w_e \quad (\text{A3})$$

$$T_t + uT_x + vT_y = -\frac{w_e \Delta T}{H} + \frac{f_2(H) I_0 - F_0}{(\rho_0 c_w H)} + \nu \nabla_H^2 T \quad (\text{A4})$$

where (u,v) are the velocity components, (τ^x, τ^y) are the wind stress components, $T = T_0 + T'$ is the SST in the mixed layer, ΔT is the temperature difference between the mixed layer and the deep layer, $H=H_0 + h$ is the depth of the mixed layer, w_e is the entrainment rate across the mixed layer base, ν is the horizontal eddy viscosity, ρ_0 is the density of water, I_0 is the net downward insolation flux at the surface, F_0 is the sum of sensible, latent and longwave radiant heat loss, c_w is the heat capacity of sea water, and $f_2(H)$ represents the proportion of I_0 absorbed within the mixed layer.

The entrainment rate is estimated by the Kraus-Turner formula calibrated by Garwood (1977):

$$w_e = \frac{2mu_*^3}{\alpha'gH\Delta T} + \frac{n}{\rho_0c_w\Delta T}(F_0 - f_1(H)I_0) \quad (A5)$$

where m is the wind mixing entrainment calibration coefficient, n is the thermal mixing entrainment calibration coefficient, u_* is the surface friction velocity, α' is the thermal expansion coefficient, and $f_1(H)$ is a function required to account for the effects of penetrating radiation on w_e .

Hirst (1986) linearized (A1) - (A4) on a basic state of no mean flow, and a mean depth H_0 and mean SST $T_0(x,y)$. The linearized equations for the perturbed quantities are:

$$u_t - \beta y v = -g' h_x + \tau^x/(r_0 H_0) - au \quad (A6)$$

$$v_t + \beta y u = -g' h_y + \tau^y/(r_0 H_0) - av \quad (A7)$$

$$h_t + (H_0 u)_x + (H_0 v)_y = -bh + K_E T' \quad (A8)$$

$$T'_t + uT'_{0x} + vT'_{0y} = \sigma h - \alpha T' \quad (A9)$$

where T' is the anomalous SST. All the coefficients, a , b , K_E , σ and α are related to m , n , F_0 , I_0 , c_w , u_* , v etc. The horizontal mixing terms in (A1-4) are approximated as: $v\nabla_H^2 \sim v \partial^2/\partial y^2 \sim -v\lambda^{-2}$ where λ is the deformation radius. Hirst (1986) estimated all the coefficients in (A7) - (A9) and concluded that $K_E T'$ is very small.

The meridional advection term vT'_{0y} is usually less important than the zonal advection term uT'_{0x} . In the equatorial oceans, the meridional scale of motion is much smaller than the zonal length scale. In fact, the trapping scales of Kelvin waves and gravest mode Rossby waves are less than 10° in latitude. Hence, u has an order of magnitude greater than v . The zonal variation of mean SST is about 7°C - 8°C across the equatorial Pacific. The mean SST variation within 10° in latitude is small. In fact,

ΔT_0 between the equator and 10°N (or 10°S) is less than 1°C in most area of the equatorial Pacific (between 120°E to 150°W) except for a small area near the eastern boundary where ΔT_0 between the equator and 10°N reaches 2 - 4°C . We can compare these two advection terms by a scaling analysis, i.e.,

$$\frac{v}{u} \sim L_y/L_x$$

$$\delta = \frac{vT'_{0y}}{uT'_{0x}} \sim (\Delta T_0)^y / (\Delta T_0)^x$$

where $(\Delta T_0)^x \sim 7^\circ\text{C}$ to 8°C is the difference of the mean SST between the eastern and western equatorial Pacific, $(\Delta T_0)^y \sim 0.5^\circ\text{C}$ - 3°C is the mean SST difference between the equator and 10°N or 10°S . In most areas, δ is very small (~ 0.1) except for a small area near the eastern boundary where δ reaches a value of about $0.2 \sim 0.4$. In our conceptual model, we neglect this term in order to simplify the equations. We should point out that the meridional advection term vT'_{0y} is not in the negligible order near the eastern boundary.

Based on the above discussions, the linearized equations (A8) and (A9) can be further simplified to

$$h_t + (H_0 u)_x + (H_0 v)_y = -bh \quad (\text{A8})$$

$$T'_t + uT'_{0x} = \sigma h - \alpha T' \quad (\text{A9})$$

Appendix B: Mean flow effects

The fully linearized equations are:

$$u_t + u_0 u_x + u u_{0x} + v u_{0y} + v_0 u_y - \beta y v = -g' h_x - a u + \tau^x / (\rho_0 H_0) \quad (B1)$$

$$v_t + u_0 v_x + u v_{0x} + v v_{0y} + v_0 v_y + \beta y u = -g' h_y - a v + \tau^y / (\rho_0 H_0) \quad (B2)$$

$$h_t + H_0 (u_x + v_y) + h_x u_0 + h_y v_0 + h(u_{0x} + v_{0y}) = -b h \quad (B3)$$

$$T_t + u T_{0x} + v T_{0y} + u_0 T_x + v_0 T_y = \sigma h - \alpha T \quad (B4)$$

where T is the anomalous SST, (u, v) are the anomalous velocity components, H_0 is the mean depth of the mixed layer, T_0 is the mean SST, and (u_0, v_0) are the velocity components of the mean currents.

From equation (B3), we can estimate the scale of h :

$$\left[\frac{\partial h}{\partial t} \right] \sim H_0 \left[\frac{\partial u}{\partial x} \right] \quad (B5)$$

therefore we have

$$[h] \sim \frac{H_0 [u][t]}{[x]} \quad (B6)$$

where $[t]$, $[x]$, $[h]$, and $[u]$ are the scales of time, zonal length, anomalous upper-layer thickness and anomalous current velocity.

The ratio of the linearized advection terms, e.g., $u_0 u_x$, to the pressure gradient $-g' h_x$ in (B1) is:

$$\frac{[u_0 u_x]}{[g' h_x]} \sim \frac{[u_0][u]}{[x]} / \frac{g'[h]}{[x]} \sim \frac{[u_0][u]}{g'[h]} \quad (B7)$$

Substituting (B6) into (B7), we obtain

$$\frac{[u_0 u_x]}{[g'h_x]} \sim \frac{[u_0][x]}{g'H_0[t]} \quad (\text{B8})$$

If we define $u^* = [x]/[t]$, which is the characteristic velocity; and $c = \sqrt{g'H_0}$, which is the Kelvin wave speed, (B8) can be written as:

$$\frac{[u_0 u_x]}{[g'h_x]} \sim \frac{[u_0]u^*}{c^2} \quad (\text{B9})$$

The Kelvin wave is the fastest traveling wave in the tropics, hence we have

$$\frac{u^*}{c} < 1 \quad (\text{B10})$$

The mean surface currents in the equatorial Pacific Ocean are complicated. Between 9°S and 5°N along the equator, the westward SEC (South Equatorial Current) dominates. The eastward NECC (North Equatorial Countercurrent) is located between 5°N and 10°N. A weak and narrow SECC (South Equatorial Countercurrent) also exists south of the SEC. Since we are mostly interested in the equatorial area, we emphasize the effects of the SEC. The SEC is a relatively weak current with a typical speed less than 20cm/s (Philander, 1990). In fact, the measurements conducted during the Hawaii-to-Tahiti Shuttle Experiment indicates that the mean current speed of SEC is about 9.7cm/s (Wyrтки and Kilonski, 1984). Stronger currents are present near the equator, e.g., 24.8 cm/s were observed between the equator and 4°N, and 14.2 cm/s was observed between the equator and 9°S (Wyrтки and Kilonski, 1984). In order to estimate (B9), 20cm/s is taken as a typical value of the mean current. With the relation (B10) we can estimate (B9) as

$$\frac{[u_0 u_x]}{[g'h_x]} < \frac{[u_0]}{c} = \frac{0.2}{2} = 0.1 \quad (\text{B11})$$

which shows that the term $[u_0 u_x]$ is at least one order smaller than the pressure term and can be neglected. Similarly, we can prove that all the other linearized advection terms in (B1) and (B2) are small. Therefore (B1) and (B2) can be simplified as:

$$u_t - \beta y v = -g' h_x - au + \tau^x / (\rho_0 H_0) \quad (\text{B12})$$

$$v_t + \beta y u = -g' h_y - av + \tau^y / (\rho_0 H_0) \quad (\text{B13})$$

Now we consider those terms associated with the mean currents in the continuity equation (B3). By using (B6), we have

$$\frac{[h_x u_0]}{[H_0 u_x]} \sim \frac{u_0}{u^*} \quad (\text{B14})$$

u^* is the characteristic velocity which is not necessarily greater than the mean current velocity u_0 . Hence the effects of the mean currents are not always negligible.

The advection terms associated with mean currents in the SST equation are discussed in Appendix E.

Appendix C: Derivation of Gill's steady state atmosphere model

Consider a two-level model of the atmosphere. There are two modes in this model, i.e., the barotropic mode and the baroclinic mode. Attention is confined to the baroclinic mode for which the horizontal components of velocity have opposite signs in the two layers. The shallow-water equations have the form

$$U_t - \beta y V = -P_x - AU \quad (C1)$$

$$V_t + \beta y U = -P_y - AV \quad (C2)$$

where (U,V) are horizontal velocities at some level representative of the lower troposphere, $-A(U,V)$ represents Rayleigh friction. The continuity equation in the lower layer is

$$H_0 (U_x + V_y) + w = 0 \quad (C3)$$

where w is the vertical velocity at some middle atmospheric level, and H_0 is the lower layer depth. The equation for the potential temperature perturbation is

$$\theta_t + (\theta_0 N^2/g) w = Q' - B\theta \quad (C4)$$

where θ_0 is the mean potential temperature, $-B\theta$ represents Newtonian cooling, N is the buoyancy frequency, and Q' is the heating rate at the middle level. The perturbation pressure P is related to θ by the hydrostatic equation, i.e.,

$$P = -H_0 g\theta/\theta_0 \quad (C5)$$

From (C3)-(C5), we may eliminate w and obtain a equation:

$$P_t + C^2 (U_x + V_y) = -Q - BP \quad (C6)$$

where $Q = (H_0 g/\theta_0)Q'$ and $C = N H_0$. The steady state version of (C1), (C2) and (C6) is the steady state model of the atmosphere. A derivation and a detailed discussion of this model are given by Gill (1982b).

Appendix D: Derivation of pressure gradients in all layers

In this appendix we derive the pressure gradients in all active layers. We assume that the density of the mixed layer is dependent on the SST anomalies, i.e.,

$$\rho_m = \rho_0 (1 - \alpha T) \quad (D1)$$

where α is the thermal expansion coefficient.

We assume that, D_m , D_1 , D_2 and D_3 are the undisturbed depths of the mixed layer, upper layer, lower layer and deep ocean. H_1 , H_2 and H_3 are the layer thicknesses of the upper, lower and deep layers. ρ_1 , ρ_2 and ρ_3 are the water densities in the upper layer, lower layer and deep ocean. These densities are assumed to be constant. The model is shown in Fig.35.

The pressures in all layers are:

$$p_m = \rho_m g [D_m + H_1 + H_2 + H_3 - z] \quad (D2)$$

$$p_1 = \rho_m g D_m + \rho_1 g [H_1 + H_2 + H_3 - z] \quad (D3)$$

$$p_2 = \rho_m g D_m + \rho_1 g H_1 + \rho_2 g [H_2 + H_3 - z] \quad (D4)$$

$$p_3 = \rho_m g D_m + \rho_1 g H_1 + \rho_2 g H_2 + \rho_3 g [H_3 - z] \quad (D5)$$

We assume that the pressure gradient vanishes in the deep layer. Hence, $\nabla p_3 = 0$ gives

$$\rho_3 \nabla H_3 = -D_m \nabla \rho_m - \rho_1 \nabla H_1 - \rho_2 \nabla H_2 \quad (D6)$$

By using (D6) to eliminate ∇H_3 , the pressure gradients in the mixed layer, upper layer and lower layer become

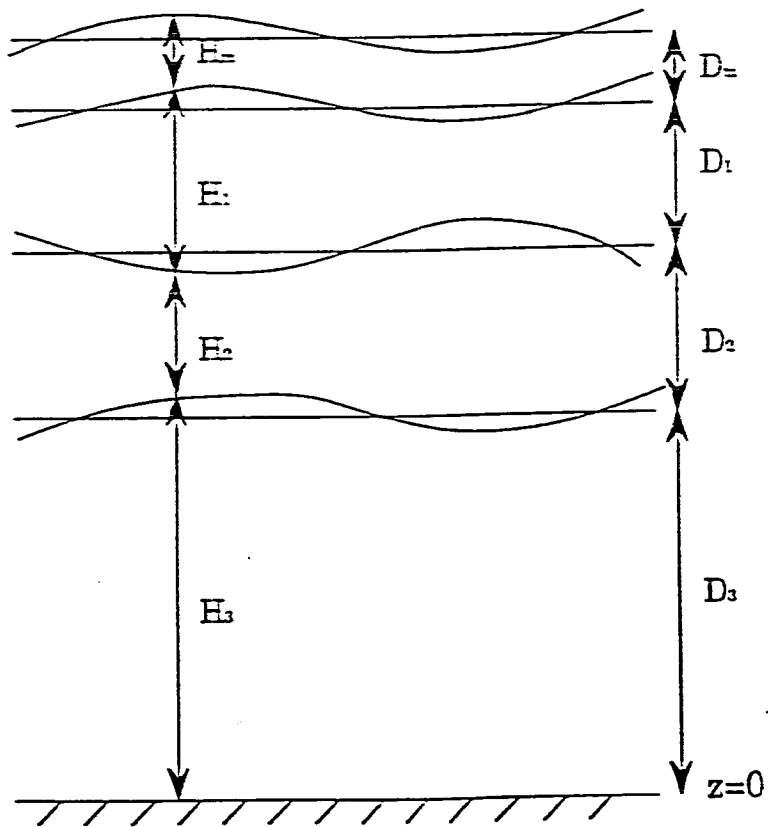


Fig. 35: The model configuration in the vertical direction.

$$\nabla p_m = -\frac{1}{2} g D_m \nabla \rho_m + g \rho_m \left[\frac{\rho_3 - \rho_1}{\rho_3} \right] \nabla H_1 + g \rho_m \left[\frac{\rho_3 - \rho_2}{\rho_3} \right] \nabla H_2 \quad (D7)$$

$$\nabla p_1 = g D_m \left[\frac{\rho_3 - \rho_2}{\rho_3} \right] \nabla \rho_m + g \rho_1 \left[\frac{\rho_3 - \rho_1}{\rho_3} \right] \nabla H_1 + g \rho_1 \left[\frac{\rho_3 - \rho_2}{\rho_3} \right] \nabla H_2 \quad (D8)$$

$$\nabla p_2 = g D_m \left[\frac{\rho_3 - \rho_2}{\rho_3} \right] \nabla \rho_m + g \rho_2 \left[\frac{\rho_3 - \rho_1}{\rho_3} \right] \nabla H_1 + g \rho_2 \left[\frac{\rho_3 - \rho_2}{\rho_3} \right] \nabla H_2 \quad (D9)$$

In all layers, there are additional pressure gradients due to the SST anomalies in the mixed layer. It is instructive to compare the SST anomaly induced pressure gradient to the bulk pressure gradients

$$\left[\frac{1}{2} g D_m \nabla \rho_m \right] = 0.5 \times g \times 50 \times \frac{[T] \alpha \rho_0}{L} \quad (D10)$$

where L is the horizontal scale of SST variations.

Now, let's consider the second term of (D7),

$$\left[g \rho_m \left[\frac{\rho_3 - \rho_1}{\rho_3} \right] \nabla H_1 \right] = g \rho_m \frac{[T_3 - T_1] \alpha \rho_0 [H_1]}{L \rho_3} \quad (D11)$$

The typical amplitude of SST variation is about $[T] = 3^\circ\text{C}$, and the temperature difference between upper layer and the deep ocean is about $[T_3 - T_1] = 25^\circ\text{C}$. The east-west thermocline variation is taken as $[H_1] = 50$ meters. Hence the ratio between (D10) and (D11) is

$$\left[\frac{1}{2} g D_m \nabla \rho_m \right] / \left[g \rho_m \left[\frac{\rho_3 - \rho_1}{\rho_3} \right] \nabla H_1 \right] = \frac{0.5 [T]}{[T_3 - T_1]} = 0.5 \times \frac{3}{25} = 0.06$$

Hence the SST anomaly induced pressure gradient is small. A similar analysis shows that effects of the SST anomaly can be neglected in the pressure gradients in the two layers below the mixed layer.

Appendix E: Effects of mean flow in the SST equation

In this appendix, we perform a scaling analysis to estimate the mean current advectations in the SST equation. The SST equation (4.7) has the form:

$$T_t = -\mathbf{u}_m \cdot \nabla T_0 - \mathbf{u}_0 \cdot \nabla T - \{M(W_0 + w) - M(W_0)\} \frac{T_0 - T_{\text{sub}}}{H_m} - M(W_0 + w) \frac{T - T_e}{H_m} - \alpha T \quad (\text{E1})$$

In this coupled model, anomalous winds are induced by the SST anomaly and anomalous ocean currents are forced by anomalous winds. From these relations, we may derive a relation between the magnitude of the SST anomaly and the magnitude of the anomalous ocean currents.

In Gill's atmosphere model, the heating of anomalous evaporation drives the anomalous winds, i.e.,

$$C^2 (U_x + V_y) = -Q - \gamma P \quad (\text{E2})$$

and the heating term Q is related to the SST anomaly by the Clausius-Clapeyron equation:

$$Q = \phi C^2 (2\beta/C)^{1/2} \left[\frac{T_{\text{ref}}}{T_0} \right]^2 \exp(b(1/T_{\text{ref}} - 1/T_0)) T \quad (\text{E3})$$

where $\phi = 1.6 \text{ m } ^\circ\text{K} / \text{s}$ and $b = 5400 \text{ } ^\circ\text{K}$ are constants. $C = 60 \text{ m/s}$ is the phase speed of internal gravity waves in the atmosphere. $T_{\text{ref}} = 303 \text{ } ^\circ\text{K}$ is

the reference temperature. The values of all these parameters are chosen the same as that used in Battisti (1988).

From (E2) we have

$$U \sim C^{-2} L_a Q \quad (\text{E4})$$

where L_a is the zonal scale of anomalous winds which is estimated by the deformation radius $(C/\beta)^{1/2} \sim 1.625 \times 10^6$ meters.

The wind stress is estimated by the aerodynamic bulk formula

$$\tau = \rho_a C_D |U| U \quad (\text{E5})$$

where ρ_a is the density of air, C_D is the wind stress drag coefficient. In this work, $\rho_a C_D = 3.2 \times 10^{-3} \text{ kg m}^{-3}$ is used (same as Zebiak, 1984). From (E3)-(E4), a relation between anomalous SST and wind stress can be derived, i.e.,

$$\tau \sim \rho_a C_D L_a^2 \phi^2 (2\beta/C) \left[\frac{T_{\text{ref}}^4}{T_0} \right] \exp(2b(1/T_{\text{ref}} - 1/T_0)) (\Delta T)^2 \quad (\text{E6})$$

where ΔT is the magnitude of the anomalous SST.

The anomalous currents in the mixed layer are dominated by the frictional Ekman flow which is governed by the following equations:

$$r_s u_s - \beta y v_s = \tau_x / (\rho_0 H_m) \quad (\text{E7})$$

$$r_s v_s + \beta y u_s = \tau_y / (\rho_0 H_m) \quad (\text{E8})$$

The Coriolis force is small near the equator, and the main balance is between the wind stress and the friction term $-r_s(u_s, v_s)$. Hence,

$$u_s \sim \tau_x / (r_s \rho_0 H_m) \quad (\text{E9})$$

From (E6) and (E9), we have

$$u_s \sim 2\rho_a C_D L_a^2 \phi^2 \beta / (r_s \rho_0 H_m C) \left[\frac{T_{\text{ref}}^4}{T_0} \right] \exp(2b(1/T_{\text{ref}} - 1/T_0)) (\Delta T)^2 \quad (\text{E10})$$

The ratio between the two zonal advection terms can be estimated now, i.e.,

$$\frac{u_0 T_x}{u T_{0x}} \sim u_0 \Delta T / (u \Delta T_0) \quad (\text{E11})$$

where u_0 and ΔT_0 are the scales of the mean zonal currents and the east-west difference of the mean SST.

In order to estimate (E11), 20 cm/s is taken as a typical value of the mean current (Appendix B). The mean SST is about 30°C in the western warm pool and about 22° C near the eastern boundary. Hence $\Delta T_0 = 8^\circ\text{C}$ is taken as the zonal mean SST difference. If u is estimated by (E10) and ΔT is taken to be 3°C, (E11) becomes

$$\begin{aligned} \delta_u &= \frac{u_0 T_x}{u T_{0x}} \sim u_0 \Delta T / (u \Delta T_0) \\ &\sim 0.18 \end{aligned} \quad (\text{E13})$$

Neelin (1991) performed a different scaling analysis with multiple time scales (fast free wave and slow SST mode) and found that δ_u ranges from 0.2 to 0.4. Strictly speaking, 0.18 is not a very small value and the neglect of $u T_{0x}$ is not rigorously justified. It also must be pointed out that the ratio of these two advection terms depends on the values of all parameters. For example, a greater value of zonal scale of winds L_a will lead to a smaller value of δ_u (the zonal wind scale is usually greater than

the deformation radius). There are a great degree of uncertainties about some physical parameters, such as the wind stress drag coefficient and friction coefficient r_s . Battisti (1988) did a sensitivity test by dropping $u_0 T_x$ from (C1) and the model solution was not significantly altered.

The mean meridional current advection $v_0 T_y$ is not always small. Near the edge of SST anomalies in the eastern Pacific, T_y is large. However, its main role is to spread the SST anomaly poleward and broaden the equatorial trapping scale. This term is not essential in producing anomalous SST near the equator (Hirst, 1990).

References

- Adamec, D., and J. J. O'Brien, 1978: The seasonal upwelling in the Gulf of Guinea due to remote forcing. *J. Phys. Oceanogr.*, **8**, 1050-1060.
- Anderson, D. L. T. and J. P. McCreary, 1985: Slowly propagating disturbances in a coupled ocean-atmosphere model. *J. Phys. Oceanogr.*, **42**, 615-629.
- Barnett, T. P., N. Graham, M. Cane, S. Zebiak, S. Dolan, J.J. O'Brien, and D. Legler, 1988: On the prediction of the El Niño of 1986-87. *Science*, **241**, 192-196.
- Battisti, D. S., 1988: The dynamics and thermodynamics of a warm event in a coupled atmosphere/ocean model. *J. Atmos. Sci.*, **45**, 2889-2919.
- Battisti, D. S. and A. C. Hirst, 1989: Interannual variability in a tropical atmosphere-ocean model: Influence of the basic state, ocean geometry and nonlinearity. *J. Atmos. Sci.*, **46**, 1687-1712.
- Battisti, D. S., A. C. Hirst and E. S. Sarachik, 1989: Instability and predictability in coupled atmosphere-ocean models. *Phil. Trans. Roy. Soc. Lond.*, **A329**, 237-247.
- Behringer, D. W., 1984: Equatorial modes in the eastern Pacific (85°W). *J. Geophys. Res.*, **89**, 3729-3731.
- Bjerknes, J., 1966: A possible response of the atmospheric Hadley circulation to equatorial anomalies of ocean temperature. *Tellus*, **18**, 820-829.
- Bjerknes, J., 1969: Atmospheric telconnections from the equatorial

- Pacific Mon. Wea. Rev.*, **97**, 163-172.
- Bryden, H. L. and E. C. Brady, 1985: Diagnostic model of the three-dimensional circulation in the upper equatorial Pacific Ocean. *J. Phys. Oceanogr.*, **15**, 1255-1273.
- Busalacchi, A. J. and J. J. O'Brien, 1980: The seasonal variability of the tropical Pacific. *J. Phys. Oceanogr.*, **10**, 1929-1952.
- Busalacchi, A. J. and J. J. O'Brien, 1981: Interannual variability of the equatorial Pacific in the 1960's. *J. Geophys. Res.*, **86**, 10901-10907.
- Busalacchi, A. J., and M. A. Cane, 1988: The effect of varying stratification on low-frequency equatorial motions. *J. Phys. Oceanogr.*, **18**, 801-812.
- Camerlengo, A. L. and J. J. O'Brien, 1980: Open boundary conditions in rotating fluids. *J. Comp. Phys.*, **35**, 12-35.
- Cane, M. A., 1979: The response of an equatorial ocean to simple wind stress patterns: I. Model formulation and analytic results. *J. Mar. Res.*, **37**, 233-252.
- Cane, M. A., and S. E. Zebiak, 1985: A theory for El Niño and the Southern Oscillation. *Science*, **228**, 1084-1087.
- Clarke, A. J., 1991: On the reflection and transmission of low-frequency energy at the irregular western Pacific Ocean boundary. *J. Geophys. Res.*, **96**, 3289-3306.
- Colin, C., C. Henin, P. Hisard, and C. Oudot, 1971: Le Courant de Cromwell dans le Pacifique central en février. *Cah. ORSTOM, Ser Oceanogr.*, **9**, 167-186.
- Donguy, J. R., 1987: Recent advances in the knowledge of the climate variations in the tropical Pacific. *Prog. Oceanogr.*, **19**, 49-85.

- Eriksen, C. C., M. B. Blumenthal, S. P. Hayes, and P. Ripa, 1983: Wind generated equatorial Kelvin waves observed across the Pacific Ocean. *J. Phys. Oceanogr.*, **13**, 1622-1640.
- Gadgil, S., P. V. Joseph and N. V. Joshi, 1984: Ocean - atmosphere coupling over monsoon regions. *Nature*, **312**, 141-143.
- Garwood, R. W., 1977: An ocean mixed layer capable of simulating climatic stress. *J. Phys. Oceanogr.*, **7**, 455-468.
- Gill, A. E., 1980: Some simple solutions for heat-induced tropical circulation. *Quart. J. Roy. Meteor. Soc.*, **106**, 447-462.
- Gill, A. E., 1982a: Changes in thermal structure of the equatorial Pacific during the 1972 El Niño as revealed by bathythermograph observations. *J. Phys. Oceanogr.*, **12**, 1373-1387.
- Gill, A. E., 1982b: Studies of moisture effects in simple atmospheric models: the stable case. *Geophys. Astrophys. Fluid Dyn.*, **19**, 119-152.
- Gill, A. E., 1985: Elements of coupled ocean-atmosphere models for the tropics. *Coupled Ocean-Atmosphere Models*, J. C. J. Nihoul, Ed., Elsevier Oceanography Series 40, Elsevier, 303-327.
- Gill, A. E. and B. A. King, 1985: The effects of a shoaling thermocline on equatorial-trapped Kelvin waves. *Dynamical Climatology*, DCTN 27, 28pp.
- Halpern, D., 1984: Upper ocean heat content in the eastern equatorial Pacific during the 1882-83 ENSO event. *Trop. Ocean-Atmos. Newslett.*, **24**, 14-16.
- Halpern, D., 1987: Observations of annual and El Niño thermal and flow variations at 0°, 110°W and 0°, 95°W during 180-1985. *J.*

- Geophys. Res.*, **92**, 8197-8212.
- Hirst, A. C., 1985: Free equatorial instabilities in simple coupled atmosphere-ocean models. *Coupled Ocean-Atmosphere Models*, J. C. J. Nihoul Ed., Elsevier Oceanography Series 40, Elsevier, 153-165.
- Hirst, A. C., 1986: Unstable and damped equatorial modes in simple coupled ocean-atmosphere models. *J. Atmos. Sci.*, **43**, 606-630.
- Hirst, A. C., 1988: Slow instabilities in tropical ocean basin-global atmosphere models. *J. Atmos. Sci.*, **45**, 830-852.
- Hirst, A. C., 1990: On simple coupled ocean-atmosphere models, equatorial instabilities, and ENSO. *International TOGA Scientific Conference Proceedings.*, World Meteorological Organization, Technical Document, No. 379, 103-110.
- Hughes, T. L., 1981: The influence of thermocline slope on equatorial thermocline displacement. *Dyn. Atmos. Oceans*, **5**, 147-157.
- Hurlburt, H. E., J. C. Kindle, and J. J. O'Brien, 1976: A numerical study of the onset of El Niño. *J. Phys. Oceanogr.*, **6**, 621-631.
- Inoue, M. and J. J. O'Brien, 1984: A forecasting model for the onset of a major El Niño. *Mon. Wea. Rev.*, **112**, 2326-2337.
- Keshavamurty, R. N., 1982: Response of the atmosphere to sea surface temperature anomalies over the equatorial Pacific and the telconnections of the Southern Oscillation. *J. Atmos. Sci.*, **39**, 1241-1259.
- Knox, R. A. and D. Halpern, 1982: Long range Kelvin wave propagation of transport variations in Pacific Ocean equatorial currents. *J. Mar. Res.*, **40** (supplement), 329-339.
- Kubota, M. and J. J. O'Brien, 1988: Variability of the upper tropical Pacific

- ocean model. *J. Geophys. Res.*, **93**, 13930-13940.
- Lau, K. M., 1981: Oscillations in a simple equatorial climate system. *J. Atmos. Sci.*, **38**, 248-261.
- Leetmaa, A., D. W. Behringer, A. Huyar, R. L. Smith, and J. Toole, 1987: Hydrographic condition in the eastern Pacific before, during and after the 1982/83 El Niño. *Prog. Oceanogr.*, **19**, 1-47.
- Levitus, S., 1982: Climatological atlas of the world ocean. *NOAA Prof. Pap.*, **13**, 173pp.
- Lighthill, M. J., 1969: Dynamic response of the Indian Ocean to the onset of the Southwest Monsoon. *Phil. Trans. R. Soc. Lond., Ser. A***265**, 45-93.
- McCreary, J. P. 1976: Eastern tropical ocean response to changing wind system - with applications to El Niño. *J. Phys. Oceanogr.*, **6**, 632-645.
- McCreary, J. P., 1983: A model of tropical ocean - atmosphere interaction. *Mon. Wea. Rev.*, **111**, 370-387.
- McCreary, J. P. and D. L. T. Anderson, 1984: A simple model of El Niño and the Southern Oscillation. *Mon. Wea. Rev.*, **112**, 934-946.
- McCreary, J. P., 1985: Modeling equatorial oceanic circulation. *Annu. Rev. Fluid Mech.*, **17**, 359-409.
- McCreary, J. P. and D. L. T. Anderson, 1991: An overview of coupled ocean-atmosphere models of El Niño and the Southern Oscillation. *J. Geophys. Res.*, **96**, 3125-3150.
- Merle, J., 1980: Seasonal variation of heat-storage in the tropical Atlantic Ocean. *Oceanol. Acta.*, **3**, 455-463.
- Moore, D. W., 1968: Planetary-gravity waves in an equatorial ocean. Ph.D dissertation, Harvard Univ., Cambridge, Mass., 201pp.

- Moore, D. W. and S. G. H. Philander, 1978: Modelling of the tropical oceanic circulation. *The Sea*, E. D. Goldberg, I. N. McCave, J. J. O'Brien, and J. H. Steele, Eds., **6**, 319-361. Wiley (Interscience), New York.
- Neelin, J. D. and I. M. Held, 1987: Modeling tropical convergence based on the moist static energy budget. *Mon. Wea. Rev.*, **115**, 3-12.
- Neelin, J. D., 1988: A simple model for surface stress and low-level flow in the tropical atmosphere driven by prescribed heating. *Quart. J. Roy. Meteor. Soc.*, **114**, 747-770.
- Neelin, J. D., 1989: A note on the interpretation of the Gill model. *J. Atmos. Sci.*, **46**, 2466-2468.
- Neelin, J. D., 1990: A hybrid coupled general circulation model for El Niño studies. *J. Atmos. Sci.*, **47**, 674-693.
- Neelin, J. D., 1990: Interannual oscillations in an ocean general circulation model coupled to a simple atmosphere model. *Phil. Trans. R. Soc. Lond.*, **A329**, 189-205.
- Neelin, J. D., 1991: The slow sea surface temperature mode and the fast-wave limit: Analytic theory for tropical interannual oscillations and experiments in a hybrid coupled model. *J. Atmos. Sci.*, **48**, 584-606.
- Neelin, J. D., M. Latif, M. A. F. Allaart, M. A. Cane, U. Cubasch, W. L. Gates, P. R. Gent, M. Ghil, C. Gordon, N. C. Lau, C. R. Mechoso, G. A. Meehl, J. M. Oberhuber, S. G. H. Philander, P. S. Schopf, K. R. Sperber, A. Sterl, T. Tokioka, J. Tribbia, and S. E. Zebiak, 1991: Tropical air-sea interaction in general circulation models. *Climate Dynamics*, in press.
- O'Brien, J. J., D. Adamec, and D. W. Moore, 1978: A simple model of

- equatorial upwelling in the Gulf of Guinea. *Geophys. Res. Lett.*, **5**, 641-644.
- Paulson, C. A., and J. J. Simpson, 1977: Irradiance measurement in the upper ocean. *J. Phys. Oceanogr.*, **7**, 952-956.
- Philander, S.G.H., T. Yamagata, and R.C. Pacanowski, 1984: Unstable air-sea interactions in the tropics. *J. Atmos. Sci.*, **41**, 604-613.
- Philander, S. G. H., 1990: *El Niño, La Niña, and the Southern Oscillation*. Academic Press, 289pp.
- Philander, S. G. H., N. C. Lau, R.C. Pacanowski, and M. J. Nath, 1989: Two different simulations of Southern Oscillation and El Niño with coupled ocean-atmosphere general circulation models. *Phil. Trans. R. Soc. Lond.*, **A329**, 167-178.
- Philander, S. G. H., 1990: A review of simulations of the Southern Oscillation. *International TOGA Scientific Conference Proceedings.*, World Meteorological Organization, Technical Document, No. 379, 87-94.
- Rasmusson, E. M., and T. H. Carpenter, 1982: Variations in tropical sea surface temperature and surface wind fields associated with the Southern Oscillation/El Niño. *Mon. Wea. Rev.*, **110**, 354-384.
- Rasmusson, E. M. and J. M. Wallace, 1983: Meteorological aspects of the El Niño/Southern Oscillation. *Science*, **222**, 1195-1202.
- Rennick, M. A., and R. L. Haney, 1986: Stable and unstable air-sea interactions in the equatorial region. *J. Atmos. Sci.*, **43**, 2937-2943.
- Schopf, P. S. and M. A. Cane, 1983: On equatorial dynamics, mixed layer physics and sea surface temperature. *J. Phys. Oceanogr.*, **13**, 917-935.

- Schopf, P. S., 1987: Coupled dynamics of the tropical ocean-atmosphere system. *Further Progress in Equatorial Oceanography*, Nova Press, 279-286.
- Schopf, P. S. and M. J. Suarez, 1988: Vacillations in a coupled ocean-atmosphere model. *J. Atmos. Sci.* **45**, 549-566.
- Seager, R., S. E. Zebiak, and M. A. Cane, 1988: A model of the tropical Pacific sea surface temperature climatology. *J. Geophys. Res.*, **93**, 1265-1280.
- Shea, D. J., K. E. Trenberth, and R. W. Reynolds, 1990: A global monthly sea surface temperature. NCAR Technical Note. NCAR/TN-345+STR. 167pp.
- Shukla, J. and J. M. Wallace, 1983: Numerical simulation of the atmospheric response to equatorial Pacific sea surface temperature anomalies. *J. Atmos. Sci.*, **40**, 1613-1630.
- Suarez, M. J. and P. S. Schopf, 1988: A delayed action oscillator for ENSO. *J. Atmos. Sci.*, **45**, 3283-3287.
- Vallis, G. K., 1986: El Niño: A chaotic dynamical system? *Science*, **232**, 243-245.
- Wakata, Y. and T. Yamagata, 1989: Time evolution of a localized sea surface temperature anomaly in coupled air-sea models. *J. Meteor. Soc. Japan.*, **67**, 264-280.
- Wakata, Y. and E. S. Sarachik, 1991: Unstable coupled atmosphere-ocean basin modes in the presence of a spatially varying basic state. *J. Atmos. Sci.*, in press.
- Webster, P. J., 1972: Response of the tropical atmosphere to local steady forcing. *Mon. Wea. Rev.*, **100**, 518-541.

- Webster, P. J., 1981: Mechanisms determining the atmospheric response to sea surface temperature anomalies. *J. Atmos. Sci.*, **40**, 2110-2124.
- Wyrтки, K., 1975: El Niño - The dynamic response of the equatorial Pacific Ocean to atmospheric forcing. *J. Phys. Oceanogr.*, **5**, 572-584.
- Wyrтки, K., 1981: An estimate of equatorial upwelling in the Pacific. *J. Phys. Oceanogr.*, **11**, 1205-1214.
- Wyrтки, K., 1982: The Southern Oscillation, ocean-atmosphere interaction and El Niño. *Marine Technology Society Journal*, **16**, 3-10.
- Wyrтки, K., 1984: The slope of sea level along the equator during the 1982/83 El Niño. *J. Geophys. Res.*, **89**, 10,419-10,424.
- Wyrтки, K., B. Kilonsky, 1984: Mean water and current structure during the Hawaii-to-Tahiti Shuttle Experiment. *J. Phys. Oceanogr.*, **14**, 242-254.
- Xie, S.P., A. Kubokawa, K. Hanawa, 1989: Oscillations with two feedback processes in a coupled ocean-atmosphere model. *J. Climate.*, **2**, 946-964.
- Yamagata, T., 1985: Stability of a simple air-sea coupled model in the tropics. *Coupled Ocean-Atmosphere Models*, J. C. J. Nihoul, Ed., Elsevier Oceanography Series 40, Elsevier, 637-658.
- Yamagata, T. and Y. Masumoto, 1989: A simple ocean-atmosphere coupled model for the origin of a warm El Niño Southern Oscillation event. *The Dynamics of the Coupled Atmosphere and Ocean*, H. Charnock and S. G. H. Philander, Ed., The Loyal Society.
- Yang, J., and L. Yu, 1991: On the propagations of equatorially trapped waves on a sloping thermocline. *J. Phys. Oceanogr.*, in press.
- Yu, L., J. J. O'Brien and J. Yang, 1991: On the remote forcing to the

- circulation in the Bay of Bengal. *J. Geophys. Res.*, in press.
- Zebiak, S. E., 1982: A simple atmospheric model of relevance to El Niño. *J. Atmos. Sci.*, **39**, 2017-2027.
- Zebiak, S. E., 1984: Tropical atmosphere-ocean interaction and the El Niño/Southern Oscillation phenomenon. Ph.D dissertation, Massachusetts Institute of Technology, 261pp.
- Zebiak, S. E., 1986: Atmospheric convergence feedback in a simple model for El Niño. *Mon. Wea. Rev.* **114**, 1263-1271.
- Zebiak, S. E. and M.A. Cane, 1987: A model El Niño - Southern Oscillation. *Mon. Wea. Rev.*, **115**, 2262-2278.
- Zebiak, S. E., 1990: Intermediate models of ENSO. *International TOGA Scientific Conference Proceedings.*, World Meteorological Organization, Technical Document, No. 379, 95-102.

Biographical Sketch

- Name: Jiayan Yang
- Date of Birth: October 30, 1962
- Place of Birth: Guangdong, The People's Republic Of China
- Education: B.S. (Applied Mathematics), Summer of 1983,
Shandong College of Oceanography, P.R. China.
M.S. (Physical Oceanography), Fall of 1987, University
of Washington.
Ph.D (Physical Oceanography), Fall of 1991, Florida
State University.
- Title of Ph.D Thesis: A coupled atmosphere-ocean model in the tropics
with various climatological backgrounds.
- Thesis Advisor: Dr. James J. O'Brien
- Publication: 1985: The solvability of one type of nonlinear singular
integral equation. *Journal of Shandong College
of Oceanography*, Vol.16, 107-115.
1991 (with Lisan Yu): On the propagation of
equatorially trapped waves on a sloping
thermocline. *Journal of Physical Oceanography*
(in press).
1991 (with L. Yu and J.J. O'Brien): On the remote
forcing to the circulations in the Bay of Bengal.
Journal of Geophysical Research (in press).
1991 (with J.J. O'Brien) A coupled atmosphere-ocean
model in the tropics with various thermocline
profiles. Submitted to: *Journal of Climate*.
1991 (with J.J. O'Brien) A simple coupled atmosphere-
ocean model in the tropics with two equilibrium
states. Submitted to: *Journal of Climate*.